

# River bank erosion and lateral accretion linked to hydrograph recession and flood duration in a mountainous snowmelt-dominated system

Nicholas A Sutfin<sup>1</sup>, Joel Rowland<sup>2</sup>, Mulu Fratkin<sup>2</sup>, Sophie Stauffer<sup>2</sup>, Rosemary Carroll<sup>3</sup>, Wendy Brown<sup>4</sup>, and Kenneth H Williams<sup>5</sup>

<sup>1</sup>Case Western Reserve University

<sup>2</sup>Los Alamos National Laboratory

<sup>3</sup>Desert Research Institute

<sup>4</sup>Rocky Mountain Biological Laboratory

<sup>5</sup>Lawrence Berkeley National Laboratory

November 30, 2022

## Abstract

Observed and projected global changes in the magnitude and frequency of river flows have potential to alter sediment dynamics in rivers, but the direction of these changes is uncertain. Linking changes in bank erosion and floodplain deposition to hydrology is necessary to understand how rivers will adjust to changes in hydrologic flow regime induced by increasing societal pressures and increased variability of climatic conditions. We present analysis based on aerial imagery, an aerial lidar dataset, intensive field surveys, and spatial analysis to quantify bank erosion, lateral accretion, floodplain overbank deposition, and a floodplain sediment budget in an 11-km long study segment of the meandering East River, Colorado, USA, over 60 years. Assuming steady state conditions over the study period, our measurements of erosion and lateral accretion close the sediment budget for a smaller 2-km long intensive study reach. We analyzed channel morphometry and snowmelt-dominated annual hydrologic indices in this mountainous system to identify factors influencing erosion and deposition in nine study sub-reaches. Results indicate channel sinuosity is an important predictor for both lateral erosion and accretion. Examination of only hydrologic indices across the study segment regardless of sub-reach morphology, indicate that the duration of flow exceeding baseflow and the slope of the annual recession limb explain 59% and 91% of the variability in lateral accretion and erosion, respectively. This work provides insight into hydrologic indices likely to influence erosion and sedimentation of rivers and reservoirs under a shifting climate and hydrologic flow regimes in snowmelt-dominated systems.

1 **River bank erosion and lateral accretion linked to hydrograph recession and flood**  
2 **duration in a mountainous snowmelt-dominated system**

3  
4 **Nicholas A Sutfin<sup>1\*</sup>, Joel Rowland<sup>1</sup>, Mulu Fratkin<sup>1</sup>, Sophie Stauffer<sup>1</sup>, Rosemary**  
5 **W.H. Carroll<sup>2</sup>, Wendy Brown<sup>3</sup>, Kenneth H. Williams<sup>3,4</sup>**

6 <sup>1</sup>Earth and Environmental Sciences Division, Los Alamos National Laboratory, Los Alamos, NM

7 <sup>2</sup>Division of Hydrologic Sciences, Desert Research Institute, Reno, NV

8 <sup>3</sup>Rocky Mountain Biological Laboratory, Gothic, CO

9 <sup>4</sup>Lawrence Berkeley National Laboratory, Berkeley, CA

10 \* Current affiliation: Dept. of Earth, Environmental, and Planetary Sciences, Case Western  
11 Reserve University, Cleveland, OH

12  
13 Corresponding authors: Nicholas A. Sutfin ([Nicholas.sutfin@case.edu](mailto:Nicholas.sutfin@case.edu)), Joel Rowland  
14 ([jrowland@lanl.gov](mailto:jrowland@lanl.gov))

15  
16 **Key Points:**

- 17 • Floodplain erosion and accretion estimated over 60 years using aerial lidar,  
18 repeat aerial imagery, field surveys, and historic flow data
- 19 • Hydrograph recession and duration of floodplain inundation explain 91% and  
20 59% of the variability in bank erosion and lateral accretion
- 21 • Results can inform potential response to shifting climatic conditions and  
22 hydrologic regimes of snowmelt-dominated rivers

23

24

25

26

27

28

29

30 **Abstract**

31           Observed and projected global changes in the magnitude and frequency of river  
32 flows have potential to alter sediment dynamics in rivers, but the direction of these  
33 changes is uncertain. Linking changes in bank erosion and floodplain deposition to  
34 hydrology is necessary to understand how rivers will adjust to changes in hydrologic flow  
35 regime induced by increasing societal pressures and increased variability of climatic  
36 conditions. We present analysis based on aerial imagery, an aerial lidar dataset, intensive  
37 field surveys, and spatial analysis to quantify bank erosion, lateral accretion, floodplain  
38 overbank deposition, and a floodplain sediment budget in an 11-km long study segment  
39 of the meandering East River, Colorado, USA, over 60 years. Assuming steady state  
40 conditions over the study period, our measurements of erosion and lateral accretion close  
41 the sediment budget for a smaller 2-km long intensive study reach. We analyzed channel  
42 morphometry and snowmelt-dominated annual hydrologic indices in this mountainous  
43 system to identify factors influencing erosion and deposition in nine study sub-reaches.  
44 Results indicate channel sinuosity is an important predictor for both lateral erosion and  
45 accretion. Examination of only hydrologic indices across the study segment regardless of  
46 sub-reach morphology, indicate that the duration of flow exceeding baseflow and the  
47 slope of the annual recession limb explain 59% and 91% of the variability in lateral accretion  
48 and erosion, respectively. This work provides insight into hydrologic indices likely to  
49 influence erosion and sedimentation of rivers and reservoirs under a shifting climate and  
50 hydrologic flow regimes in snowmelt-dominated systems.

51

52

## 53 **Plain Language Summary**

54 Changing climatic conditions are poised to alter the timing and magnitude of  
55 precipitation, snowpack, snowmelt and the balance of water and sediment within river  
56 corridors. Understanding how these changes affect the stability of land along rivers is  
57 important for securing infrastructure, maintaining healthy ecosystems, preserving water  
58 quality, and understanding the fate and transport of contaminated sediment. This  
59 research uses aerial imagery, laser topographic scanning technology, field  
60 measurements of water and soil, and historical river flow data to examine linkages  
61 between river flows and erosion and deposition of sediment along the floodplain of a  
62 mountain over 60 years. Results show that river bank erosion is linked to the rate at  
63 which the river flows decrease following snowmelt-driven peaks and that the amount of  
64 sediment that is deposited along the river banks is linked to the duration of flooding;  
65 both are influenced by channel sinuosity. These results have important implications for  
66 understanding how rivers and freshwater resources may be impacted by shifting climatic  
67 conditions and hydrologic regimes.

## 68 **1 Introduction**

69 A large number of studies have quantified long-term channel migration and  
70 episodic bank erosion, but these approaches do not fully examine the link between  
71 changes in river flows and the timing of river bank erosion, particularly in snowmelt-  
72 dominated systems. Rapid changes in river flows likely strongly influence river bank  
73 stability and erosion on seasonal scales (Wolman, 1959; Simon et al., 2002). Annual  
74 hydrologic trends including the magnitude, frequency, timing, duration, and rate of  
75 change in discharge are important aspects of river flow regimes that influence aquatic  
76 and riparian habitat (Poff et al., 1997) and sediment dynamics including erosion and  
77 deposition along floodplains (Wohl et al., 2015). More specific investigation of hydrologic

78 flow regimes have been examined using various hydrologic indices to provide insight  
79 into riverine ecosystems (Richter et al., 1996) and germination of riparian vegetation  
80 (Benjankar et al., 2014; Caponi et al., 2019). These changes that characterize annual  
81 hydrologic flow regimes across all climatic zones can include very rapid changes in  
82 discharge, such as those in flashy rainfall dominated systems. Alteration of natural flow  
83 regimes induced by dams and flow regulation – common in snowmelt dominated  
84 systems – can mimic these rapid changes and greatly alter sediment regimes and  
85 riverine habitat (Richter et al., 1996; Poff et al., 1997; Lenhart et al., 2013).

86         While understanding the mechanisms and timing of bank erosion is fundamental  
87 to landscape evolution and risk to infrastructure, it is also crucial for nutrient and carbon  
88 dynamics and potential impact to water resources. The rate at which banks erode and  
89 rivers migrate substantially influence nutrient and carbon dynamics (Sekely et al., 2002;  
90 Sutfin et al., 2016), ecosystem habitat (Naiman et al., 2010), and the fate and transport  
91 of contaminants bound to floodplain sediment (Macklin et al., 2006; Rhoades et al.,  
92 2009). Changes in erosion and deposition along floodplains can greatly alter carbon  
93 storage along floodplains (Noe & Hupp, 2005; Hoffmann et al., 2009; Omengo et al.,  
94 2018; Scott & Wohl, 2018; Lininger et al., 2019), which is substantially higher within  
95 snowmelt-dominated mountainous headwater systems (Wohl et al., 2012; Sutfin et al.,  
96 2016; Sutfin & Wohl, 2017). Contaminants adsorbed to mineral facies and organic  
97 matter in floodplain and bank sediment of mountain streams, such as the heavy metals  
98 from the mining spill along the Animas River in Colorado, USA, (Rodriguez-Freire et al.,  
99 2016), are susceptible to erosion and pose a risk for downstream water quality and  
100 ecosystems. The research presented here is motivated by our efforts to quantify carbon  
101 storage and dynamics in a mountainous region along the floodplain of the East River  
102 near Crested Butte, Colorado, USA. The general goals of this research were to quantify

103 erosion and deposition along the East River and to link these observations to past  
104 hydrologic conditions.

105 Many researchers have used remotely sensed imagery to examine bank erosion  
106 and lateral accretion over years to decades (James E. Pizzuto, 1994; Micheli & Kirchner,  
107 2002a, 2002b; S. S. Day et al., 2013b, 2013a; Lenhart et al., 2013; Rowland et al., 2016;  
108 Schook et al., 2017; Schwenk et al., 2017; Caponi et al., 2019). Using these data as a  
109 basis for understanding river migration rates, modeling efforts seek to understand the  
110 physically-based drivers of channel migration over long time scales (i.e.,  $10^2$  to  $10^5$   
111 years) (Howard, 1996; Güneralp & Rhoads, 2009; G. Parker et al., 2011; Bogoni et al.,  
112 2017), or use near-bank velocities to estimate bank erosion over shorter time scales  
113 (Darby et al., 2007; Gary Parker et al., 1982; J. E. Pizzuto & Meckelnburg, 1989).

114 Physically based models of bank erosion provide understanding of cantilever  
115 failures, slip or rotational failures, and planar shear resulting from undercutting, positive  
116 pore pressure, and excess bank shear stress, respectively (Thorne & Tovey, 1981;  
117 Simon et al., 2000; Langendoen & Simon, 2008; Langendoen & Alonso, 2008). Available  
118 models tend to use bankfull flow conditions to model bank erosion (Langendoen &  
119 Alonso, 2008) and past work indicates that more erosion is likely to occur at high flow  
120 conditions. However, changes in flow have also been identified as potential drivers for  
121 bank failure because positive pore pressure of saturated banks combined with the loss  
122 of supporting pressure when stage declines make slip and rotational bank failures likely  
123 (Rinaldi & Casagli, 1999). Thus, additional hydrologic indices such as the rate of change  
124 offer the potential to provide a more robust understanding of the hydrologic drivers of  
125 bank erosion.

126 Effectively linking floodplain erosion and accretion to hydrology requires the  
127 assumption of minimal changes in sediment supply and are simplified by the assumption

128 of steady state and a balanced sediment budget over the time period examined.  
129 Sediment budgets at the watershed scale must consider the production of sediment from  
130 weathering and erosion, elements of storage within the basin, sediment transport  
131 processes, and the resulting sediment yield (Dietrich et al., 1982; Gellis & Walling,  
132 2013). Sediment budgets for only floodplains, however, may be simplified needing only  
133 to account for the time averaged balance of erosion and deposition along the floodplain  
134 alone (Reid & Dunne, 2016). Examples of floodplain sediment accounting includes those  
135 in the southwestern United States by Gellis et al. (2012) and in the Le Sueur watershed  
136 in Minnesota, USA, by Belmont et al., (2011) and Day et al., (2013). Here, we use a  
137 floodplain sediment budget to constrain estimates of floodplain erosion and  
138 sedimentation along a subalpine meandering river using a combination of field  
139 observations, remotely sensed imagery and lidar, and GIS spatial analysis.

140 We studied the connections between hydrology and sediment flux of the East  
141 River floodplain, using (1) repeat aerial imagery to quantify lateral erosion and accretion  
142 over a 60-year period, (2) measurement of floodplain fine sediment depth, (3) an aerial  
143 lidar digital elevation model (DEM) and (4) empirical relationships with characteristics of  
144 the flow regime to identify hydrologic drivers of river bank erosion and lateral accretion.  
145 From this work, we developed an empirical relationship between hydrology and  
146 sediment fluxes on decadal time scales to address the primary goal to determine what  
147 morphometric variables (e.g., sinuosity, channel slope, width) and hydrologic indices  
148 (e.g., peak magnitude, timing of peak, slope of the recession limb) best explain observed  
149 floodplain erosion and accretion on the snowmelt-dominated East River. We also  
150 calculated a sediment budget to verify our accounting of eroded and accreted floodplain  
151 sediment and used the results to examine a practical and cost-effective way to estimate

152 hydrologic influence on floodplain erosion and accretion that does not require the  
153 intensive fieldwork and lidar analysis employed in this study.

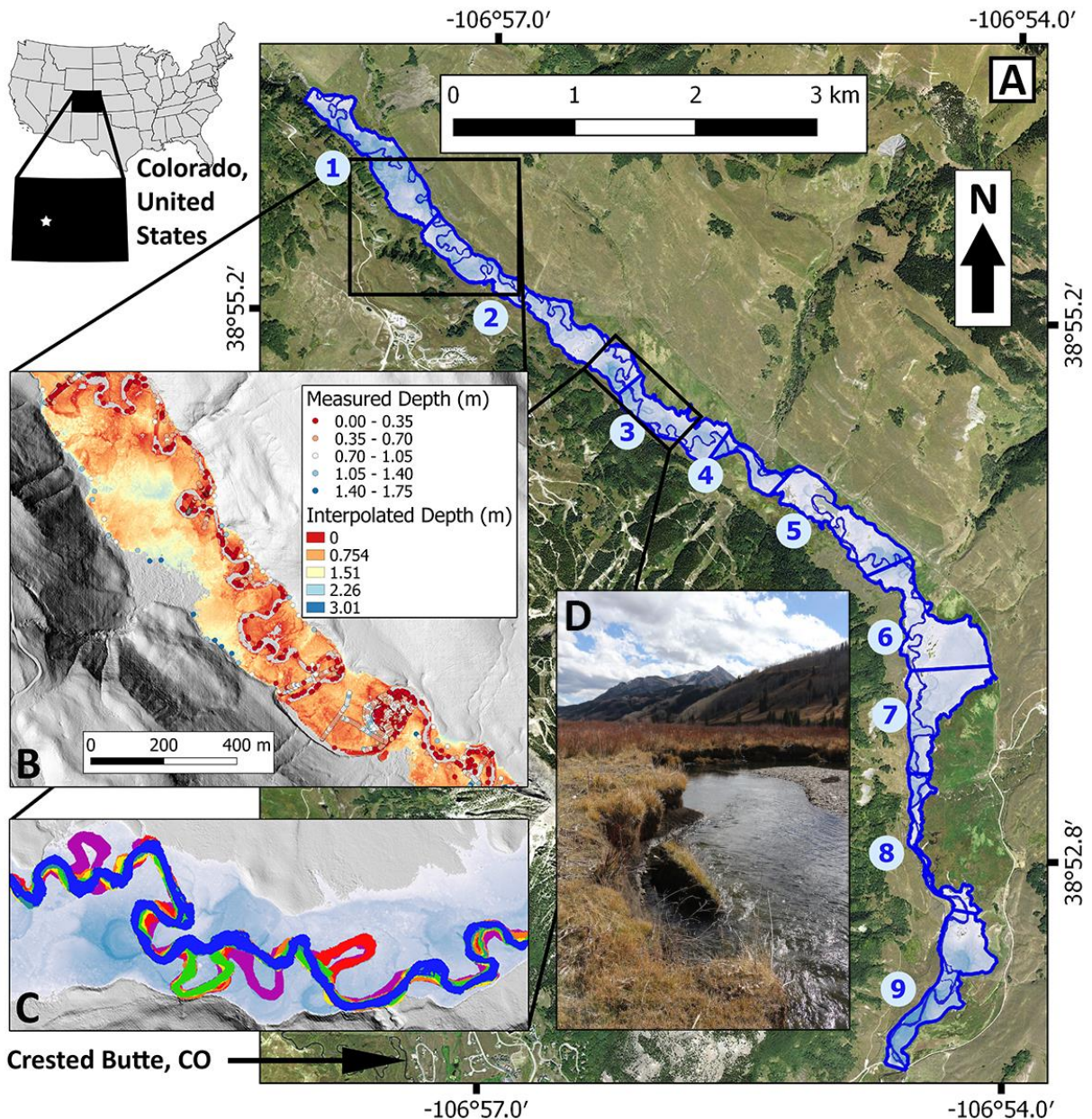
154

## 155 **2 Study Area**

156 We studied an 11-km long segment of the East River approximately 3.5 km down  
157 valley from Gothic, CO, (Figure 1) near Crested Butte. At the downstream end of the  
158 study segment, the East River drains approximately 134 km<sup>2</sup> and has an annual average  
159 precipitation of 64 cm (SNOTEL, 2017). The floodplain lies directly downstream of steep,  
160 confined, mountainous tributaries that incise through sandstones, mudstones, shales,  
161 granodiorite and metamorphosed byproducts of the uplifted White Rock pluton in the Elk  
162 Mountains of Colorado (Gaskill et al., 1991). Within the floodplain reach, the East River  
163 is a gravel-cobble bed, sinuous alluvial river approximately 20-m wide on average and  
164 bounded by lateral Pinedale glacial moraines, landslide deposits, and outcrops of  
165 Mancos Shale along the bed and valley walls. Sedges, grasses, and willows dominate  
166 the vegetation along the floodplain with isolated trees, dominantly blue spruce, scattered  
167 along the reach, but rarely located along the river banks. Throughout the floodplain,  
168 extensive beaver activity results in dams, lodges and the introduction of large wood from  
169 the surrounding hillslopes. Floodplain fine overbank sediment is dominated by silt-size  
170 particles with varying proportions of sand, clay, and minimal gravel content (Malenda et  
171 al., 2019). Beneath fine sediment, the floodplain is composed of gravel and cobbles, and  
172 contains lenses of finer, sorted material. Erosion of underlying gravels and undercutting  
173 of fine overbank sediment commonly result in cantilever failure of grass-covered blocks  
174 along the East River 11-km long study segment (Figure 1D, S1).

175 The East River is a typical snowmelt-dominated system, which is characterized  
176 by a gradual rising limb as temperatures warm and snow melts in the spring months of

177 April and May. An annual peak flow commonly occurs in the latter half of May or early  
178 half of June after peak snowmelt, followed by a gradual recession limb that takes place  
179 over weeks to months at which discharge returns to some baseflow condition sometime  
180 between September and November.



181  
182 **Figure 1.** Map of study area on the East River near Crested Butte, Colorado, USA. The  
183 floodplain was delineated by “flooding” a 0.5-m resolution lidar digital elevation model  
184 along the 11-km long study segment, which was divided into 9 study reaches (A) based  
185 on changes in valley slope. The depth of fine sediment was measured across the  
186 floodplain at 1847 points and interpolated across the upper 2 km, intensive study reach

187 (B) consisting of reach 1 and approximately half of reach 2, ending at the downstream  
188 extent of the black box in (A). Masks of the river channel, depicted in various colors,  
189 were derived for all seven time periods (C), and used to determine lateral accretion and  
190 erosion, typically occurring as cantilever failures in the study area (D). Shades of blue  
191 indicate relative depth of water across the delineated floodplain in A and C.

192 Limited land-use impacts have influenced the watershed upstream of the 11-km  
193 long study segment of the East River. From 1880 to 1890, a silver mine operated along  
194 Copper Creek upstream of Gothic, CO, the present location of the Rocky Mountain  
195 Biological Laboratory. The mining area is now designated as US Forest Service (USFS)  
196 national forest and wilderness area. Land use along the 11-km long study segment  
197 consists of small privately owned parcels and U.S. Forest Service (USFS) land, on which  
198 ranchers graze cattle for limited portions of the year (Theobald et al., 1996). Limited  
199 property access restricted our field investigations to the upper 2 km, intensive study  
200 reach (Figure 1A; Reach 1 and half of reach 2). Although flow diversions exist within the  
201 11-km long study segment, they were present prior to beginning of the study period in  
202 1955 and they primarily capture runoff from tributaries before they reach the East River.

203

### 204 **3 Materials and Methods**

205 Spatial analysis of aerial lidar, repeat aerial imagery, surface water flow  
206 measurements and historical hydrologic flow analysis, measurements of floodplain fine  
207 sediment depth, and multiple linear regression were used to examine linkages between  
208 hydrology and bank erosion, accretion, and channel migration rates over 60 years.

#### 209 *3.1 Terrain Analysis and Study Reach Delineation*

210 Aerial lidar was collected in August of 2015 for the entire East River watershed.  
211 Average bare-ground point cloud density of lidar was 4.29 points/m<sup>2</sup> resulting in a total  
212 accuracy with root mean squared error of 0.05 m at the 95% confidence level. A hydro-  
213 flattened, bare-ground DEM with a horizontal resolution of 0.5 m derived from the lidar

214 point cloud data was used for all topographic analysis. Using the valley slope, we divided  
215 the ~11-km long floodplain segment into nine study reaches. We calculated the valley  
216 slope using a best-fit line of elevation points extracted from the 2015 DEM and spaced  
217 every 10 meters down the valley center. We detrended the slope of the 9 sub-reaches  
218 using the raster calculator in QGIS and recombined them to generate a floodplain DEM  
219 with zero down-valley slope and a maximum total relief of 5.44 m. We artificially  
220 entrenched the flat lidar water surface by 2 meters and used the *r.fill.dir* Grass tool in  
221 QGIS to flood the detrended DEM at a depth of six meters to delineate the approximate  
222 extent of the floodplain. We verified the digitally delineated floodplain extent with field  
223 observations of distinct breaks in slope, such as the base of lateral moraines, toes of  
224 alluvial fans, and abutments to incised bedrock outcrops.

### 225 *3.2 Channel Position and Movement using Aerial Imagery*

226 We used aerial images from seven dates (i.e., 1955, 1973, 1983, 1990, 2001,  
227 2012, 2015) obtained from the US Geological Survey, US Department of Agriculture,  
228 and the US Forest Service to delineate the channel, measure channel widths, sinuosity,  
229 and lateral erosion and accretion over time. All imagery was resampled to 1-m resolution  
230 to allow direct comparison between images. We georeferenced the 2015 imagery using  
231 the 2015 lidar DEM dataset as a reference using >6 control points including the corners  
232 of buildings, intersections of roads and fences, and the base of mature trees. All other  
233 images were georeferenced (if not already done so by the source agency) through  
234 comparison with similar point types in the 2015 georeferenced image.

235 To analyze channel characteristics and compare changes over time, we  
236 generated binary channel masks for each set of aerial imagery. For color imagery  
237 between 1973 and 2015, we generated masks of bankfull river extent using red-green-  
238 blue (RGB) color bands and the normalized difference water index (NDWI) to classify the

239 channel water surface in each image (Figure 1C; McFeeters, 1996) using the object-  
240 oriented classification software, eCognition. To control for variations in water levels  
241 between images, regions of tan and grey gravel and sand bars devoid of vegetation and  
242 exposed, un-vegetated bank faces were included in the channel mask as an estimate of  
243 bankfull extent (Gurnell, 1997; Richard et al., 2005; Mount & Louis, 2005; Fisher et al.,  
244 2013; Rowland et al., 2016; Donovan et al., 2019). The black and white 1955 USDA  
245 photos required manual delineation of the channel mask.

246 Metrics calculated to quantify the channel and floodplain attributes for the nine  
247 valley reaches and entire 11-km long study segment included: valley, floodplain, and  
248 channel areas; valley and channel lengths; elevation change along the reach; valley and  
249 channel slopes; sinuosity; average channel width; and valley confinement. The channel  
250 area relative to the area of delineated valley floor defined valley confinement as a proxy  
251 for potential of the floodplain to accommodate channel migration, dissipate energy  
252 during overbank flow, and facilitate overbank deposition. Channel sinuosity measures  
253 the channel length divided by the straight down-valley length. Channel slope was  
254 calculated as the valley slope divided by channel sinuosity. Channel width, linear  
255 erosion, and accretion rates were determined for each bank pixel using the Spatially  
256 Continuous Riverbank Erosion and Accretion Measurements algorithm (SCREAM;  
257 Rowland et al., 2016).

258 Linear rates represent the distance that a river bank face moves in a given time  
259 interval by measuring the Euclidean distance between a bank pixel in one river mask  
260 and the closest bank pixel at the subsequent river mask. Eroded and accreted floodplain  
261 areas derived from SCREAM were divided by the number of years within that time  
262 period and the channel length to estimate linear rates of erosion and accretion. Three  
263 sources of error are associated with our measurements of linear change: image

264 registration, image classification and the accuracy of SCREAM output (Rowland et al.,  
265 2016). Average estimated registration error for the 1-m imagery from 1973 to 2015 was  
266 0.58 m. Poor image quality of the 1955 photographs prevented direct estimates of error  
267 using this method, so we have assigned a registration error equal to two times the  
268 highest error (1.2 m) in areas for the period between 1955-1973. Errors associated with  
269 area-based erosion and accretion measurements as a result of image mis-registration  
270 for each time period were assigned as percentage of change in areas following the  
271 methodology detailed in Rowland et al. (2016). Total measurement errors were  
272 estimated by combining registration, classification, and methodological errors in  
273 quadrature (Rowland et al. 2016)) (Table S1).

### 274 *3.3 Vertical Accretion Rates*

275 We estimated long-term vertical accretion rates using a combination of field-  
276 based measurements of fine-grained deposit thickness and changes in channel position  
277 from aerial imagery between 1973 and 2015. Images from 1955 were excluded from this  
278 analysis because of the uncertainty associated with the poor-quality images. In 2016,  
279 along the upper 2 km, intensive study reach (Figure 1A, reach 1 and half of reach 2), we  
280 measured thickness of fine-grained deposits at 324 locations on 21 transects by  
281 inserting a soil probe into the floodplain surface until refusal at bedrock or gravel-size  
282 material (>2mm). Mean migration rate was estimated from SCREAM output and the  
283 distance to each transect point from the channel was converted into duration since  
284 channel occupation by dividing by the bend averaged migration rate (Figure S2). More  
285 detailed analysis to examine vertical accretion rates in conjunction with the channel  
286 migration rate over each time period was conducted and outlined in the supplemental  
287 information (Figure S2), but suspected point bar erosion did not produce robust results  
288 that support continuous vertical accretion for each time period. Instead, we used the total

289 depth to represent an average deposition rate over the time period examined. The  
290 measured depth of fine sediment ( $d_i$ ) was then divided by the duration since occupation  
291 by the river channel ( $t_i$ , when fine sediment depth would have been equal to zero) to  
292 estimate a mean vertical accretion rate ( $\bar{a}_i$ ; Equation 1).

$$293 \quad \bar{a}_i = \frac{d_i}{t_i} \quad (1)$$

294 Potential predictors of floodplain vertical accretion rates, across the upper 2 km,  
295 intensive study reach were assessed through stepwise multiple linear regression.  
296 Variables examined for this analysis were similar to those described above, with the  
297 following additions. Distance from the channel was measured in the field. Relative  
298 elevation from the bankfull stage at the transect was extracted from the lidar at the top of  
299 point bars were bar sand/gravel transitioned into vegetation cover. Along each transect,  
300 channel width, valley width, and the ratio between the two (valley confinement) were  
301 measured from the imagery in GIS. Localized valley slope, channel slope, and sinuosity  
302 were measured using GIS extending approximately 50 m upstream to 50 m downstream  
303 of the transect. Mean values of radius of curvature, lateral accretion rate, and erosion  
304 rate were calculated along each meander bend. Measurements were denoted as either  
305 being on the inside or outside of a bend. The angle of each transect was used as a  
306 proxy for the angle of each river bend relative to the down valley direction from 0-90°.

### 307 *3.4 Estimating floodplain sediment volumes*

308 Areas of accretion and deposition from the SCREAM analysis were converted to  
309 sediment volumes using measured sediment depths. In our analysis, we only estimate  
310 volumes of fine grained (less ~ 2mm in grain diameter) sediments deposited on top of  
311 the gravel-rich channel and point bar deposits. In addition to the soil probe  
312 measurements collected on point bar transects (Section 3.3), 1,587 measurements were

313 made along the upper 2 km intensive study reach (Figure 1A, Reaches 1 and 2; Sutfin &  
314 Rowland, 2019). We subtracted these depth measurements from the DEM elevations  
315 using the *raster calculator* in QGIS to calculate an absolute elevation of underlying  
316 gravel/bedrock. We then generated a triangular irregular network (TIN) of the  
317 gravel/bedrock surface elevation using the *interpolate* tool in QGIS. By subtracting  
318 elevations of this interpolated surface from the ground surface elevations, we created a  
319 spatially continuous isopach map of fine-grained floodplain sediment.

320 This interpolated fine-sediment map represents conditions in 2015. At the  
321 location of the current channel the fine sediment has values of zero, as such, areas of  
322 historical floodplain erosion that intersected the 2015 channel did not have accurate  
323 values of the floodplain volume eroded. To correct for this error we interpolated 2015  
324 fine-sediment thickness across the channel using a 3 m buffer that extended beyond the  
325 locally thin deposits covering active point bars. We used the *close gap* Saga tool in  
326 QGIS (threshold = 0.1) to create the corrected isopach map. We calculated eroded  
327 volumes by multiplying the areas of eroded regions derived from the aerial imagery for  
328 each time interval by the interpolated isopach map of fine sediment within those mapped  
329 areas.

330 Using the estimated vertical accretion rates from our soil probe transects we  
331 estimated an average deposition rate for laterally accreted regions along the channel  
332 and developed a multiple linear regression model to estimate overbank deposition on the  
333 stable floodplain surface in response to floods. For the laterally accreted areas, we used  
334 the average migration rates at the bends determined using the probe transects  
335 described above in section 3.3 to determine the portion of contemporary floodplain that  
336 would have been formed by lateral accretion during the 42 years between 1973 and  
337 2015. A reach-based average migration rate and resulting mean migration distance

338 along the probe transects were used to estimate an average vertical accretion rate from  
339 all points within the mean migration distance for the entire period between 1973-2015  
340 (Table S2). This average rate was multiplied by the mapped accretion areas from the  
341 aerial photos and SCREAM output to provide a volume of laterally accreted sediments.

342 Overbank deposition rates beyond 10 m were calculated for each cell utilizing  
343 another multiple linear regression model including only the two strongest predictor  
344 variables, distance from the channel and relative elevation from the channel (Figure S3).  
345 The *proximity grid* Saga tool in QGIS was used to create a grid based on distance from  
346 the channel for images from the six years. Floodplain elevation relative to the channel  
347 was calculated by subtracting the minimum elevation from the detrended 2015 DEM  
348 floodplain surface (derivation described above in section 3.1). This assigned a relative  
349 elevation to every raster pixel. The river channel buffered by three meters on both sides  
350 was subtracted from the relative elevation grid and the *close gap* tool in QGIS was used  
351 to interpolate elevations across the channel.

352 The distance-from-channel raster and the detrended-valley DEM were used as  
353 input to the vertical accretion rate regression model equation in the raster calculator to  
354 generate raster grids of estimated overbank deposition rates for all six time periods.  
355 Overbank sediment deposition estimates of volume were made by multiplying calculated  
356 rates by the number of years in the respective time interval, summing all pixel values for  
357 each period, and multiply that value by the area of each pixel (0.25 m<sup>2</sup>). Vertical  
358 accretion within abandoned channels was estimated using the lateral accretion rate of  
359 3.3 cm y<sup>-1</sup> within the first 10 m from the channel for periods following cutoff occurrence.  
360 Aggradation of previously abandoned channels was based on the relative vertical and  
361 horizontal distance from the active bankfull channel at distances exceeding 10 m. Rates

362 of volume of sediment accreted and eroded during each time period were estimated by  
363 dividing the total volume of sediment by the number of years in each time period.

### 364 *3.5 Streamflow Data and Hydrologic Analysis*

365 Streamflow was measured 22 times near the Crested Butte city water pump  
366 house in the upper 2 km, intensive study reach, from October, 1<sup>st</sup>, 2014, to September,  
367 30<sup>th</sup>, 2017, and a stage-discharge rating curve was created against stage data recorded  
368 every 15 minutes ( $r^2 = 0.99$ ) (Carroll & Williams, 2019). To extend the flow record prior to  
369 2014, we regressed measured discharge at the 2-km intensive study reach against data  
370 from the US Geological Survey stream gage on the East River at Almont (gage #  
371 09112500) 40 km downstream ( $r^2 = 0.97$ ; Figure 3A). Using this regression, we  
372 generated a synthetic hydrograph for the study site from 1934-2018 using the Almont  
373 streamflow data (Table S3). A comparison of the synthetic hydrograph and flows  
374 measured between 2014 and 2018 showed a strong agreement with a Nash-Sutcliffe  
375 Efficiency coefficient (NSE) of 0.97 (Figure 3B). Flow frequency analysis was conducted  
376 on the entire synthetic hydrograph to determine annual statistics for the continuous 82  
377 years. Analysis of possible hydrological drivers for erosion and deposition examined the  
378 synthetic hydrograph from 1955 to 2015 to correspond with the aerial imagery analysis.

379 We used R software (R Core Team, 2017) to extract synthetic hydrograph  
380 characteristic between 1955 and 2015. An average minimum flow value of  $0.49 \text{ m}^3 \text{ s}^{-1}$   
381 during the low-flow months of October, November, December, January, February, and  
382 March were used as a reference baseflow condition. Bankfull flow was estimated as  $8$   
383  $\text{m}^3 \text{ s}^{-1}$  based on field observations and hydrologic analysis indicates an approximate  
384 recurrence interval of 1.2 years. The mean value for the day of the year on which peak  
385 flow occurred, the last day exceeding bankfull flow conditions, and the last day  
386 exceeding baseflow conditions were calculated for each time period. The maximum and

387 mean values within each time period were calculated for annual hydrograph peak  
388 magnitude, peak timing, annual volume of discharge, the annual volume of water above  
389 bankfull flow, duration between the first and last day of flow exceeding baseflow, the  
390 number of days on which baseflow occurred, the annual volume of discharge exceeding  
391 bankfull, duration between the first and last day of flow exceeding bankfull flow, the  
392 number of days on which bankfull flow occurred, and the cumulative number of days  
393 since the last bankfull flow, the total recession limb slope from the annual maximum  
394 peak to baseflow, the bankfull recession limb slope from bankfull stage to baseflow, and  
395 the number of peaks above bankfull flow. Recession slopes were estimated as the slope  
396 of the line between peak discharge and the first occurrence of baseflow conditions.

397 A secondary analysis was conducted to examine diel fluctuations in discharge  
398 associated with the slope of the recession limb of each annual hydrograph. A regression  
399 analysis of 15-minute streamflow data from the same USGS gauge and measured flow  
400 at the study site from 2015-2019 yielded an  $r^2 = 0.94$ . This regression was used to  
401 extend the study site discharge data to span the duration of the 15-minute data from  
402 1988-2019. Maximum and minimum daily values were determined using hourly data and  
403 the number and magnitude of diel fluctuations exceeding  $6 \text{ m}^3\text{s}^{-1}$  within a window of 5 to  
404  $10 \text{ m}^3\text{s}^{-1}$  were summed. Correlations were examined between the recession limb slope  
405 and the number, the summed magnitude, and the average magnitude of diel fluctuations  
406 to occur within the defined recession window.

### 407 *3.6 Statistical Analyses*

408 The number of potential variables for all multivariate regression models used to identify  
409 significant predictors was reduced to minimize collinearity of predictor variables prior to  
410 multiple linear regression. Starting with the most strongly correlated variable and working  
411 sequentially through variables with decreasing correlation values, variables were

412 eliminated as potential predictors for the regression model if they were moderately cross  
413 correlated ( $r > 0.7$ ) with another more strongly correlated variable (Dormann et al., 2013)  
414 already selected as a predictor. Stepwise multiple linear regression was conducted  
415 using the *stats* package *lm* function in R statistical software to examine possible  
416 predictor variables and determine the best regression model for: (1) the area of accreted  
417 and (2) the area of eroded floodplain along nine study reaches, and (3) vertical  
418 floodplain deposition rate estimated from measurements of floodplain fine sediment  
419 depth along the upper 2 km, intensive study reach over the 6 time periods. Multiple  
420 linear regression assumptions of normality and homoscedasticity of model residuals  
421 were met with power transformations and verified using the Shapiro-Wilk normality test  
422 (*shapiro.test* function) and the non-constant error variance test in R (*ncv.test* function),  
423 for which details are provided in supporting material. Variables were included in stepwise  
424 multiple linear regression to identify the best regression model based on minimizing the  
425 Akaike Information Criteria (AIC).

## 426 **4. Results**

### 427 *4.1 Channel and floodplain metrics*

428 The floodplain delineation of the entire 11-km long study segment resulted in a valley  
429 bottom area of 2.65 km<sup>2</sup> with a total valley length of 10.62 km and a total valley slope of  
430 0.64%. Despite the occurrence of 21 channel chute cutoffs in the 60-year time period,  
431 channel slope and the sinuosity for the entire river segment remained relatively constant  
432 during the six periods examined. Channel slope along the entire 11-km long study  
433 segment varied from 0.34 to 0.36% over the 60-year time period. Sinuosity fluctuated  
434 about a mean value of  $1.81 \pm 0.04$  m/m (SD) with a minimum and maximum of 1.77 to  
435 1.89 (Table 1).

436 **Table 1.** Morphological characteristics of the entire East River study segment derived from remotely sensed imagery and lidar for  
 437 each time period. Channel width was calculated as a mean of channel width pixel values from SCREAM and standard deviations of  
 438 those averages are provided following each mean.

Year	Floodplain area (km <sup>2</sup> )	Channel Area (km <sup>2</sup> )	Channel Length (km)	Sinuosity (m/m)	Channel slope (%)	Confinement (m <sup>2</sup> /m <sup>2</sup> )	Mean channel width (m)
1955	2193.6	459.0	20.08	1.89	0.339	0.17	25 ± 2
1973	2254.0	398.7	19.29	1.82	0.353	0.15	20 ± 2
1983	2222.3	430.3	18.80	1.77	0.362	0.16	23 ± 3
1990	2295.4	357.3	18.90	1.78	0.361	0.13	19 ± 3
2001	2275.4	377.3	19.39	1.83	0.352	0.14	21 ± 3
2011	2296.2	356.5	18.81	1.77	0.362	0.13	19 ± 1
2015	2312.2	340.4	18.98	1.79	0.359	0.13	17 ± 1

439

440 **Table 2.** Morphological characteristics of nine study reaches derived from remotely sensed imagery and lidar. Values are averaged  
 441 from the seven images spanning 60 years and standard deviations of those averages are provided following each mean.

Reach	Valley area (m <sup>2</sup> )	Valley Length (m)	Valley slope (%)	Floodplain area (m <sup>2</sup> )	Channel Area (m <sup>2</sup> )	Channel Length (m)	Sinuosity (m/m)	Channel slope (%)	Confinement (m <sup>2</sup> /m <sup>2</sup> )	Channel width (m)
1	344236	1471	0.94	294462	49774 ± 6292	2860 ± 130	1.94 ± 0.09	0.48 ± 0.02	0.14 ± 0.02	18 ± 3
2	489119	2126	0.74	405784	83334 ± 6234	4735 ± 143	2.23 ± 0.07	0.33 ± 0.01	0.17 ± 0.01	18 ± 2
3	232658	910	0.55	199873	32785 ± 6046	1740 ± 99	1.91 ± 0.11	0.29 ± 0.02	0.14 ± 0.03	19 ± 3
4	93445	595	0.86	76134	17311 ± 1495	903 ± 60	1.52 ± 0.10	0.57 ± 0.04	0.19 ± 0.02	20 ± 2
5	330488	1142	0.68	283494	46994 ± 5334	2419 ± 170	2.12 ± 0.15	0.32 ± 0.02	0.14 ± 0.02	20 ± 2
6	378666	924	0.56	344169	34497 ± 4194	1448 ± 248	1.57 ± 0.27	0.37 ± 0.06	0.09 ± 0.01	22 ± 3
7	302210	855	0.33	271371	30839 ± 6166	1490 ± 116	1.74 ± 0.14	0.19 ± 0.02	0.10 ± 0.02	21 ± 3
8	126101	1175	0.54	89108	36992 ± 2469	1583 ± 26	1.35 ± 0.02	0.40 ± 0.01	0.29 ± 0.02	23 ± 3
9	355743	1420	0.46	299779	55965 ± 8114	2001 ± 53	1.41 ± 0.04	0.33 ± 0.01	0.16 ± 0.02	23 ± 4

442

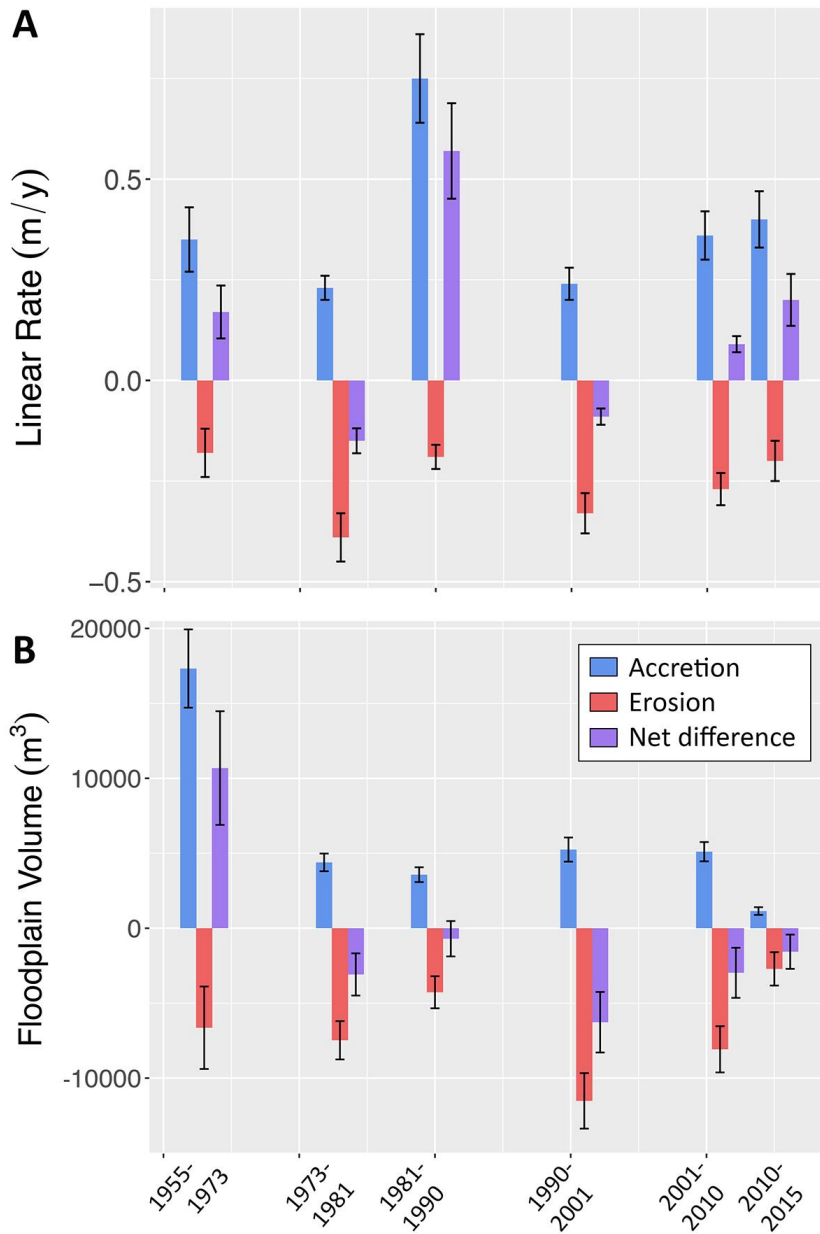
443 Valley slope ranged from 0.33% to 0.94% along each of the 9 delineated study reaches  
444 with a mean of  $0.36 \pm 0.19\%$  (SD; Table 2). Mean valley confinement for the time period was  
445  $0.16 \pm 0.02 \text{ m}^2/\text{m}^2$  (mean  $\pm$  SD). Study reach 8 is the most confined reach ( $C_v = 0.29 \pm 0.02$ ) and  
446 is located toward the downstream end of the 11-km long study segment where the tributary  
447 alluvial fan from Brush Creek constricts the East River valley. Reach sinuosity (P) averaged  
448 over the time period is also lowest in study reach 8 at  $1.35 \pm 0.02 \text{ m/m}$  (Figure 2). The highest  
449 reach mean sinuosity ( $P = 2.23 \pm 0.07$ ) occurred in reach 2, which is moderately confined ( $C_v =$   
450  $0.17 \pm 0.01$ ) (Table 2).

451 Averaged over all time periods, channel width generally increased from upstream  
452 reaches to downstream reaches (Table 2). Although the channel mean width fluctuated with  
453 intervals of widening followed by narrowing, there was a net overall decrease over the 60-year  
454 time period. The average channel width for the entire 11-km long study segment decreased  
455 from a high of  $25 \pm 2 \text{ m}$  in 1955 to a minimum of  $17 \pm 1 \text{ m}$  in 2015. The greatest width reduction  
456 ( $\sim 5 \text{ m}$ ) occurred between 1955 and 1973, but a substantial decrease of  $>4 \text{ m}$  also occurred  
457 during two time periods between 2001 and 2015.

#### 458 *4.2 Channel Migration and Floodplain Area*

459 The net balance between total area of eroded and accreted floodplain by the East River  
460 varied over the six time periods, with estimated accretion greater than erosion in four out of six  
461 time periods (Table 3). Over the entire 60-year period accretion exceeded erosion by  $120,036 \pm$   
462  $43,973 \text{ m}^2$ , equal to 5.3% of the total area of the valley bottom. This accretion total includes the  
463 area of 21 abandoned channels arising from meander bend cutoffs. The highest rate of change  
464 in floodplain sediment balance occurred from 1983-1990 with a mean accretion rate outpacing  
465 erosion by a factor of four (Table 3; Figure 2). There was an observed decrease in channel  
466 width during this period, followed by a period dominated by erosion and channel widening. The

467 period between 1973 and 1983 was dominated by the largest erosion rates observed in this  
468 study, and was accompanied by an observed increase in channel width (Table 1, 3; Figure 2A).



469  
470 **Figure 2** Bar plots of estimated accretion, erosion, and net difference (accretion minus erosion)  
471 in linear rates along the entire 11-km long study segment (A) and volume of floodplain fine  
472 sediment along the upper 2 km, intensive study reach (B) during each time period examined  
473 over the 60 year study period.

474  
475

**Table 3.** Area accreted and eroded across the entire 11-km long study segment and hydrologic flow indices on the East River during the six time periods of the study.

	1955-1973	1973-1983	1983-1990	1990-2001	2001-2011	2011-2015	Mean	Total
Duration (years)	18 ± 0.3	10 ± 0.3	7 ± 0.3	11 ± 0.3	10 ± 0.3	4 ± 0.3	10 ± 0.3	60 ± 0.8
Accretion (m <sup>2</sup> )	125529 ± 27774	45276 ± 6339	99194 ± 13887	50226 ± 8036	70686 ± 9189	30156 ± 7539	70178 ± 12127	421067 ± 34789
Erosion (m <sup>2</sup> )	-64915 ± 25388	-74670 ± 12694	-24569 ± 6142	-69550 ± 11128	-52358 ± 9948	-14969 ± 6137	-50172 ± 11906	-301031 ± 33224
Net Change (m <sup>2</sup> )	60614 ± 37629	-29394 ± 14188	74625 ± 15185	-19324 ± 13726	18328 ± 13543	15187 ± 9721	20006 ± 17332	120036 ± 48106
Accretion Rate (m <sup>2</sup> y <sup>-1</sup> )	6974 ± 1548	4528 ± 652	14171 ± 2095	4566 ± 744	7069 ± 949	7539 ± 1987	7474 ± 1329	44846 ± 3551
Erosion Rate (m <sup>2</sup> y <sup>-1</sup> )	-3606 ± 1412	-7467 ± 1294	-3510 ± 893	-6323 ± 1030	-5236 ± 1010	-3742 ± 1566	-4981 ± 1201	-29884 ± 2999
Mean linear Accretion Rate (m y <sup>-1</sup> )	0.347 ± 0.077	0.235 ± 0.034	0.754 ± 0.111	0.242 ± 0.039	0.365 ± 0.049	0.401 ± 0.106	0.390 ± 0.069	2.343 ± 0.186
Mean Linear Erosion Rate (m y <sup>-1</sup> )	-0.180 ± 0.070	-0.387 ± 0.067	-0.187 ± 0.048	-0.334 ± 0.054	-0.270 ± 0.052	-0.199 ± 0.083	-0.259 ± 0.062	-1.557 ± 0.156
Mean Day of Peak Flow	152.7	162	156.3	151.5	147	155.3	154.13 ± 5.06	
Mean Peak Flow (m <sup>3</sup> s <sup>-1</sup> )	11.84	11.6	12.9	12.35	11.31	10.15	11.69 ± 0.94	
Max Peak Flow (m <sup>3</sup> s <sup>-1</sup> )	22.56	18.32	21.86	23.74	16.02	15.49	19.67 ± 3.53	
Mean Bankfull Duration (days)	31.3	38.1	41	36.1	29.3	25.5	33.55 ± 5.84	
Max Bankfull Duration (days)	61	48	64	63	47	31	52.33 ± 12.86	
Mean Days Above Bankfull Flow	20.3	24	22.6	23.8	18.5	12.8	20.33 ± 4.26	
Max Days Above Bankfull Flow	59	46	62	56	47	30	50.00 ± 11.71	
Mean Duration Above Baseflow (days)	215.5	218	255.1	230.9	263	278.5	243.50 ± 25.82	
Max Duration Above Baseflow (days)	362	331	364	305	364	349	345.83 ± 23.74	
Mean Days Above Baseflow	232.1	217.8	266.7	243.9	259.8	245.5	244.30 ± 17.86	
Max Days Above Baseflow	281	261	362	275	316	272	294.50 ± 37.97	
Mean Days Since Bankfull Flow	267	327.1	349.6	261.3	345.3	455.3	334.27 ± 70.58	
Max Days Since Bankfull Flow	925	904	935	579	944	901	864.67 ± 140.96	
Mean Day Baseflow Ends	280.2	288.6	304	305.3	291	321.3	298.40 ± 14.73	
Mean Day Bankfull Flow Ends	173.3	181.9	176.8	172.7	170.3	173	174.67 ± 4.11	
Mean No. Peaks Above Bankfull		1.9	2	1.8	1.4	0.5	1.52 ± 0.61	
Maximum No. Peaks Above Bankfull	3	4	5	4	3	1	3.33 ± 1.37	
Mean Total Recession Slope (m <sup>3</sup> s <sup>-1</sup> day <sup>-1</sup> )	0.094	0.087	0.083	0.077	0.079	0.056	0.08 ± 0.01	
Max Total Recession Slope (m <sup>3</sup> s <sup>-1</sup> day <sup>-1</sup> )	0.149	0.142	0.097	0.13	0.124	0.085	0.12 ± 0.03	
Mean Bankfull Recession Slope (m <sup>3</sup> s <sup>-1</sup> day <sup>-1</sup> )	0.076	0.064	0.059	0.058	0.066	0.047	0.06 ± 0.01	
Max Bankfull Recession Slope (m <sup>3</sup> s <sup>-1</sup> day <sup>-1</sup> )	0.12	0.086	0.082	0.075	0.091	0.05	0.08 ± 0.02	
Mean Total Annual Volume (km <sup>3</sup> )	0.060	0.059	0.067	0.065	0.057	0.051	0.060 ± 0.006	
Max Total Annual Volume (km <sup>3</sup> )	0.109	0.081	0.103	0.110	0.087	0.077	0.094 ± 0.015	
Mean Bankfull Volume (km <sup>3</sup> )	0.027	0.034	0.037	0.033	0.027	0.024	0.031 ± 0.005	
Max Bankfull Volume (km <sup>3</sup> )	0.074	0.047	0.072	0.073	0.050	0.031	0.058 ± 0.018	

480 Measured total depths of floodplain fine sediment above gravel and bedrock across the  
481 floodplain ranged from 0 to 141 cm with a mean value of  $41 \pm 25$  cm (Table S2). A reach-based  
482 average migration rate of  $0.24 \pm 0.05$  m  $y^{-1}$  resulted in a mean migration distance of  $\sim 10.0 \pm 2.1$  m  
483 along the probe transects for the entire period between 1973-2015 (Table S2). Error presented  
484 in the values above were propagated from the mean standard deviation of the estimated mean  
485 migration rates derived from the SCREAM analysis. Using our estimated vertical accretion rates  
486 at each point, we estimated an average vertical accretion rate of  $3.3 \pm 0.3$  cm  $y^{-1}$  among all points  
487 within the closest 10 m from the channel. The best performing multiple linear regression model  
488 explains  $\sim 60\%$  of the variability in vertical accretion rates ( $r^2=0.60$ ,  $p<0.001$ ) using distance from  
489 the channel, relative elevation from the channel, valley confinement, local channel slope (all with  
490  $p<0.001$ ), and whether the survey point was on the inside of a bend ( $p=0.023$ ; Table S4). A cell-  
491 by-cell multiple linear regression model of estimates of vertical accretion rates ( $r_{va}$ ) across the  
492 floodplain (Figure S2) for each time period was developed based on distance from the channel  
493 ( $p<0.001$ ) and relative elevation from the channel ( $p<0.001$ ). This model, readily parameterized  
494 from remotely-sensed data, explained  $\sim 54\%$  of the variability in long-term vertical accretion  
495 rates over the 42-year time period between 1973 and 2015 ( $r^2=0.54$ ,  $p<0.001$ ) such that more  
496 deposition occurred closer to the channel and at lower elevations across the floodplain (Figure  
497 S2).

#### 498 *4.4 Eroded and Accreted Sediment Volumes*

499 Estimated volumes of eroded and accreted sediment from the upper 2 km, intensive  
500 study reach were used to examine changes in volumes of floodplain sediment over the six time  
501 periods. Sediment input to and output from the floodplain during the six time periods ranged  
502 from  $1145 \pm 258$  to  $17,324 \pm 2610$  m<sup>3</sup> and  $2713 \pm 113$  to  $11519 \pm 1851$  m<sup>3</sup>, respectively (Table 4).  
503 The difference between accreted and eroded volumes represent the net sediment change,

504 which ranged from  $-6273 \pm 2018$  (where negative values indicate net erosion) to  $10,683 \pm 3792$   
505  $\text{m}^3$  of sediment (Figure 2B, Table 4).

506 Estimated eroded volume exceeded accreted volume in all but one (i.e., 1955-1973) of  
507 the six periods examined in this study resulting in a net loss of sediment over the total 60-year  
508 time period between 1955 and 2015 (Figure 2B). Although the resulting estimated sediment  
509 balance after 60 years was a net loss of  $3919 \text{ m}^3$  across the floodplain during the 60-year  
510 period, this net difference falls within the error of the estimate (i.e.,  $\pm 5091 \text{ m}^3$ ) and suggest  
511 closure of the sediment budget.

512 **Table 4.** Floodplain area and sediment volume eroded, accreted, and the net change between accretion and erosion along the  
 513 upper 2 km, intensive study reach.

	1955 - 1973	1973 - 1983	1983 - 1990	1990 - 2001	2001 - 2011	2011 - 2015	Total
Duration (y)	18 ± 0.3	10 ± 0.3	7 ± 0.3	11 ± 0.3	10 ± 0.3	4 ± 0.3	
Area eroded (m <sup>2</sup> ) <sup>a</sup>	12228 ± 5060	12428 ± 2113	7341 ± 1835	16774 ± 2684	13317 ± 2530	3752 ± 1538	
Mean Depth of Eroded bank material (m)	0.54 ± 0.01	0.60 ± 0.01	0.58 ± 0.01	0.69 ± 0.01	0.61 ± 0.01	0.72 ± 0.01	
<b>Volume Eroded (m<sup>3</sup>)<sup>b</sup></b>	<b>-6640 ± 2751</b>	<b>-7476 ± 1277</b>	<b>-4272 ± 1071</b>	<b>-11519 ± 1851</b>	<b>-8080 ± 1541</b>	<b>-2713 ± 1113</b>	<b>-40700 ± 4169</b>
Mean erosion rate (m <sup>3</sup> /y)	-369 ± 153	-748 ± 130	-610 ± 155	-1047 ± 171	-808 ± 156	-678 ± 283	
Mean bank area erosion rate (m <sup>2</sup> /y) <sup>c</sup>	-0.02 ± 0.01	-0.04 ± 0.01	-0.03 ± 0.01	-0.06 ± 0.01	-0.04 ± 0.01	-0.04 ± 0.02	
Point bar area of accretion from (m <sup>2</sup> ) <sup>d</sup>	28392 ± 4356	12391 ± 1735	14534 ± 2035	13612 ± 2178	14493 ± 1884	7403 ± 1851	
Mean vertical accretion within eroded areas (m) <sup>e</sup>	0.59 ± 0.01	0.33 ± 0.01	0.23 ± 0.01	0.36 ± 0.01	0.33 ± 0.01	0.13 ± 0.01	
Estimated accretion along point bars (m <sup>3</sup> ) <sup>f</sup>	16865 ± 2608	4089 ± 587	3357 ± 493	4941 ± 803	4783 ± 640	977 ± 255	
Overbank deposition (m <sup>3</sup> ) <sup>g</sup>	459 ± 92	302 ± 61	213 ± 44	305 ± 62	322 ± 66	168 ± 36	
<b>Total volume accreted (m<sup>3</sup>)<sup>h</sup></b>	<b>17324 ± 2610</b>	<b>4391 ± 590</b>	<b>3570 ± 495</b>	<b>5246 ± 806</b>	<b>5105 ± 643</b>	<b>1145 ± 258</b>	<b>36780 ± 2921</b>
Mean accretion rate (m <sup>3</sup> /y)	962.43 ± 145.87	439.11 ± 60.462	509.97 ± 73.961	476.9 ± 74.406	510.54 ± 66.126	286.16 ± 67.924	
<b>Net volume (m<sup>3</sup>)</b>	<b>10684 ± 3792</b>	<b>-3085 ± 1407</b>	<b>-702 ± 1179</b>	<b>-6273 ± 2018</b>	<b>-2975 ± 1670</b>	<b>-1568 ± 1142</b>	<b>-3920 ± 5091</b>

<sup>a</sup> Area eroded from banks estimated by SCREAM (Rowland et al., 2016)

<sup>b</sup> Volume calculated directly in GIS

<sup>c</sup> Mean vertical area of bank eroded estimated as the mean erosion rate divided by the total channel length

<sup>d</sup> Area of point bar accretion estimated by SCREAM

<sup>e</sup> Vertical accretion estimated as the product of the duration of each time period and accretion rates derived from measured probe transect of fine floodplain sediment depths described in section 3.3

<sup>f</sup> Volume of accretion estimated as the product of accreted areas identified by SCREAM and mean vertical accretion rates

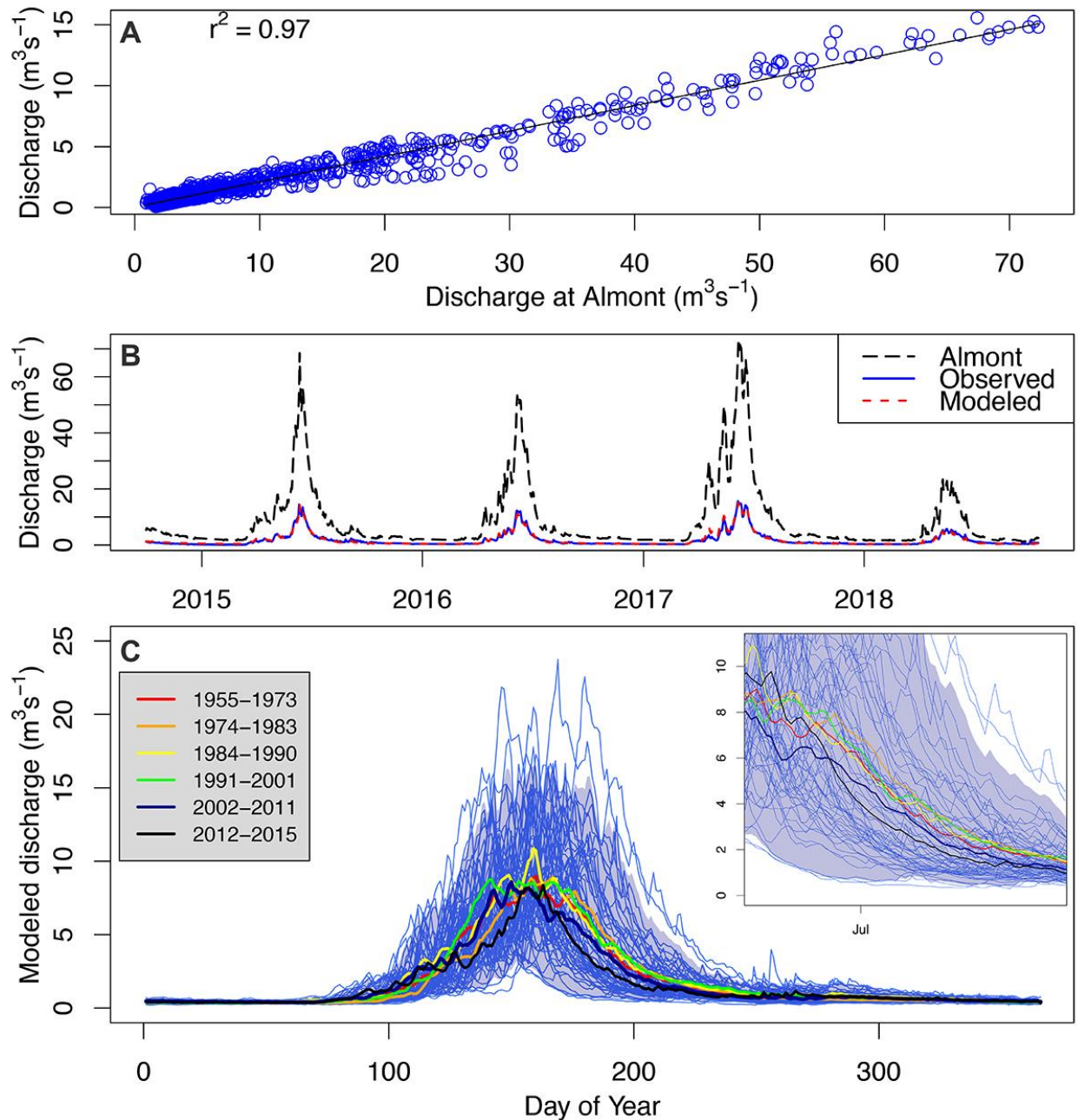
<sup>g</sup> Estimates of overbank deposition derived from the regression model described in section 3.4 in which vertical accretion rates of each DEM cell were summed and the total was multiplied by the number of years in each time period.

<sup>h</sup> The sum of accreted volumes from point bars and overbank deposition

514  
515  
516  
517  
518  
519  
520  
521  
522

523 *4.5 Hydrologic linkages with floodplain sediment*

524           Although each of the six time periods studied do not span equal time intervals, average  
525 flow conditions were similar for most time periods, with one drier and one wetter period (Figure  
526 3C; Table 3). Peak discharge typically occurred within the second half of May, throughout June,  
527 and secondary peaks during high flow years sometimes occurred at the beginning of May and  
528 the beginning of July (Figure 3C; Table S3). The mean annual and peak discharges within the  
529 reach averaged 1.9 and 12.1 m<sup>3</sup> s<sup>-1</sup> respectively from 1935 to 2017. The period between 2012  
530 and 2015 was a relatively dry interval with the least average number of days above both  
531 baseflow conditions and bankfull stage, the least mean and max annual volume of flow, the  
532 lowest maximum and mean peak flow, and the lowest mean and maximum total recession slope  
533 of all time periods (Table 3). Conversely, the period between 1991 and 2001 was a relatively  
534 wet interval with the highest mean duration above baseflow, the highest maximum peak flow, a  
535 relatively high total annual volume of discharge, and a relatively high number of peaks above  
536 bankfull flow conditions.



537

538 **Figure 3** Modeled discharge at the East River study site and Almont stream gauge. (A) Linear  
 539 regression between measured discharge at Almont and the study site ( $r^2=0.97$ ), (B) discharge  
 540 at the two sites for the 2015 to 2018 water years including modeled discharge at the study site  
 541 based on the regression analysis (NSE=0.97). (C) Modeled annual hydrographs for the 60-year  
 542 study period (1955-2015) and an inset closeup of the hydrograph recession limbs. Thin, light  
 543 blue lines are annual hydrographs, the shaded blue area is the 95% confidence interval, and  
 544 colored lines represent mean hydrographs for the six time periods.

545

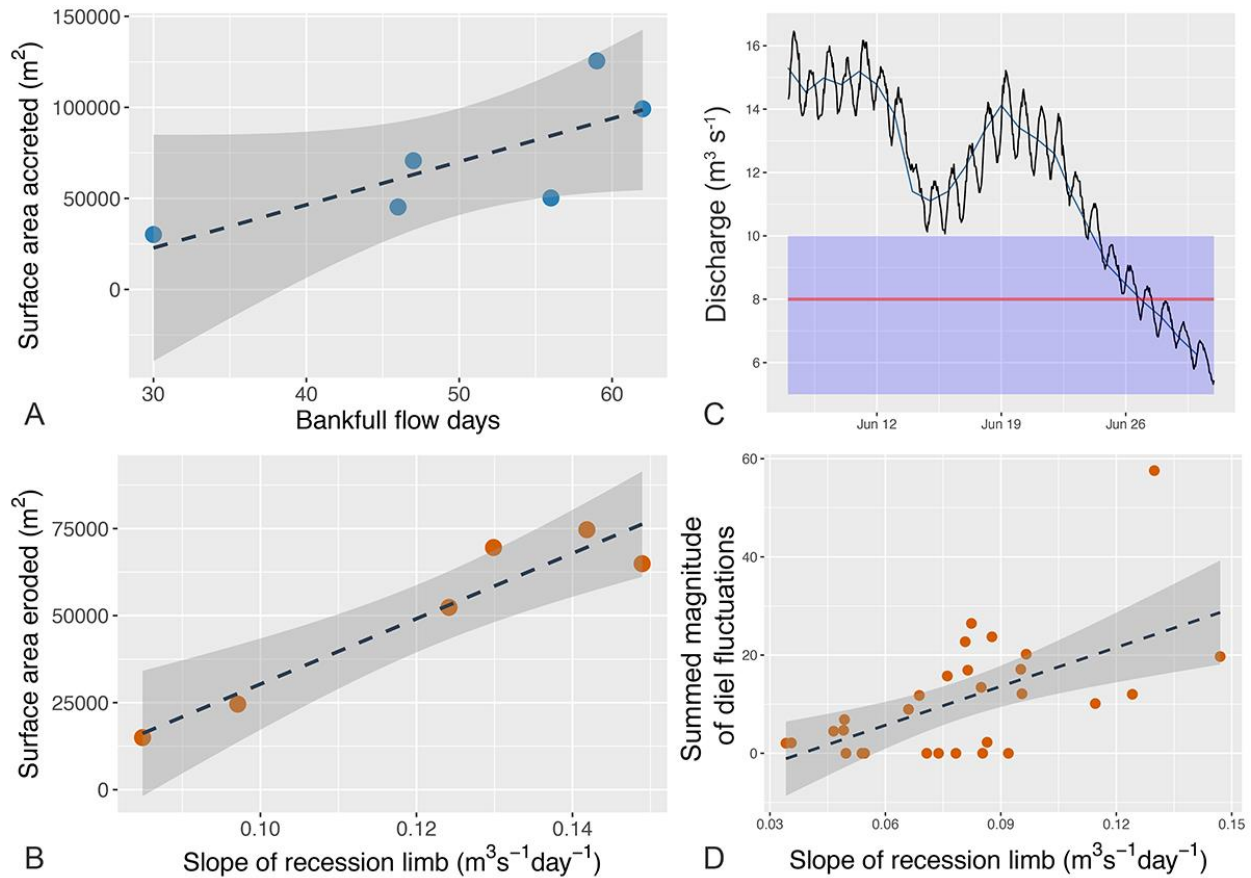
546 Multiple stepwise linear regression indicates that floodplain sediment exchange along the nine  
547 study reaches during the six time intervals are explained primarily by the hydrologic conditions  
548 and the sinuosity of the channel at the beginning of each period (Table S5). Laterally accreted  
549 area ( $A_L$ ) with the appropriate power transformation ( $\lambda = 0.26263$ ) was most significantly  
550 influenced by a positive correlation with sinuosity ( $P$ ;  $p < 0.0001$ ), the maximum number of days  
551 above the reference baseflow condition ( $D_{base}$ ;  $p < 0.05$ ), the mean channel width ( $w$ ) of the  
552 study reach ( $p < 0.05$ , and the maximum bankfull recession limb slope ( $R_{bf}$ ) ( $r^2 = 0.55$ ,  $p < 0.1$ ).

$$553 \quad A_L^{0.26263} = -6.591 + 0.015D_{base} + 3.142P + 0.240w + 21.432 R_{bf} \quad (2)$$

554 The area of floodplain erosion ( $E_A$ ) across the nine study reaches over the 6 periods was best  
555 explained by a positive correlation with the maximum total recession limb slope from peak to  
556 baseflow conditions ( $R_{total}$ ;  $p < 0.0001$ ) and sinuosity ( $P$ ;  $p < 0.001$ ) and a negative correlation with  
557 the maximum time between the first and last day flow exceeded baseflow ( $T_{base}$ ) ( $r^2 = 0.59$ ,  $p <$   
558  $0.05$ ; Table S5).

$$559 \quad E_A^{0.10101} = 2.058 + 5.190 R_{total} + 0.157 P - 0.002 T_{base} \quad (3)$$

560 Because our multiple linear regression analyses explained only about 55-60% of the  
561 variability in observed area of accretion and erosion and many variables examined require  
562 detailed analysis of imagery and lidar, we examined an additional simpler regression model  
563 using only the most significant variables that describe hydrologic conditions. Because sinuosity  
564 across the entire 11-km long study segment remains relatively constant and channel width  
565 similarly adjusts on a decadal time scale (Tables 1, 2), channel morphology maintains a quasi-  
566 steady state over the course of the study period. This means that changes in erosion and  
567 accretion may be explained by hydrology alone on a larger scale, under the primary  
568 assumptions of consistent sediment supply proportional to discharge. Such an approach is  
569 appealing because changes in hydrology are more easily measured by stream gauging, which  
570 allows predictions using future projections in climate variability.



571

572 **Figure 4** Linear regression of eroded and accreted areas and diel fluctuations. Each point  
 573 represents each of the six time intervals for which data from all nine study reaches are  
 574 combined. (A) The number of days that flow exceeded bankfull flow conditions is a significant  
 575 predictor of accreted area ( $r^2=0.59$ ,  $p = 0.074$ ) and (B) the maximum slope within each time  
 576 frame of the total recession limb from peak to baseflow is a significant predictor of eroded area  
 577 ( $r^2=0.91$ ,  $p = 0.003$ ). (C) Fluctuations in discharge in response to snowmelt during daily warming  
 578 and cooling cycles can exceed  $3 \text{ m}^3 \text{ s}^{-1}$ , but do not show a strong correlation with the slope of  
 579 the recession limb ( $r^2=0.29$ ) (D). In A, B, and D, the dashed lines represent the linear regression  
 580 model and the gray shaded area represents the 95% confidence intervals. In C the red line  
 581 represents the bankfull flow stage and the blue shaded area represents the window in which diel  
 582 fluctuations were examined.

583

584 Our analysis did not show a strong correlation between the maximum slope of the  
 585 recession limb and number of, the summed magnitude, or the mean magnitude of diel  
 586 fluctuations in discharge ( $Q = 8 \text{ m}^3 \text{ s}^{-1}$ ) within the defined bankfull window ( $5 < Q_{\text{bf}} < 12 \text{ m}^3 \text{ s}^{-1}$ ),  
 587 but this topic requires more attention, particularly in snowmelt-dominated system that could  
 588 change under a shifting climate.

589

590 Multiple linear regression to examine the role of hydrologic drivers alone on floodplain  
591 sediment dynamics across the entire 11-km long study segment – in contrast to the regression  
592 analyses that examined morphologic variables in addition to hydrologic variable across the nine  
593 study reaches – identified similar variables as the most significant predictors of erosion and  
594 accretion found in those other regression analyses. Examining hydrology alone, lateral accretion  
595 across the entire 11-km long study segment was best explained by the maximum number of  
596 days flow was above bankfull stage ( $r^2 = 0.59$ ,  $p = 0.074$ ; Figure 4A). The most significant  
597 hydrologic variable for explaining the area of erosion along the 11-km long study segment was  
598 the mean slope of the hydrograph recession from peak to baseflow conditions ( $r^2 = 0.91$ ,  $p =$   
599  $0.003$ ; Figure 4B).

#### 600 **4. Discussion**

##### 601 4.1 Temporal variability of channel widening and narrowing

602 On the East River, we observed that progressive increases in sinuosity were truncated  
603 by channel cutoffs. This autocyclic pattern was punctuated with alternating periods of channel  
604 narrowing and widening, which occur in tandem to maintain a relatively stable sinuosity on the  
605 order of decades over the 11-km long study segment (Table 1; Figure 2A). The period between  
606 2012 and 2015 is the only exception in this alternating pattern and may have arisen from a  
607 reduction in erosion associated with the lowest maximum total recession slope in the study  
608 period. Channel reaches are more likely to experience deposition and lateral accretion following  
609 channel widening as flows spread out, flow depth decreases, and competency to transport  
610 sediment declines. Germination of riparian species during high flows stabilize point bars,  
611 resulting in channel narrowing that can force flow to outer banks and encourage subsequent  
612 bank erosion (Merritt & Cooper, 2000; Zen et al., 2017). This type of feedback appears to have  
613 occurred on the East River where narrowing induced increases in flow depth, velocity, and

614 boundary shear stress would have driven bank undercutting of the fine sediment facilitating  
615 cantilever failure of saturated banks. Thus a window of opportunity for vegetation establishment  
616 on bars (Balke et al., 2014; Caponi et al., 2019) followed by a substantial duration of overbank  
617 flow that undercut banks would facilitate such a cyclical pattern. Propagation of cyclical patterns  
618 of narrowing and widening have commonly been observed in the field (Hooke, 2008; Cantelli et  
619 al., 2004) and modeled to match field observations after channel avulsions or bifurcations  
620 (Kleinhans et al., 2011) like the chute cutoffs that occur on the East River.

621

#### 622 4.2 Balancing the floodplain sediment budget and accretion

623 Of all the sources of possible error (i.e., lateral erosion and accretion, interpolation of  
624 sediment volumes across the channel, and estimates of floodplain vertical accretion), vertical  
625 accretion represents the most uncertain component of the sediment budget. Estimates of  
626 deposition along point bars and areas adjacent to the channel are relatively robust because they  
627 are based on measured long-term average deposition rates, but overbank deposition across the  
628 entire floodplain based on our multiple linear regression contains uncertainty that cannot fully be  
629 quantified. Our approach used a bulk depth of total sediment deposited over the 42 year period  
630 between 1973 and 2015, which does not account for deposition and subsequent erosion  
631 occurring at time scales shorter than our averaging.

632 Our regression analysis of lateral accretion does however examine hydrologic indices  
633 that can incorporate the influences of annual events into the time period in which those events  
634 occur (e.g., maximum bankfull volume, maximum cumulative days since last bankfull flow). The  
635 duration between flow events has been referred to as the “window of opportunity” for riparian  
636 vegetation to germinate and has been shown to be highly correlated with point bar accretion  
637 (Balke et al., 2014; Zen et al., 2017; Caponi et al., 2019). Correlation were low between lateral  
638 accretion and the maximum ( $r=0.232$ ) and mean ( $r=-0.346$ ) cumulative days since the last  
639 bankfull flow and although the latter was higher, our results indicate a negative correlation

640 (Table S6). These variables were also eliminated for consideration in the optimal stepwise linear  
641 regression model because of cross correlation ( $r = -0.79$ ) with the most significant hydrologic  
642 variable in the regression analysis, duration of overbank flow exceeding bankfull stage.

643 Our results linking (1) duration of overbank flows to lateral accretion and (2) distance  
644 from the channel and relative elevation with overbank deposition support published research  
645 that documents overbank deposition as a function of the duration of inundation and distance  
646 from the channel (Asselman & Middelkoop, 1995; Hupp et al., 2008; G. Day et al., 2008).

647

#### 648 4.3 *Linkages between hydrology and observed bank erosion*

649 Although the study presented here does not examine annual trends, our multiple  
650 regression analysis results of nine study reaches and the simple relationship in Figure 4B  
651 suggests that the slope of the peak annual recession limb is strongly linked to the occurrence of  
652 bank erosion on the East River. While sinuosity and the maximum duration between the first  
653 and last day of flow exceeding baseflow conditions are also significant predictors in the multiple  
654 linear regression analysis ( $p < 0.01$ ), the recession limb slope has a higher significance  
655 ( $p < 0.0001$ ). Although the volume of discharge above bankfull flow has been shown to be linked  
656 to erosion (Surian, et al., 2015), this variable was eliminated from the analysis as a potential  
657 predictor because of a strong correlation with the mean number of bankfull days ( $r = 0.98$ ). Other  
658 variables eliminated from consideration as predictors for erosion because of high correlation  
659 with the maximum total recession limb include variants of: the duration of baseflow, the bankfull  
660 slope of the recession limb, and the cumulative number of days since the last bankfull flow.

661 The importance of the recession limb slope is emphasized by the fact that the maximum  
662 total recession slope alone explains 91% of the variability in bank erosion when considering the  
663 entire 11-km long study segment without separation into the nine study reaches. Past work by  
664 Pizzuto (1994) in a snowmelt dominated system determined that elevated discharge for

665 approximately 7 days on the Powder River, Montana suggested a steep recession limb in 1978  
666 may have been partially responsible for observed bank erosion on the order of 30% of the  
667 channel width. Temporal resolution of aerial imagery does not provide the frequency needed to  
668 examine past erosion on annual time scales on the East River. Hooke (1979) outlined a similar  
669 challenge when examining the connection between bank erosion and hydrologic flow conditions  
670 in temperate systems, because the study lacked the temporal resolution necessary to examine  
671 the role of the recession limb in the observed rainfall-induced storm hydrograph peaks. The role  
672 of the recession limb as a mechanism for bank erosion, however, likely varies substantially  
673 between the temperate stormy system examined by Hooke and snowmelt-dominated discharge  
674 of the East River.

675         Several mechanisms for river bank failures have been identified in prior research, as  
676 described briefly in the introduction, but findings presented here that link flow conditions to  
677 erosion may include a combination of mechanisms. On the East River, we observed that high  
678 flows eroded underlying fluvial gravels resulting in planar cantilever failures of the fine grained  
679 upper portion of the bank (Figure 1D, S1). Bank failures as a result of changes in river stage  
680 may be triggered by a loss of confining pressure or slip failures resulting from positive pore  
681 pressure, where slow drainage in saturated overlying banks of fine sediment cannot drain fast  
682 enough to keep pace with the decline in stage (Rinaldi & Casagli, 1999). Positive pore pressure  
683 is likely the case in stormy systems that experience flash floods with dramatic changes in  
684 discharge occurring over the course of a single day or several hours, but could likely play a  
685 partial role in bank erosion on the East River.

686         Shifting oblique directions in subsurface hydraulic gradient observed on the East River  
687 (Malenda et al., 2019), could change the magnitude and direction of confining pressure on the  
688 outside of river bends where erosion occurs and shifts hyporheic flow toward apposing meander  
689 bends. This change in hydraulic gradient could produce a positive pore pressure along banks  
690 with a seepage face, triggering bank erosion (Rinaldi & Casagli, 1999; Fox et al., 2007).

691 Although it is possible that some bank failures in the study area have been triggered by positive  
692 pore pressure, these types of failures often occur along much higher banks (>4m) composed of  
693 heterogeneous bank material, and slump scarps commonly provide evidence of occurrence  
694 (Simon et al., 2000; Langendoen & Simon, 2008; S. S. Day et al., 2013b). Slumps scarps are  
695 not observed on the East River, and cantilevers failures are the primary mechanism of bank  
696 failure.

697 Loss in confining pressure, provides a conceptual explanation for the link between  
698 observed cantilever failures and the slope of the recession limb in our analysis. Following  
699 undercutting during flows at or exceeding bankfull discharge, the gradual decline in flow stage  
700 occurring over the course of days to weeks and characteristic of snowmelt-dominated systems  
701 is likely to allow silt-dominated soils to drain so that undercut banks are no longer fully saturated  
702 (Figure 4). The loss of supporting pressure with declining stage can result in tension cracks of  
703 undercut banks that trigger bank failure (Rinaldi & Casagli, 1999). These cracks can be  
704 exacerbated by the weight of nearly saturated banks and repeat loss of supporting pressure  
705 from large diel fluctuations in discharge ( $2$  to  $5 \text{ m}^3\text{s}^{-1}$ ) during peak flow recessions on the East  
706 River near bankfull stage ( $\sim 8 \text{ m}^3\text{s}^{-1}$ ; Figure 4C). These rapid changes in discharge ( $Q$ ) equate to  
707 daily changes in flow depth ( $d$ ) of approximately 20 to 30 cm at the gauging station which has  
708 an approximate bankfull width ( $w$ ) of 14 m. Our analysis of diel fluctuations on an hourly time  
709 step from using USGS gage data from 1988 to 2018, however, does not show a strong  
710 correlation with the slope of the recession limb (Figure 4D), but this possible mechanism  
711 requires additional attention.

712

#### 713 *4.4 Influence of shifting hydrologic regimes on floodplain sediment fluxes*

714 Observed increases in erosion linked to the total slope of the annual recession limb  
715 along the snowmelt-dominated East River in CO are likely to exist in other snowmelt-dominated  
716 systems that constitute a majority of rivers in the western USA (Li et al., 2017) and rivers above

717 40° latitude globally (Adam et al., 2009). Predicted increase in the frequency and severity of  
718 storms and floods (Bates et al., 2008) could make extreme floods in mountainous regions – like  
719 the one that occurred in the Colorado Front Range in 2013 – more common, which could greatly  
720 alter floodplain sediment dynamics and residence times (Sutfin & Wohl, 2019). Observed  
721 changes in snowpack (Stewart, 2009), upward shifts in the rainfall-snowfall transition (Kampf &  
722 Lefsky, 2016), rapid warming and earlier snowmelt (Clow, 2009), increased rain-on-snow  
723 events, are altering snow-melt dominated hydrographs (Stewart et al., 2004; Clow, 2009; Kampf  
724 & Lefsky, 2016; Praskievicz, 2016; Painter et al., 2018). The coldest snowmelt regimes are  
725 likely to experience increased spring hydrograph peaks, whereas transitional snowmelt regimes  
726 may experience lower spring peaks and more winter peak events (Nijssen et al., 2001). Rain-  
727 on-snow events in winter months could produce hydrograph peaks that exceed spring peaks in  
728 snowmelt dominated systems. Although observations and projections of floods do not indicate  
729 an increase in magnitude across rivers with all types of flow regimes, floods are occurring more  
730 often (Hirsch & Archfield, 2015; Mallakpour & Villarini, 2015), which means more variability and  
731 more frequent recession limbs in otherwise predictable and consistent snowmelt-dominated  
732 systems. These changes would by definition shift otherwise predictable snowmelt dominated  
733 systems to more flashy systems with increased variability and more rapidly rising and receding  
734 limbs, but how changes could influence sediment dynamics are uncertain.

735         The changes in annual average snowpack and timing of snowmelt are poised to change  
736 the variables identified in this study as important for both erosion and accretion, but the direction  
737 of these changes is unknown. If a link between diel fluctuations and recession slope exists in  
738 snowmelt-dominated systems stronger than that presented here, increased frequency of flood  
739 peaks may not result in a substantial increase in bank erosion. However, if the link between the  
740 recession slope and cantilever bank erosion occurs independently of diel fluctuations, increased  
741 frequency and flashiness of flood peaks could equate to a significant increase in bank erosion  
742 and alteration of floodplain sediment budgets. Because our results and other studies have

743 shown a positive correlation between floodplain accretion and the duration of overbank flow  
744 (Asselman & Middelkoop, 1995; Hupp et al., 2008), flashier systems could limit overbank  
745 deposition while encouraging bank erosion.

746

## 747 **Conclusion**

748 Analysis of aerial imagery, aerial lidar data, and field measurements of depth of  
749 floodplain fine sediment suggest that the floodplain sediment budget along the East River study  
750 segment is balanced over the 60-year study period. Empirical relationships between 60 years of  
751 discharge data, channel morphometry of nine study reaches, and observed bank erosion and  
752 accretion suggest that channel sinuosity is a significant factor for both erosion and accretion and  
753 that channel width is a significant factor for the latter. In addition, the maximum slope of the  
754 recession limb from the peak to baseflow and bankfull stage to baseflow as well as the duration  
755 of flow above baseflow and bankfull conditions are significant hydrologic indices correlated with  
756 erosion and accretion. The role of the hydrologic variables becomes more evident when  
757 erosion and accretion are examined across the entire 11-km long study segment, rather than  
758 the nine study reaches. Sixty percent of the variability in accretion is explained by the maximum  
759 number of flow days exceeding bankfull stage and 91% of erosion is explained by the maximum  
760 slope of the annual peak recession limb within each time period. We posit that diel fluctuations  
761 during the annual recession on the order of 25% of the bankfull flow play a role in observed  
762 cantilever failures, but our analysis does not show a strong relationship between recession  
763 slope and diel fluctuations. Projected changes and increased variability in flow regimes of  
764 snowmelt-dominated systems are likely to influence the variables identified here as important for  
765 floodplain sediment dynamics in other regions.

766

## 767 **Acknowledgement:**

768 This work was funded by an Early Career award to Rowland by the Subsurface Biogeochemical  
769 Research Programs within the U.S. Department of Energy Office of Science, Biological and  
770 Environmental Research Program. This material is partially based upon work supported through  
771 the Lawrence Berkeley National Laboratory's Watershed Function Scientific Focus Area  
772 (operated by the University of California) funded by the U.S. Department of Energy (DOE),  
773 Office of Science, Office of Biological and Environmental Research contract DE-AC02-  
774 05CH11231. We thank the Rocky Mountain Biological Research Station for their support and  
775 Meghan King and Anastasia Piliouras for their assistance in the field. All data used for this study  
776 are provided in the manuscript, as supplemental materials, and in Sutfin & Rowland (2019) and  
777 Carroll & Williams (2019). The R code used to extract hydrologic parameters are provided as  
778 supplemental Supporting Information as cited in the text. This manuscript was greatly improved  
779 by comments from two anonymous reviewers and the associate editor.

780

## 781 **References**

- 782 Adam, J. C., Hamlet, A. F., & Lettenmaier, D. P. (2009). Implications of global climate change  
783 for snowmelt hydrology in the twenty-first century. *Hydrological Processes*, 23(7), 962–  
784 972. <https://doi.org/10.1002/hyp.7201>
- 785 Asselman, N. E. M., & Middelkoop, H. (1995). Floodplain sedimentation: Quantities, patterns  
786 and processes. *Earth Surface Processes and Landforms*, 20(6), 481–499.  
787 <https://doi.org/10.1002/esp.3290200602>
- 788 Balke, T., Herman, P. M. J., & Bouma, T. J. (2014). Critical transitions in disturbance-driven  
789 ecosystems: identifying Windows of Opportunity for recovery. *Journal of Ecology*,  
790 102(3), 700–708. <https://doi.org/10.1111/1365-2745.12241>
- 791 Bates, B., Kundzewicz, Z. W., Wu, S., Burkett, V., Doell, P., Gwary, D., et al. (2008). *Climate*  
792 *Change and Water. Technical Paper of the Intergovernmental Panel on Climate Change.*

793 Belmont, P., Gran, K. B., Schottler, S. P., Wilcock, P. R., Day, S. S., Jennings, C., et al. (2011).  
794 Large Shift in Source of Fine Sediment in the Upper Mississippi River. *Environmental*  
795 *Science & Technology*, 45(20), 8804–8810. <https://doi.org/10.1021/es2019109>

796 Benjankar, R., Burke, M., Yager, E., Tonina, D., Egger, G., Rood, S. B., & Merz, N. (2014).  
797 Development of a spatially-distributed hydroecological model to simulate cottonwood  
798 seedling recruitment along rivers. *Journal of Environmental Management*, 145, 277–288.  
799 <https://doi.org/10.1016/j.jenvman.2014.06.027>

800 Bogoni, M., Putti, M., & Lanzoni, S. (2017). Modeling meander morphodynamics over self-  
801 formed heterogeneous floodplains. *Water Resources Research*, 53(6), 5137–5157.  
802 <https://doi.org/10.1002/2017WR020726>

803 Cantelli, A., Paola, C., & Parker, G. (2004). Experiments on upstream-migrating erosional  
804 narrowing and widening of an incisional channel caused by dam removal. *Water*  
805 *Resources Research*, 40(3). <https://doi.org/10.1029/2003WR002940>

806 Caponi, F., Koch, A., Bertoldi, W., Vetsch, D. F., & Siviglia, A. (2019). When Does Vegetation  
807 Establish on Gravel Bars? Observations and Modeling in the Alpine Rhine River.  
808 *Frontiers in Environmental Science*, 7. <https://doi.org/10.3389/fenvs.2019.00124>

809 Carroll, R., & Williams, K. (2019). Discharge data collected within the East River for the  
810 Lawrence Berkeley National Laboratory Watershed Function Science Focus Area (water  
811 years 2015-2018), Watershed Function SFA. *EES-DIVE: Deep Insight for Earth Science*.  
812 <http://dx.doi.org/10.21952/WTR/1495380>

813 Clow, D. W. (2009). Changes in the Timing of Snowmelt and Streamflow in Colorado: A  
814 Response to Recent Warming. *Journal of Climate*, 23(9), 2293–2306.  
815 <https://doi.org/10.1175/2009JCLI2951.1>

816 Darby, S. E., Rinaldi, M., & Dapporto, S. (2007). Coupled simulations of fluvial erosion and  
817 mass wasting for cohesive river banks. *Journal of Geophysical Research: Earth Surface*,  
818 *112*(F3). <https://doi.org/10.1029/2006JF000722>

819 Day, G., Dietrich, W. E., Rowland, J. C., & Marshall, A. (2008). The depositional web on the  
820 floodplain of the Fly River, Papua New Guinea. *Journal of Geophysical Research: Earth*  
821 *Surface*, *113*. [https://doi.org/10.1029/2006JF000622@10.1002/\(ISSN\)2169-](https://doi.org/10.1029/2006JF000622@10.1002/(ISSN)2169-9011.PAPUA1)  
822 [9011.PAPUA1](https://doi.org/10.1002/(ISSN)2169-9011.PAPUA1)

823 Day, S. S., Gran, K. B., Belmont, P., & Wawrzyniec, T. (2013a). Measuring bluff erosion part 1:  
824 terrestrial laser scanning methods for change detection. *Earth Surface Processes and*  
825 *Landforms*, *38*(10), 1055–1067. <https://doi.org/10.1002/esp.3353>

826 Day, S. S., Gran, K. B., Belmont, P., & Wawrzyniec, T. (2013b). Measuring bluff erosion part 2:  
827 pairing aerial photographs and terrestrial laser scanning to create a watershed scale  
828 sediment budget. *Earth Surface Processes and Landforms*, *38*(10), 1068–1082.  
829 <https://doi.org/10.1002/esp.3359>

830 Dietrich, W. E., Dunne, T., Humphrey, N. F., & Reid, L. M. (1982). Construction of sediment  
831 budgets for drainage basins. In: *Sediment Budgets and Routing in Forested Drainage*  
832 *Basins: Proceedings of the Symposium; 31 May - 1 June 1982; Corvallis, Oregon. Gen.*  
833 *Tech. Rep. PNW-141. Portland, Oregon: Pacific Northwest Forest and Range*  
834 *Experiment Station, Forest Service, U.S. Department of Agriculture; 1982: 5-23.*  
835 Retrieved from <https://www.fs.usda.gov/treearch/pubs/7749>

836 Donovan, M., Belmont, P., Notebaert, B., Coombs, T., Larson, P., & Souffront, M. (2019).  
837 Accounting for uncertainty in remotely-sensed measurements of river planform change.  
838 *Earth-Science Reviews*, *193*, 220–236. <https://doi.org/10.1016/j.earscirev.2019.04.009>

839 Dormann, C. F., Elith, J., Bacher, S., Buchmann, C., Carl, G., Carré, G., et al. (2013).  
840 Collinearity: a review of methods to deal with it and a simulation study evaluating their  
841 performance. *Ecography*, 36(1), 27–46. [https://doi.org/10.1111/j.1600-](https://doi.org/10.1111/j.1600-0587.2012.07348.x)  
842 [0587.2012.07348.x](https://doi.org/10.1111/j.1600-0587.2012.07348.x)

843 Fisher, G. B., Bookhagen, B., & Amos, C. B. (2013). Channel planform geometry and slopes  
844 from freely available high-spatial resolution imagery and DEM fusion: Implications for  
845 channel width scalings, erosion proxies, and fluvial signatures in tectonically active  
846 landscapes. *Geomorphology*, 194, 46–56.  
847 <https://doi.org/10.1016/j.geomorph.2013.04.011>

848 Fox, G. A., Wilson, G. V., Simon, A., Langendoen, E. J., Akay, O., & Fuchs, J. W. (2007).  
849 Measuring streambank erosion due to ground water seepage: correlation to bank pore  
850 water pressure, precipitation and stream stage. *Earth Surface Processes and Landforms*,  
851 32(10), 1558–1573. <https://doi.org/10.1002/esp.1490>

852 Gaskill, D. L., Mutschler, F. E., Kramer, J. H., Thomas, J. A., & Zahony, S. G. (1991). Geologic  
853 map of the Gothic quadrangle, Gunnison County, Colorado. Geologic Quadrangle Map  
854 GQ-1689, sale 1:24,000, Gunnison, Colorado: U.S. Geological Survey.

855 Gellis, A. C., & Walling, D. E. (2013). Sediment Source Fingerprinting (Tracing) and Sediment  
856 Budgets as Tools in Targeting River and Watershed Restoration Programs. In A. Simon,  
857 S. J. Bennett, & J. M. Castro (Eds.), *Geophysical Monograph Series* (pp. 263–291).  
858 Washington, D. C.: American Geophysical Union.  
859 <https://doi.org/10.1029/2010GM000960>

860 Gellis, A. C., Pavich, M. J., Ellwein, A. L., Aby, S., Clark, I., Wieczorek, M. E., & Viger, R.  
861 (2012). Erosion, storage, and transport of sediment in two subbasins of the Rio Puerco,  
862 New Mexico. *GSA Bulletin*, *124*(5–6), 817–841. <https://doi.org/10.1130/B30392.1>

863 Güneralp, İ., & Rhoads, B. L. (2009). Empirical analysis of the planform curvature-migration  
864 relation of meandering rivers. *Water Resources Research*, *45*(9), W09424.  
865 <https://doi.org/10.1029/2008WR007533>

866 Gurnell, A. M. (1997). Channel change on the River Dee meanders, 1946–1992, from the  
867 analysis of air photographs. *Regulated Rivers: Research & Management*, *13*(1), 13–26.  
868 [https://doi.org/10.1002/\(SICI\)1099-1646\(199701\)13:1<13::AID-RRR420>3.0.CO;2-W](https://doi.org/10.1002/(SICI)1099-1646(199701)13:1<13::AID-RRR420>3.0.CO;2-W)

869 Hirsch, R. M., & Archfield, S. A. (2015). Flood trends: Not higher but more often. *Nature*  
870 *Climate Change*, *5*(3), 198–199. <https://doi.org/10.1038/nclimate2551>

871 Hoffmann, T., Glatzel, S., & Dikau, R. (2009). A carbon storage perspective on alluvial sediment  
872 storage in the Rhine catchment. *Geomorphology*, *108*(1), 127–137.  
873 <https://doi.org/10.1016/j.geomorph.2007.11.015>

874 Hooke, J. M. (1979). An analysis of the processes of river bank erosion. *Journal of Hydrology*,  
875 *42*(1), 39–62. [https://doi.org/10.1016/0022-1694\(79\)90005-2](https://doi.org/10.1016/0022-1694(79)90005-2)

876 Hooke, J. M. (2008). Temporal variations in fluvial processes on an active meandering river over  
877 a 20-year period. *Geomorphology*, *100*(1), 3–13.  
878 <https://doi.org/10.1016/j.geomorph.2007.04.034>

879 Howard, A. D. (1996). Modeling Channel Evolution and Floodplain Morphology. *Floodplain*  
880 *Processes*, 15–62.

881 Hupp, C. R., Demas, C. R., Kroes, D. E., Day, R. H., & Doyle, T. W. (2008). Recent  
882 sedimentation patterns within the central Atchafalaya Basin, Louisiana. *Wetlands*, 28(1),  
883 125–140. <https://doi.org/10.1672/06-132.1>

884 Kampf, S. K., & Lefsky, M. A. (2016). Transition of dominant peak flow source from snowmelt  
885 to rainfall along the Colorado Front Range: Historical patterns, trends, and lessons from  
886 the 2013 Colorado Front Range floods. *Water Resources Research*, 52(1), 407–422.  
887 <https://doi.org/10.1002/2015WR017784>

888 Kleinhans, M. G., Cohen, K. M., Hoekstra, J., & IJmker, J. M. (2011). Evolution of a bifurcation  
889 in a meandering river with adjustable channel widths, Rhine delta apex, The Netherlands.  
890 *Earth Surface Processes and Landforms*, 36(15), 2011–2027.  
891 <https://doi.org/10.1002/esp.2222>

892 Langendoen, E. J., & Alonso, C. V. (2008). Modeling the Evolution of Incised Streams: I. Model  
893 Formulation and Validation of Flow and Streambed Evolution Components. *Journal of*  
894 *Hydraulic Engineering*, 134(6), 749–762. [https://doi.org/10.1061/\(ASCE\)0733-](https://doi.org/10.1061/(ASCE)0733-9429(2008)134:6(749))  
895 [9429\(2008\)134:6\(749\)](https://doi.org/10.1061/(ASCE)0733-9429(2008)134:6(749))

896 Langendoen, E. J., & Simon, A. (2008). Modeling the Evolution of Incised Streams. II:  
897 Streambank Erosion. *Journal of Hydraulic Engineering*, 134(7), 905–915.  
898 [https://doi.org/10.1061/\(ASCE\)0733-9429\(2008\)134:7\(905\)](https://doi.org/10.1061/(ASCE)0733-9429(2008)134:7(905))

899 Lenhart, C. F., Titov, M. L., Ulrich, J. S., Nieber, J. L., & Suppes, B. J. (2013). The Role of  
900 Hydrologic Alteration and Riparian Vegetation Dynamics in Channel Evolution along the  
901 Lower Minnesota River. *Transactions of the American Society of Agricultural and*  
902 *Biological Engineers*, 56(2), 549–561.

903 Li, D., Wrzesien, M. L., Durand, M., Adam, J., & Lettenmaier, D. P. (2017). How much runoff  
904 originates as snow in the western United States, and how will that change in the future?  
905 *Geophysical Research Letters*, *44*(12), 6163–6172.  
906 <https://doi.org/10.1002/2017GL073551>

907 Lininger, K. B., Wohl, E., Rose, J. R., & Leisz, S. J. (2019). Significant Floodplain Soil Organic  
908 Carbon Storage Along a Large High-Latitude River and its Tributaries. *Geophysical  
909 Research Letters*, *46*(4), 2121–2129. <https://doi.org/10.1029/2018GL080996>

910 Macklin, M. G., Brewer, P. A., Hudson-Edwards, K. A., Bird, G., Coulthard, T. J., Dennis, I. A.,  
911 et al. (2006). A geomorphological approach to the management of rivers contaminated by  
912 metal mining. *Geomorphology*, *79*(3), 423–447.  
913 <https://doi.org/10.1016/j.geomorph.2006.06.024>

914 Malenda, H. f., Sutfin, N. a., Guryan, G., Stauffer, S., Rowland, J. c., Williams, K. h., & Singha,  
915 K. (2019). From Grain to Floodplain: Evaluating heterogeneity of floodplain  
916 hydrostatigraphy using sedimentology, geophysics, and remote sensing. *Earth Surface  
917 Processes and Landforms*, *0*(0). <https://doi.org/10.1002/esp.4613>

918 Mallakpour, I., & Villarini, G. (2015). The changing nature of flooding across the central United  
919 States. *Nature Climate Change*, *5*(3), 250–254. <https://doi.org/10.1038/nclimate2516>

920 McFeeters, S. K. (1996). The use of the Normalized Difference Water Index (NDWI) in the  
921 delineation of open water features. *International Journal of Remote Sensing*, *17*(7),  
922 1425–1432. <https://doi.org/10.1080/01431169608948714>

923 Merritt, D. M., & Cooper, D. J. (2000). Riparian vegetation and channel change in response to  
924 river regulation: a comparative study of regulated and unregulated streams in the Green

925 River Basin, USA. *Regulated Rivers: Research & Management*, 16(6), 543–564.  
926 [https://doi.org/10.1002/1099-1646\(200011/12\)16:6<543::AID-RRR590>3.0.CO;2-N](https://doi.org/10.1002/1099-1646(200011/12)16:6<543::AID-RRR590>3.0.CO;2-N)

927 Micheli, E. R., & Kirchner, J. W. (2002a). Effects of wet meadow riparian vegetation on  
928 streambank erosion. 1. Remote sensing measurements of streambank migration and  
929 erodibility. *Earth Surface Processes and Landforms*, 27(6), 627–639.  
930 <https://doi.org/10.1002/esp.338>

931 Micheli, E. R., & Kirchner, J. W. (2002b). Effects of wet meadow riparian vegetation on  
932 streambank erosion. 2. Measurements of vegetated bank strength and consequences for  
933 failure mechanics. *Earth Surface Processes and Landforms*, 27(7), 687–697.  
934 <https://doi.org/10.1002/esp.340>

935 Mount, N., & Louis, J. (2005). Estimation and propagation of error in measurements of river  
936 channel movement from aerial imagery. *Earth Surface Processes and Landforms*, 30(5),  
937 635–643. <https://doi.org/10.1002/esp.1172>

938 Naiman, R. J., Decamps, H., & McClain, M. E. (2010). *Riparia: Ecology, Conservation, and*  
939 *Management of Streamside Communities*. Elsevier.

940 Nijssen, B., O'Donnell, G. M., Hamlet, A. F., & Lettenmaier, D. P. (2001). Hydrologic  
941 Sensitivity of Global Rivers to Climate Change. *Climatic Change*, 50(1), 143–175.  
942 <https://doi.org/10.1023/A:1010616428763>

943 Noe, G. B., & Hupp, C. R. (2005). Carbon, nitrogen, and phosphorus accumulation in  
944 floodplains of atlantic coastal plain rivers, usa. *Ecological Applications*, 15(4), 1178–  
945 1190. <https://doi.org/10.1890/04-1677>

946 Omengo, F. O., Geeraert, N., Bouillon, S., & Govers, G. (2018). Deposition and fate of organic  
947 carbon in floodplains along a tropical semiarid lowland river (Tana River, Kenya).

948 *Journal of Geophysical Research: Biogeosciences*, 1131–1143.  
949 [https://doi.org/10.1002/2015JG003288@10.1002/\(ISSN\)2169-8961.CNFLOI1](https://doi.org/10.1002/2015JG003288@10.1002/(ISSN)2169-8961.CNFLOI1)

950 Painter, T. H., Skiles, S. M., Deems, J. S., Brandt, W. T., & Dozier, J. (2018). Variation in  
951 Rising Limb of Colorado River Snowmelt Runoff Hydrograph Controlled by Dust  
952 Radiative Forcing in Snow. *Geophysical Research Letters*, 45(2), 797–808.  
953 <https://doi.org/10.1002/2017GL075826>

954 Parker, G., Shimizu, Y., Wilkerson, G. V., Eke, E. C., Abad, J. D., Lauer, J. W., et al. (2011). A  
955 new framework for modeling the migration of meandering rivers. *Earth Surface  
956 Processes and Landforms*, 36(1), 70–86. <https://doi.org/10.1002/esp.2113>

957 Parker, Gary, Sawai, K., & Ikeda, S. (1982). Bend theory of river meanders. Part 2. Nonlinear  
958 deformation of finite-amplitude bends. *Journal of Fluid Mechanics*, 115, 303–314.  
959 <https://doi.org/10.1017/S0022112082000767>

960 Pizzuto, J. E., & Meckelnburg, T. S. (1989). Evaluation of a linear bank erosion equation. *Water  
961 Resources Research*, 25(5), 1005–1013. <https://doi.org/10.1029/WR025i005p01005>

962 Pizzuto, James E. (1994). Channel adjustments to changing discharges, Powder River, Montana.  
963 *GSA Bulletin*, 106(11), 1494–1501. [https://doi.org/10.1130/0016-  
964 7606\(1994\)106<1494:CATCDP>2.3.CO;2](https://doi.org/10.1130/0016-7606(1994)106<1494:CATCDP>2.3.CO;2)

965 Poff, N. L., Allan, J. D., Bain, M. B., Karr, J. R., Prestegard, K. L., Richter, B. D., et al. (1997).  
966 The Natural Flow Regime. *BioScience*, 47(11), 769–784.  
967 <https://doi.org/10.2307/1313099>

968 Praskievicz, S. (2016). Impacts of Projected Climate Changes on Streamflow and Sediment  
969 Transport for Three Snowmelt-Dominated Rivers in the Interior Pacific Northwest. *River  
970 Research and Applications*, 32(1), 4–17. <https://doi.org/10.1002/rra.2841>

971 Reid, L., & Dunne, T. (2016). Sediment budgets as an organizing framework in fluvial  
972 geomorphology. In: Kondolf, G.M.; Piégay, H., Eds. *Tools in Fluvial Geomorphology*.  
973 Chichester, UK: John Wiley & Sons, Ltd: 357-379. Chapter 16, 357–379.  
974 <https://doi.org/10.1002/9781118648551>

975 Rhoades, E. L., O’Neal, M. A., & Pizzuto, J. E. (2009). Quantifying bank erosion on the South  
976 River from 1937 to 2005, and its importance in assessing Hg contamination. *Applied*  
977 *Geography*, 29(1), 125–134. <https://doi.org/10.1016/j.apgeog.2008.08.005>

978 Richard, G. A., Julien, P. Y., & Baird, D. C. (2005). Statistical analysis of lateral migration of  
979 the Rio Grande, New Mexico. *Geomorphology*, 71(1), 139–155.  
980 <https://doi.org/10.1016/j.geomorph.2004.07.013>

981 Richter, B. D., Baumgartner, J. V., Powell, J., & Braun, D. P. (1996). A Method for Assessing  
982 Hydrologic Alteration within Ecosystems. *Conservation Biology*, 10(4), 1163–1174.  
983 <https://doi.org/10.1046/j.1523-1739.1996.10041163.x>

984 Rinaldi, M., & Casagli, N. (1999). Stability of streambanks formed in partially saturated soils  
985 and effects of negative pore water pressures: the Sieve River (Italy). *Geomorphology*,  
986 26(4), 253–277. [https://doi.org/10.1016/S0169-555X\(98\)00069-5](https://doi.org/10.1016/S0169-555X(98)00069-5)

987 Rodriguez-Freire, L., Avasarala, S., Ali, A.-M. S., Agnew, D., Hoover, J. H., Artyushkova, K., et  
988 al. (2016). Post Gold King Mine Spill Investigation of Metal Stability in Water and  
989 Sediments of the Animas River Watershed. *Environmental Science & Technology*,  
990 50(21), 11539–11548. <https://doi.org/10.1021/acs.est.6b03092>

991 Rowland, J. C., Shelef, E., Pope, P. A., Muss, J., Gangodagamage, C., Brumby, S. P., & Wilson,  
992 C. J. (2016). A morphology independent methodology for quantifying planview river

993 change and characteristics from remotely sensed imagery. *Remote Sensing of*  
994 *Environment*, 184, 212–228. <https://doi.org/10.1016/j.rse.2016.07.005>

995 Schook, D. M., Rathburn, S. L., Friedman, J. M., & Wolf, J. M. (2017). A 184-year record of  
996 river meander migration from tree rings, aerial imagery, and cross sections.  
997 *Geomorphology*, 293, 227–239. <https://doi.org/10.1016/j.geomorph.2017.06.001>

998 Schwenk, J., Khandelwal, A., Fratkin, M., Kumar, V., & Foufoula-Georgiou, E. (2017). High  
999 spatiotemporal resolution of river planform dynamics from Landsat: The RivMAP  
1000 toolbox and results from the Ucayali River. *Earth and Space Science*, 4(2),  
1001 2016EA000196. <https://doi.org/10.1002/2016EA000196>

1002 Scott, D. N., & Wohl, E. E. (2018). Geomorphic regulation of floodplain soil organic carbon  
1003 concentration in watersheds of the Rocky and Cascade Mountains, USA. *Earth Surface*  
1004 *Dynamics*, 6(4), 1101–1114. <https://doi.org/10.5194/esurf-6-1101-2018>

1005 Sekely, A. C., Mulla, D. J., & Bauer, D. W. (2002). Streambank slumping and its contribution to  
1006 the phosphorus and suspended sediment loads of the blue earth river, minnesota. *Journal*  
1007 *of Soil and Water Conservation*, 57(5), 243–250.

1008 Simon, A., Curini, A., Darby, S. E., & Langendoen, E. J. (2000). Bank and near-bank processes  
1009 in an incised channel. *Geomorphology*, 35(3), 193–217. [https://doi.org/10.1016/S0169-](https://doi.org/10.1016/S0169-555X(00)00036-2)  
1010 [555X\(00\)00036-2](https://doi.org/10.1016/S0169-555X(00)00036-2)

1011 Simon, A., Thomas, R. E., Curini, A., & Shields, F. D. (2002). Case Study: Channel Stability of  
1012 the Missouri River, Eastern Montana. *Journal of Hydraulic Engineering*, 128(10), 880–  
1013 890. [https://doi.org/10.1061/\(ASCE\)0733-9429\(2002\)128:10\(880\)](https://doi.org/10.1061/(ASCE)0733-9429(2002)128:10(880))

1014 Stewart, I. T. (2009). Changes in snowpack and snowmelt runoff for key mountain regions.  
1015 *Hydrological Processes*, 23(1), 78–94. <https://doi.org/10.1002/hyp.7128>

1016 Stewart, I. T., Cayan, D. R., & Dettinger, M. D. (2004). Changes in Snowmelt Runoff Timing in  
1017 Western North America under a 'Business as Usual' Climate Change Scenario. *Climatic*  
1018 *Change*, 62(1), 217–232. <https://doi.org/10.1023/B:CLIM.0000013702.22656.e8>

1019 Sutfin, N. A., & Rowland, J. C. (2019). Depth and elevation of floodplain fine sediment along  
1020 the East River near Crested Butte, Colorado measured in 2016 and 2017. Incorporating  
1021 the Hydrological Controls on Carbon Cycling in Floodplain Ecosystems into Earth  
1022 System Models (ESMs). *ESS-Dive: Deep Insight for Earth Science Data*.  
1023 <https://doi.org/doi:10.15485/1574502>

1024 Sutfin, N. A., & Wohl, E. (2017). Substantial soil organic carbon retention along floodplains of  
1025 mountain streams. *Journal of Geophysical Research: Earth Surface*, 122(7), 1325–1338.  
1026 <https://doi.org/10.1002/2016JF004004>

1027 Sutfin, N. A., & Wohl, E. (2019). Elevational differences in hydrogeomorphic disturbance  
1028 regime influence sediment residence times within mountain river corridors. *Nature*  
1029 *Communications*, 10(1), 2221. <https://doi.org/10.1038/s41467-019-09864-w>

1030 Sutfin, N. A., Wohl, E. E., & Dwire, K. A. (2016). Banking carbon: a review of organic carbon  
1031 storage and physical factors influencing retention in floodplains and riparian ecosystems.  
1032 *Earth Surface Processes and Landforms*, 41(1), 38–60. <https://doi.org/10.1002/esp.3857>

1033 Surian, N., Barban, M., Ziliani, L., Monegato, G., Bertoldi, W., & Comiti, F. (2015). Vegetation  
1034 turnover in a braided river: frequency and effectiveness of floods of different  
1035 magnitude. *Earth Surface Processes and Landforms*, 40(4), 542–558.  
1036 <https://doi.org/10.1002/esp.3660>

1037 Theobald, D. M., Gosnell, H., & Riebsame, W. E. (1996). Land Use and Landscape Change in  
1038 the Colorado Mountains II: A Case Study of the East River Valley. *Mountain Research*  
1039 *and Development*, 16(4), 407–418. <https://doi.org/10.2307/3673990>

1040 Thorne, C. R., & Tovey, N. K. (1981). Stability of composite river banks. *Earth Surface*  
1041 *Processes and Landforms*, 6(5), 469–484. <https://doi.org/10.1002/esp.3290060507>

1042 Wohl, E., Dwire, K., Sutfin, N., Polvi, L., & Bazan, R. (2012). Mechanisms of carbon storage in  
1043 mountainous headwater rivers. *Nature Communications*, 3, 1263.  
1044 <https://doi.org/10.1038/ncomms2274>

1045 Wohl, E., Bledsoe, B. P., Jacobson, R. B., Poff, N. L., Rathburn, S. L., Walters, D. M., &  
1046 Wilcox, A. C. (2015). The Natural Sediment Regime in Rivers: Broadening the  
1047 Foundation for Ecosystem Management. *BioScience*, 65(4), 358–371.  
1048 <https://doi.org/10.1093/biosci/biv002>

1049 Wolman, M. G. (1959). Factors Influencing Erosion of a Cohesive River Bank. *American*  
1050 *Journal of Science*, 257(3), 204–216. <https://doi.org/10.2475/ajs.257.3.204>

1051 Zen, S., Gurnell, A. M., Zolezzi, G., & Surian, N. (2017). Exploring the role of trees in the  
1052 evolution of meander bends: The Tagliamento River, Italy. *Water Resources Research*,  
1053 53(7), 5943–5962. <https://doi.org/10.1002/2017WR020561>

1054

Year	Floodplain area (km <sup>2</sup> )	Channel			
		Channel Area (km <sup>2</sup> )	Length (km)	Sinuosity (m/m)	Channel slope (%)
1955	2193.6	459.0	20.08	1.89	0.339%
1973	2254.0	398.7	19.29	1.82	0.353%
1983	2222.3	430.3	18.80	1.77	0.362%
1990	2295.4	357.3	18.90	1.78	0.361%
2001	2275.4	377.3	19.39	1.83	0.352%
2011	2296.2	356.5	18.81	1.77	0.362%
2015	2312.2	340.4	18.98	1.79	0.359%

Confinement (m <sup>2</sup> /m <sup>2</sup> )	Mean channel width (m)
0.17	25 ± 2
0.15	20 ± 2
0.16	23 ± 3
0.13	19 ± 3
0.14	21 ± 3
0.13	19 ± 1
0.13	17 ± 1

Reach	Valley area (m <sup>2</sup> )	Valley Length (m)	Valley slope (%)	Floodplain area (m <sup>2</sup> )	Channel Area (m2)
1	344236	1471	0.94	294462	49774 ± 6292
2	489119	2126	0.74	405784	83334 ± 6234
3	232658	910	0.55	199873	32785 ± 6046
4	93445	595	0.86	76134	17311 ± 1495
5	330488	1142	0.68	283494	46994 ± 5334
6	378666	924	0.56	344169	34497 ± 4194
7	302210	855	0.33	271371	30839 ± 6166
8	126101	1175	0.54	89108	36992 ± 2469
9	355743	1420	0.46	299779	55965 ± 8114

<b>Channel Length (m)</b>	<b>Sinuosity (m/m)</b>	<b>Channel slope (%)</b>	<b>Confinement (m<sup>2</sup>/m<sup>2</sup>)</b>	<b>Channel</b>
2860 ± 130	1.94 ± 0.09	0.48 ± 0.02	0.14 ± 0.02	18
4735 ± 143	2.23 ± 0.07	0.33 ± 0.01	0.17 ± 0.01	18
1740 ± 99	1.91 ± 0.11	0.29 ± 0.02	0.14 ± 0.03	19
903 ± 60	1.52 ± 0.10	0.57 ± 0.04	0.19 ± 0.02	20
2419 ± 170	2.12 ± 0.15	0.32 ± 0.02	0.14 ± 0.02	20
1448 ± 248	1.57 ± 0.27	0.37 ± 0.06	0.09 ± 0.01	22
1490 ± 116	1.74 ± 0.14	0.19 ± 0.02	0.1 ± 0.02	21
1583 ± 26	1.35 ± 0.02	0.4 ± 0.01	0.29 ± 0.02	23
2001 ± 53	1.41 ± 0.04	0.33 ± 0.01	0.16 ± 0.02	23

**width (m)**

---

± 3

± 2

± 3

± 2

± 2

± 3

± 3

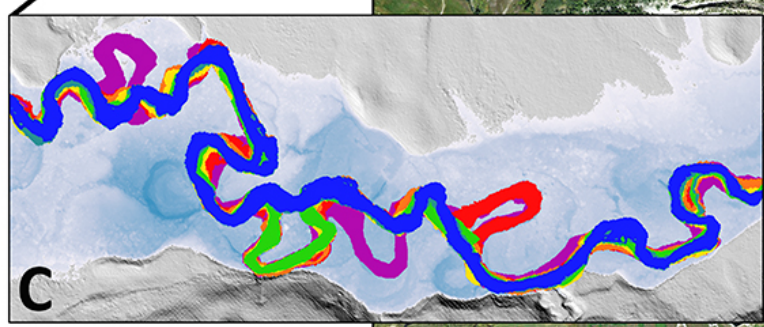
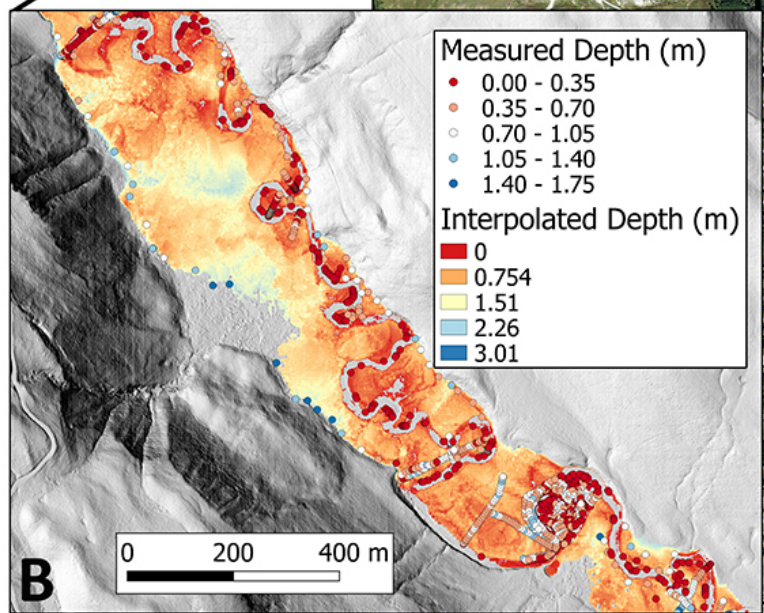
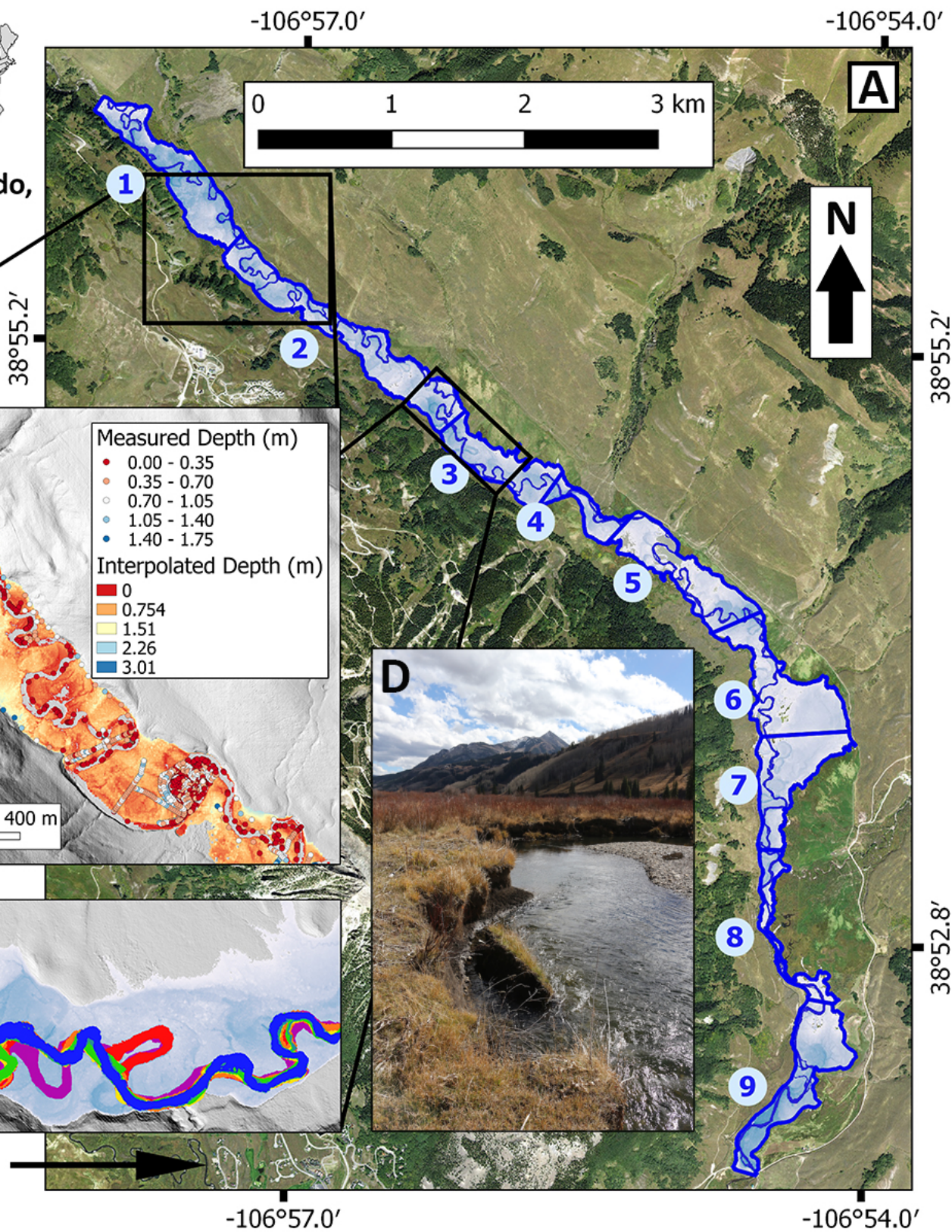
± 3

± 4

	1955-1973	1973-1983	1983-1990	1990-2001	2001-2011	2011-2015	Mean	Total
Duration (years)	18 ± 0.3	10 ± 0.3	7 ± 0.3	11 ± 0.3	10 ± 0.3	4 ± 0.3	10 ± 0.3	60 ± 0.8
Accretion (m <sup>2</sup> )	125529 ± 27774	45276 ± 6339	99194 ± 13887	50226 ± 8036	70686 ± 9189	30156 ± 7539	70178 ± 12127	421067 ± 34789
Erosion (m <sup>2</sup> )	-64915 ± 25388	-74670 ± 12694	-24569 ± 6142	-69550 ± 11128	-52358 ± 9948	-14969 ± 6137	-50172 ± 11906	-301031 ± 33224
Net Change (m <sup>2</sup> )	60614 ± 37629	-29394 ± 14188	74625 ± 15185	-19324 ± 13726	18328 ± 13543	15187 ± 9721	20006 ± 17332	120036 ± 48106
Accretion Rate (m <sup>2</sup> y <sup>-1</sup> )	6974 ± 1548	4528 ± 652	14171 ± 2095	4566 ± 744	7069 ± 949	7539 ± 1987	7474 ± 1329	44846 ± 3551
Erosion Rate (m <sup>2</sup> y <sup>-1</sup> )	-3606 ± 1412	-7467 ± 1294	-3510 ± 893	-6323 ± 1030	-5236 ± 1010	-3742 ± 1566	-4981 ± 1201	-29884 ± 2999
Mean linear Accretion Rate (m y <sup>-1</sup> )	0.347 ± 0.077	0.235 ± 0.034	0.754 ± 0.111	0.242 ± 0.039	0.365 ± 0.049	0.401 ± 0.106	0.390 ± 0.069	2.343 ± 0.186
Mean Linear Erosion Rate (m y <sup>-1</sup> )	-0.180 ± 0.070	-0.387 ± 0.067	-0.187 ± 0.048	-0.334 ± 0.054	-0.270 ± 0.052	-0.199 ± 0.083	-0.259 ± 0.062	-1.557 ± 0.156
Mean Day of Peak Flow	152.7	162	156.3	151.5	147	155.3	154.13 ± 5.06	
Mean Peak Flow (m <sup>3</sup> s <sup>-1</sup> )	11.84	11.6	12.9	12.35	11.31	10.15	11.69 ± 0.94	
Max Peak Flow (m <sup>3</sup> s <sup>-1</sup> )	22.56	18.32	21.86	23.74	16.02	15.49	19.67 ± 3.53	
Mean Bankfull Duration (days)	31.3	38.1	41	36.1	29.3	25.5	33.55 ± 5.84	
Max Bankfull Duration (days)	61	48	64	63	47	31	52.33 ± 12.86	
Mean Days Above Bankfull Flow	20.3	24	22.6	23.8	18.5	12.8	20.33 ± 4.26	
Max Days Above Bankfull Flow	59	46	62	56	47	30	50.00 ± 11.71	
Mean Duration Above Baseflow (days)	215.5	218	255.1	230.9	263	278.5	243.50 ± 25.82	
Max Duration Above Baseflow (days)	362	331	364	305	364	349	345.83 ± 23.74	
Mean Days Above Baseflow	232.1	217.8	266.7	243.9	259.8	245.5	244.30 ± 17.86	
Max Days Above Baseflow	281	261	362	275	316	272	294.50 ± 37.97	
Mean Days Since Bankfull Flow	267	327.1	349.6	261.3	345.3	455.3	334.27 ± 70.58	
Max Days Since Bankfull Flow	925	904	935	579	944	901	864.67 ± 140.96	
Mean Day Baseflow Ends	280.2	288.6	304	305.3	291	321.3	298.40 ± 14.73	
Mean Day Bankfull Flow Ends	173.3	181.9	176.8	172.7	170.3	173	174.67 ± 4.11	
Mean No. Peaks Above Bankfull		1.9	2	1.8	1.4	0.5	1.52 ± 0.61	
Maximum No. Peaks Above Bankfull	3	4	5	4	3	1	3.33 ± 1.37	
Mean Total Recession Slope (m <sup>3</sup> s <sup>-1</sup> day <sup>-1</sup> )	0.094	0.087	0.083	0.077	0.079	0.056	0.08 ± 0.01	
Max Total Recession Slope (m <sup>3</sup> s <sup>-1</sup> day <sup>-1</sup> )	0.149	0.142	0.097	0.13	0.124	0.085	0.12 ± 0.03	
Mean Bankfull Recession Slope (m <sup>3</sup> s <sup>-1</sup> day <sup>-1</sup> )	0.076	0.064	0.059	0.058	0.066	0.047	0.06 ± 0.01	
Max Bankfull Recession Slope (m <sup>3</sup> s <sup>-1</sup> day <sup>-1</sup> )	0.12	0.086	0.082	0.075	0.091	0.05	0.08 ± 0.02	
Mean Total Annual Volume (km <sup>3</sup> )	0.060	0.059	0.067	0.065	0.057	0.051	0.060 ± 0.006	
Max Total Annual Volume (km <sup>3</sup> )	0.109	0.081	0.103	0.110	0.087	0.077	0.094 ± 0.015	
Mean Bankfull Volume (km <sup>3</sup> )	0.027	0.034	0.037	0.033	0.027	0.024	0.031 ± 0.005	
Max Bankfull Volume (km <sup>3</sup> )	0.074	0.047	0.072	0.073	0.050	0.031	0.058 ± 0.018	

	1955 - 1973	1973 - 1983	1983 - 1990	1990 - 2001	2001 - 2011	2011 - 2015	Totals
Duration (y)	18 ± 0.3	10 ± 0.3	7 ± 0.3	11 ± 0.3	10 ± 0.3	4 ± 0.3	
Area Eroded from SCREAM (m <sup>2</sup> )	12228 ± 5060	12428 ± 2113	7341 ± 1835	16774 ± 2684	13317 ± 2530	3752 ± 1538	
Mean Depth of Eroded (m)	0.54 ± 0.01	0.60 ± 0.01	0.58 ± 0.01	0.69 ± 0.01	0.61 ± 0.01	0.72 ± 0.01	
<b>Volume Eroded (m<sup>3</sup>)</b>	<b>-6640 ± 2751</b>	<b>-7476 ± 1277</b>	<b>-4272 ± 1071</b>	<b>-11519 ± 1851</b>	<b>-8080 ± 1541</b>	<b>-2713 ± 1113</b>	<b>-40700 ± 4169</b>
Mean erosion rate (m <sup>3</sup> /y)	-369 ± 153	-748 ± 130	-610 ± 155	-1047 ± 171	-808 ± 156	-678 ± 283	
Mean bank area erosion rate (m <sup>2</sup> /y) <sup>c</sup>	#REF! ± #REF!	#REF! ± #REF!	#REF! ± #REF!	#REF! ± #REF!	#REF! ± #REF!	#REF! ± #REF!	
Point bar area of accretion from SCREAM (m <sup>2</sup> )	28392 ± 4356	12391 ± 1735	14534 ± 2035	13612 ± 2178	14493 ± 1884	7403 ± 1851	
Mean vertical accretion within eroded areas (m)	0.59 ± 0.01	0.33 ± 0.01	0.23 ± 0.01	0.36 ± 0.01	0.33 ± 0.01	0.13 ± 0.01	
Estimated accretion along point bars (m <sup>3</sup> )	16865 ± 2608	4089 ± 587	3357 ± 493	4941 ± 803	4783 ± 640	977 ± 255	
Overbank deposition from regression (m <sup>3</sup> )	459 ± 92	302 ± 61	213 ± 44	305 ± 62	322 ± 66	168 ± 36	
<b>Total volume accreted (m<sup>3</sup>)</b>	<b>17324 ± 2610</b>	<b>4391 ± 590</b>	<b>3570 ± 495</b>	<b>5246 ± 806</b>	<b>5105 ± 643</b>	<b>1145 ± 258</b>	<b>36780 ± 2921</b>
Mean accretion rate (m <sup>3</sup> /y)	962.43 ± 145.87	439.11 ± 60.462	509.97 ± 73.961	476.9 ± 74.406	510.54 ± 66.126	286.16 ± 67.924	
<b>Net volume (m<sup>3</sup>)</b>	<b>10684 ± 3792</b>	<b>-3085 ± 1407</b>	<b>-702 ± 1179</b>	<b>-6273 ± 2018</b>	<b>-2975 ± 1670</b>	<b>-1568 ± 1142</b>	<b>-3920 ± 5091</b>

Figure 1.

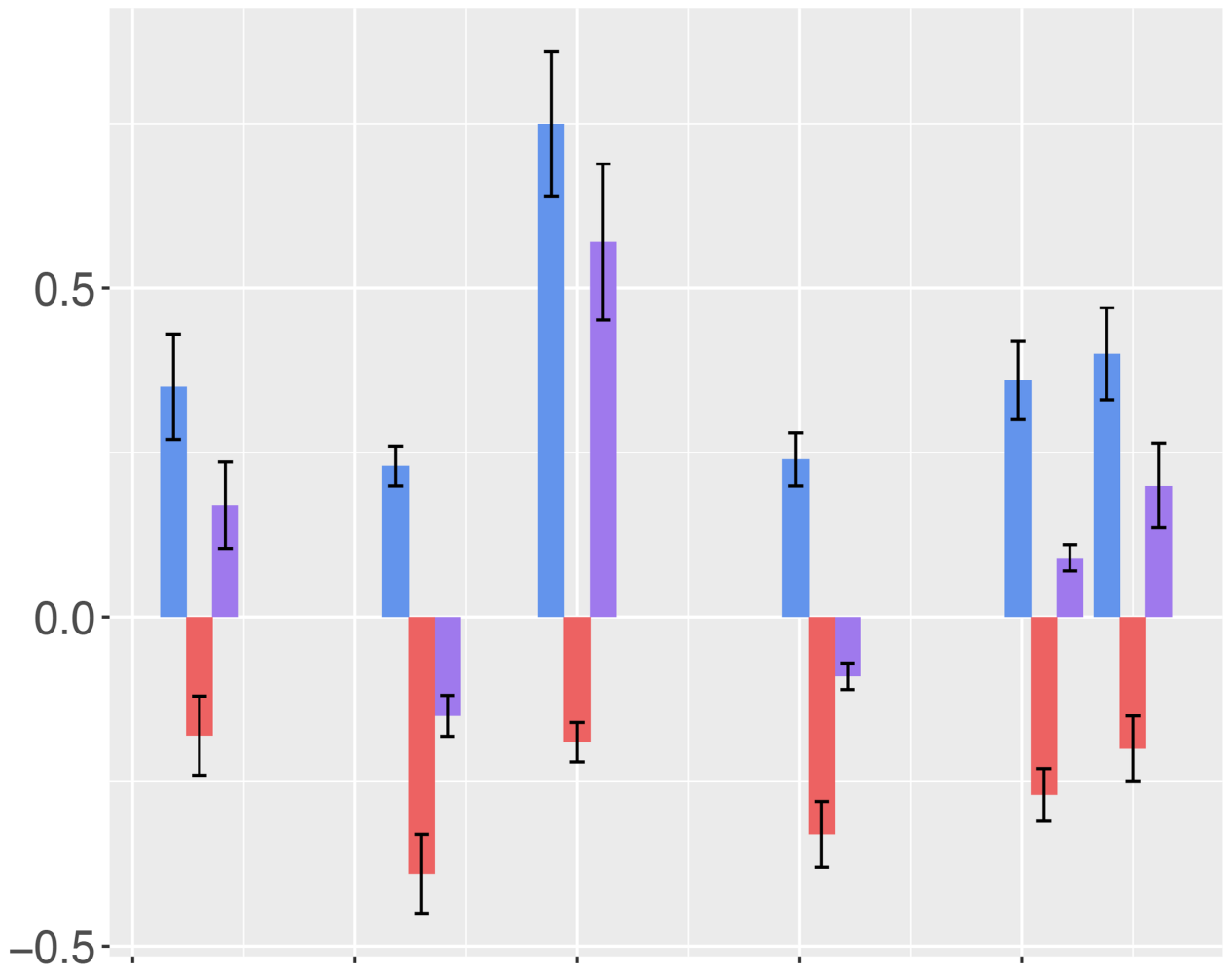


Crested Butte, CO

-106°57.0' -106°54.0'

Figure 2.

**A**  
Linear Rate (m/y)



**B**  
Floodplain Volume (m<sup>3</sup>)

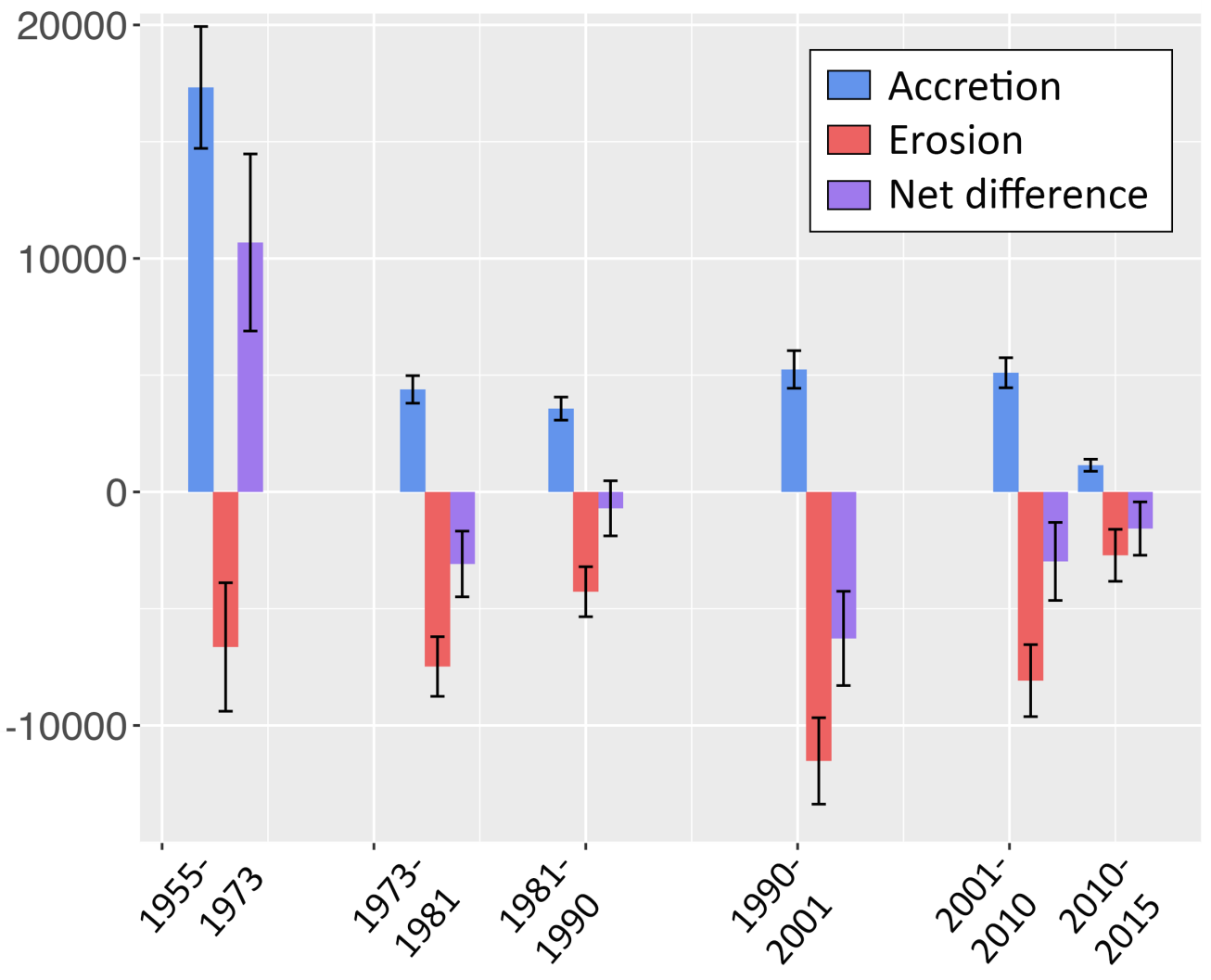


Figure 3.

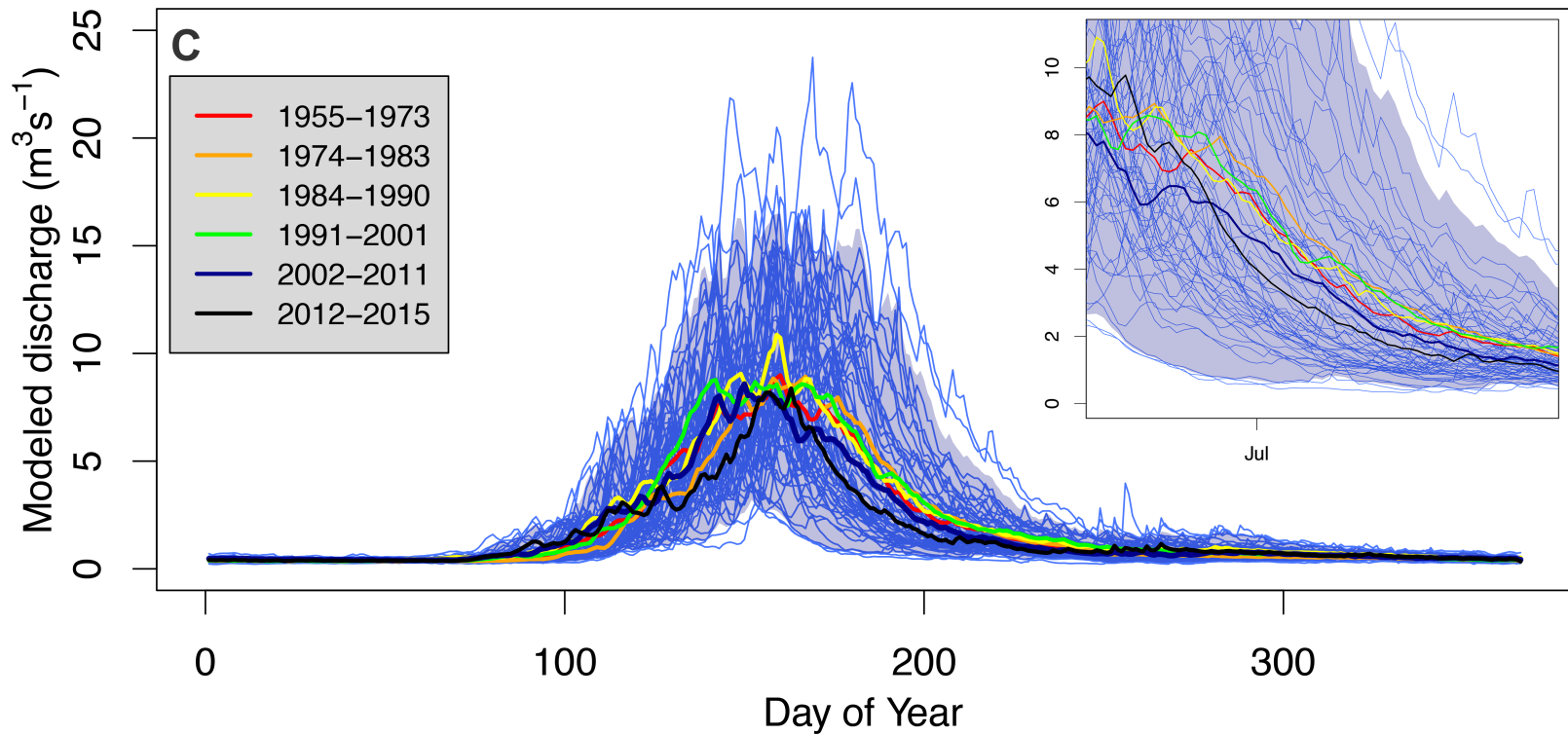
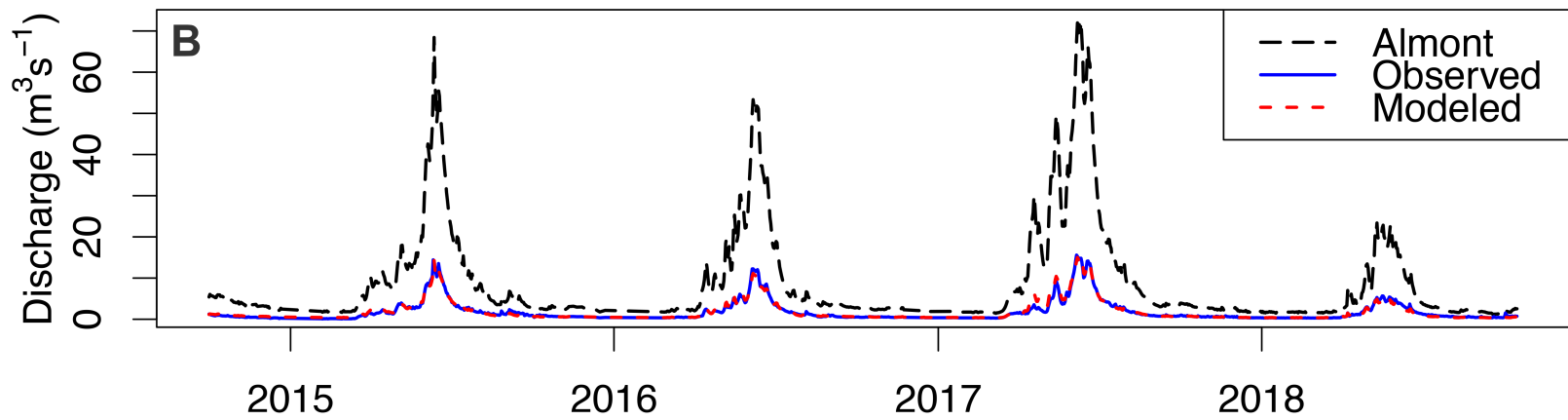
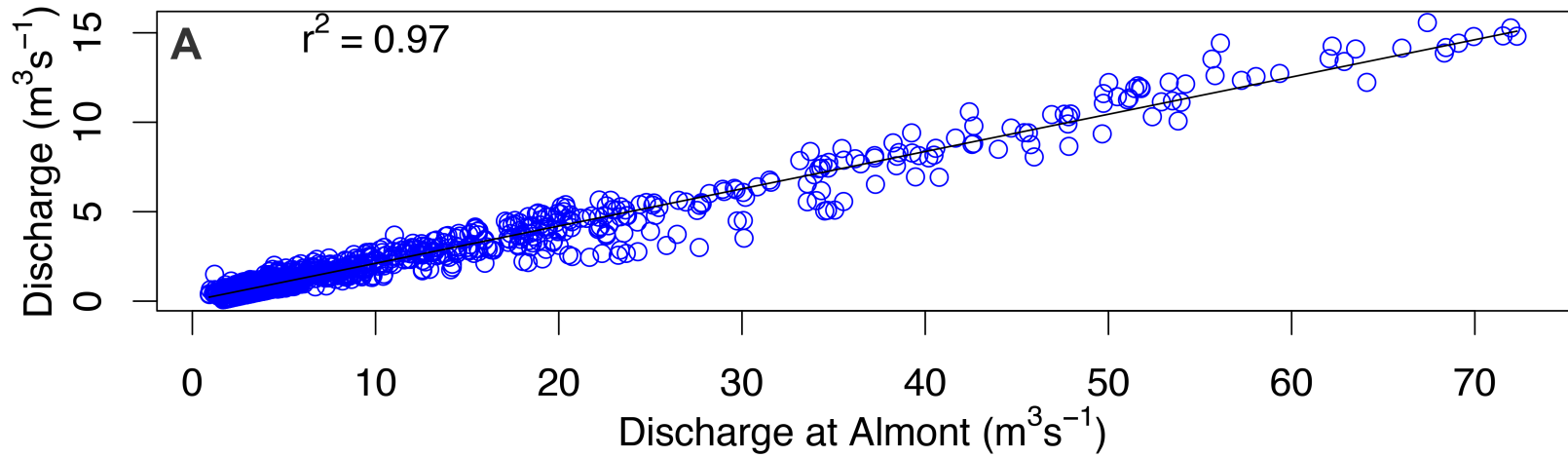
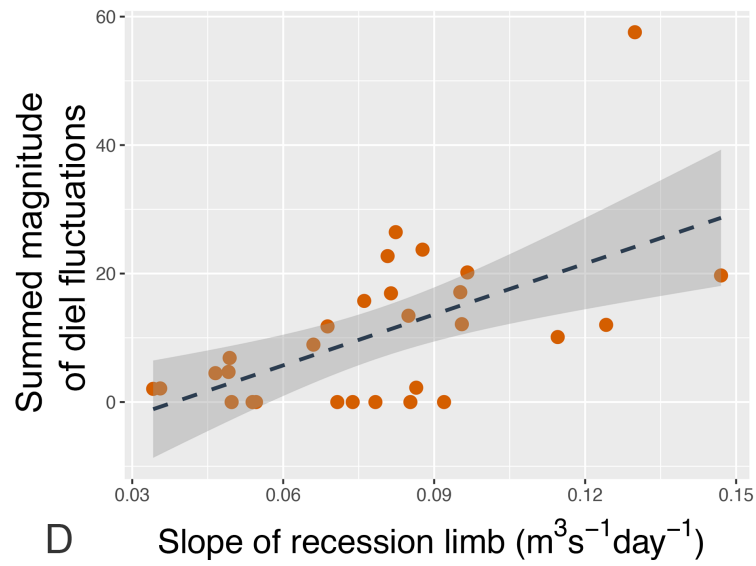
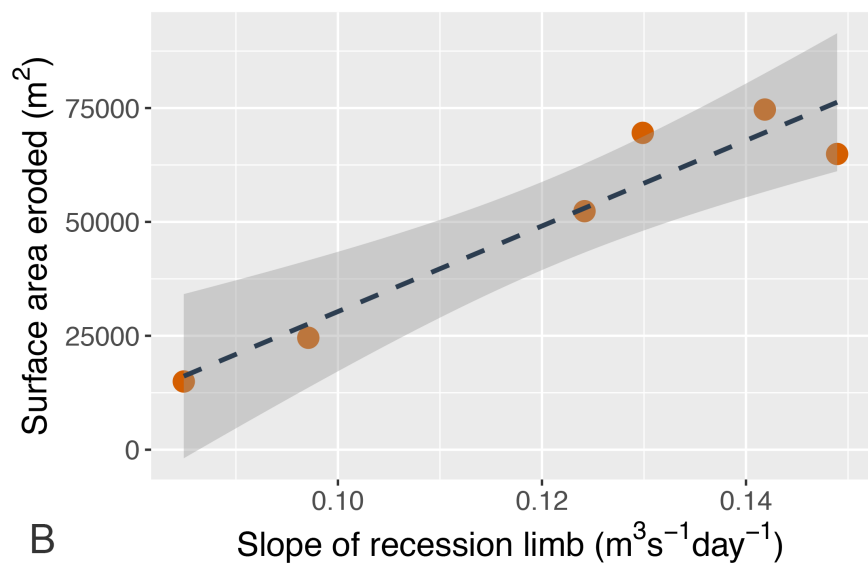
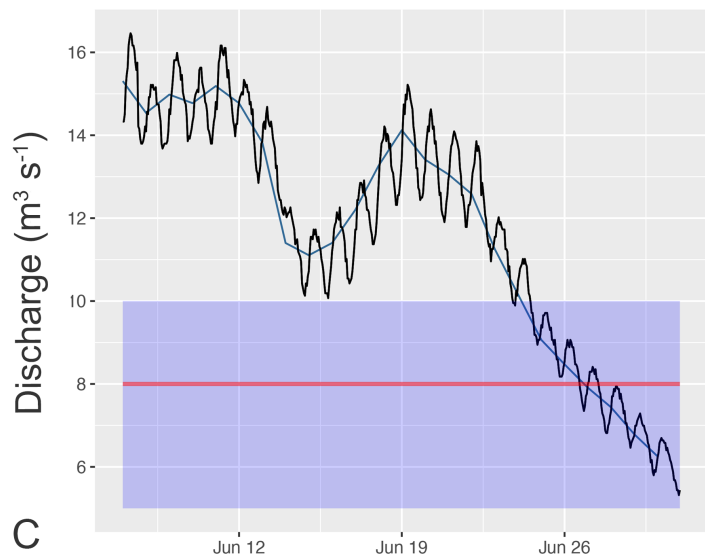
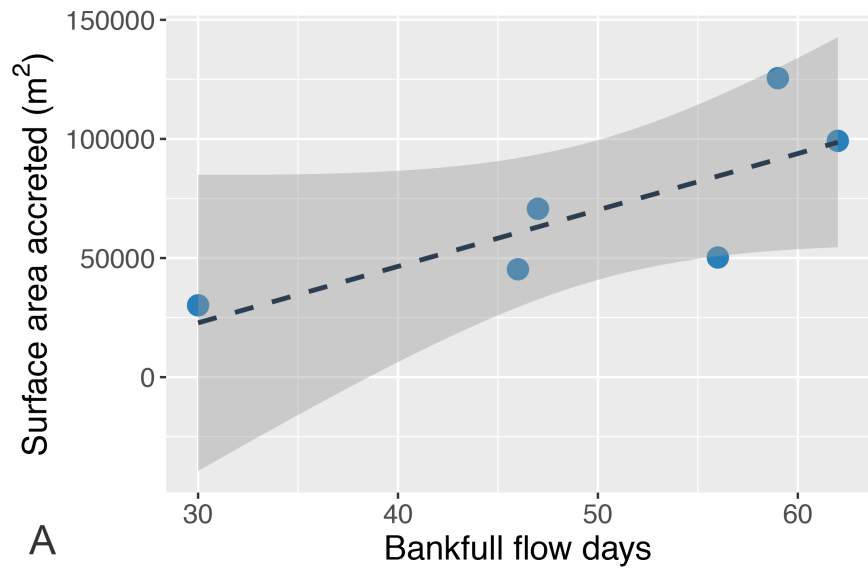


Figure 4.



```
# This code will examine to hydrograph dataset, select matching days
# and times and conduct a regression that can be used to fill in missing data
# Author: Nicholas A. Sutfin
# Date: Oct. 18th 2017, last modified May 8th, 2020
```

```
library("plyr")
#library("smwrBase", lib.loc=~ /R/win-library/3.2")
library("lattice") #, lib.loc="C:/Program Files/R/R-3.3.0/library")
library("lubridate")
library("hydroGOF")
```

```
# Set user space
loadpath = '/Users/NicholasSutfin/Documents/EastRiver/ER_Rcode/'
savepath = '/Users/NicholasSutfin/Documents/EastRiver/ER_Rcode/Baseflow_1.91_BestFit/' #
Calculating slope as line between 1st and last points (2p)
setwd(loadpath)
```

```
All_DailyQ_1935_2020 = read.csv("All_DailyQ_1935_2020.csv", stringsAsFactors = F)
#"All_DailyQ_1910_2020.csv", stringsAsFactors = F)
```

```
# Load Almont data for 2015-2017 as csv file, convert to SI units, code the date as a date, and
define the year
```

```
Alm_Q <- read.csv("ER_AlmQ_2015-2019.csv", header=TRUE)
Alm_Q$Q_cfs = as.numeric(as.character(Alm_Q$Q_cfs))
Alm_Q$Alm_Q_cms = Alm_Q$Q_cfs*0.0283168
Alm_DailyQ = as.data.frame(Alm_Q)
Alm_DailyQ = ddply(Alm_DailyQ, ~date, summarise, Alm_Q_cms = mean(Alm_Q_cms))
Alm_Qdaily <- Alm_DailyQ[order(as.Date(Alm_DailyQ$date, format="%m/%d/%y")),]
Alm_Qdaily$date = as.Date(Alm_Qdaily$date, "%m/%d/%y")
Alm_Qdaily$year = year(Alm_Qdaily$date)
Alm_Qdaily$month = month(Alm_Qdaily$date)
Alm_Qdaily$Calday = day(Alm_Qdaily$date)
Alm_Qdaily$day = yday(Alm_Qdaily$date)
```

```
# Load Pump house data for 2015-2017 as csv file, convert to SI units, code the date as a date,
and define the year
```

```
#PH_Qdaily <- read.csv("ER_PH_2015-17Q.csv", header=TRUE )
PH_Data <- read.csv("ER_PHQ_2014-2018.csv", header=TRUE)
PH_DailyQ = ddply(PH_Data, ~date, summarise, PHQ_cms = mean(PHQ_cms))
PH_Qdaily <- PH_DailyQ[order(as.Date(PH_DailyQ$date, format="%m/%d/%y")),]
PH_Qdaily$date = as.Date(PH_Qdaily$date, "%m/%d/%y")
PH_Qdaily$year = year(PH_Qdaily$date)
PH_Qdaily$month = month(PH_Qdaily$date)
PH_Qdaily$Calday = day(PH_Qdaily$date)
```

```
PH_Qdaily$day = yday(PH_Qdaily$Date)
names(PH_Qdaily)[2]<-paste("PH_Q_cms")
```

```
#
```

---

```
# Find matching dates and create new dataset
DailyQ_diff <- setdiff(PH_Qdaily$Date, Alm_Qdaily$Date)
DailyQ_int <- intersect(PH_Qdaily$Date, Alm_Qdaily$Date)
```

```
# Find PH Q data for dates overlapping the with Almont gage
PH_DailyQ_match <- PH_Qdaily[PH_Qdaily$Date %in% DailyQ_int, ]
# Find Almont gauge data that overlaps with pump house study site data
Alm_DailyQ_match <- Alm_Qdaily[Alm_Qdaily$Date %in% DailyQ_int, ]
# Merge the two overlapping datasets side by side by matching dates
All_DailyQ_15_18 <- cbind(Alm_DailyQ_match, PH_DailyQ_match)
```

```
rows = length(All_DailyQ_15_18$PH_Q_cms) #[All_DailyQ_15_18$day > 105 &
All_DailyQ_15_18$day < 319])
Qmat <- matrix(0, rows, 3)
Q = as.data.frame(Qmat)
names(Q)[1]=paste("PH")
names(Q)[2]=paste("AL")
names(Q)[3]=paste("day")
```

```
# April 15th = 105 Nov 15th = 319, so 104-320 is good
Q$PHDate = All_DailyQ_15_18$Date[which(is.na(All_DailyQ_15_18$PH_Q_cms) == FALSE)]
#[All_DailyQ_15_18$day > 105 & All_DailyQ_15_18$day < 319]
Q$PH = All_DailyQ_15_18$PH_Q_cms[which(is.na(All_DailyQ_15_18$PH_Q_cms) == FALSE)]
#[All_DailyQ_15_18$day > 105 & All_DailyQ_15_18$day < 319]
Q$ALDate = All_DailyQ_15_18$Date[which(is.na(All_DailyQ_15_18$PH_Q_cms) == FALSE)]
#[All_DailyQ_15_18$day > 105 & All_DailyQ_15_18$day < 319]
Q$AL = All_DailyQ_15_18$Alm_Q_cms[which(is.na(All_DailyQ_15_18$Alm_Q_cms) == FALSE)]
#[All_DailyQ_15_18$day > 105 & All_DailyQ_15_18$day < 319]
Q$day = All_DailyQ_15_18$day[which(is.na(All_DailyQ_15_18$Alm_Q_cms) == FALSE)]
#[All_DailyQ_15_18$day > 105 & All_DailyQ_15_18$day < 319]
```

```
Qreg <- lm(Q$PH ~ Q$AL, data = Q)
summary(Qreg)
Qreg # adjusted R squared = 0.97
```

```
# For all days: PHQ = -0.081804 + 0.211284(Alm)
# Excluding frozen days, regression output: PHQ = 0.010948 + 0.211611(Alm)
```

```
par(mfrow=c(1,1), mar=c(4,5,2,2), cex = 1.5, lwd = 1)
```

```

plot(All_DailyQ_15_18$Alm_Q_cms, All_DailyQ_15_18$PH_Q_cms, col = "blue",
     xlab = expression(paste("Discharge at Almont (m3, s-1,"))),
     ylab = expression(paste("Discharge (m3, s-1,")))
lines(All_DailyQ_15_18$Alm_Q_cms, Qreg$coefficients[1] +
      Qreg$coefficients[2]*All_DailyQ_15_18$Alm_Q_cms,
      col = "black")
par(cex = 1)
#points(Q$AL, Q$PH, pch = 19, col = "red")
text(10, 15, expression("r2 ~" = 0.97"), cex = 1.5)

# Load Almont discharge data from 1910 to 2020, cut data to timeframe of interest (1955-2015)
# and convert to cms
# _____
Alm_Qdaily_1910_2020 <- read.csv("Alm_Q_cfs_1910_2020.csv", header=TRUE)
Alm_Qdaily_1910_2020$Alm_Q_cms = Alm_Qdaily_1910_2020$Alm_Q_cfs*0.0283168
Alm_Qdaily_1910_2020$Date = as.Date(Alm_Qdaily_1910_2020$Date, "%m/%d/%Y")

All_DailyQ_1910_2020 = Alm_Qdaily_1910_2020
All_DailyQ_1910_2020$year = format(All_DailyQ_1910_2020$Date, "%Y")
All_DailyQ_1910_2020$month = format(All_DailyQ_1910_2020$Date, "%m")
All_DailyQ_1910_2020$day = format(All_DailyQ_1910_2020$Date, "%d")
All_DailyQ_1910_2020$yday = yday(All_DailyQ_1910_2020$Date)
All_DailyQ_1910_2020$Mod_PH_Q_cms = Qreg$coefficients[1] +
Qreg$coefficients[2]*All_DailyQ_1910_2020$Alm_Q_cms

# Use regression to extend daily Q for PH based on Almont flow
# _____
# regression output: PHQ = x + y(Alm)
par(mfrow=c(1,1), mar=c(4,5,3,2), cex = 1.5)
All_DailyQ_2014_2020 = All_DailyQ_1910_2020[37987:length(Alm_Qdaily_1910_2020$Date), ]

# _____
# plot observed vs. modeled data for East River and calculate Nash-Sutcliffe and RMSE
par(mfrow=c(1,1), mar=c(4,4,2,2), cex = 1.1)

Date = All_DailyQ_2014_2020$Date
Modeled_PHQ = subset(All_DailyQ_2014_2020, Date > "2014-9-30")
#min(WaterYear15):max(WaterYear15)))

# Select only unique values
Observed_PHQ = All_DailyQ_15_18[,c(3,9)]

```

```

PH_Q_int <- intersect(Observed_PHQ$Date[order(Observed_PHQ$Date)],
Modeled_PHQ$Date[order(Modeled_PHQ$Date)])
Modeled_Q_match <- Modeled_PHQ[Modeled_PHQ$Date %in% PH_Q_int, ]
Observed_Q_match <- Observed_PHQ[Observed_PHQ$Date %in% PH_Q_int, ]
PHQ_15_18 = cbind(Modeled_Q_match, Observed_Q_match)

Qreg2 <- lm(PHQ_15_18$PH_Q_cms ~ PHQ_15_18$Alm_Q_cms, data = All_DailyQ_15_18)
summary(Qreg2)
Qreg2

```

```

par(mfrow=c(1,1), mar=c(4,5,2,2), cex = 1.5, lwd = 1)
# Plot Almont flow data
plot(All_DailyQ_15_18$Date, All_DailyQ_15_18$Alm_Q_cms, lwd = 2, type = "l",
     col = "black", xlab = "Year", ylab = expression(paste("Discharge (m3", "s-1", "))), lty =
5, cex = 1.5)
# Plot observed ER study site flow data
lines(PHQ_15_18$Date[order(PHQ_15_18$Date)],
      PHQ_15_18$PH_Q_cms[order(PHQ_15_18$Date)], lty = 1, col = "blue", lwd = 2, type = "l",
      xlab = expression(paste("Discharge (m3", "s-1", "))), ylab = "Time (years)")
#polygon(PHQ_15_17$date, PHQ_15_17[,5], col = "blue")

```

```

# Plot modeled ER study site flow data
lines(PHQ_15_18$Date[order(PHQ_15_18$Date)],
      PHQ_15_18$Mod_PH_Q_cms[order(PHQ_15_18$Date)], col = 'red', lwd = 2, lty = 2)
legend("topright", col = c("black", "blue", "red"), lty = c(5,1,2),
      lwd = 2, legend = c('Almont', 'Observed', 'Modeled'))

```

```

NSE(PHQ_15_18[,10],PHQ_15_18[,8])
text(10, 15, expression("NSE = 0.97"), cex = 1.5)
# Nash-Sutcliffe coefficient = 0.97

```

```

# _____

```

```

# Format data for hydrograph analysis
write.csv(All_DailyQ_2014_2020,"All_DailyQ_2014_2020.csv")
write.csv(All_DailyQ_1910_2020,"All_DailyQ_1910_2020.csv")

```

```

ER_Q_35_20 <- All_DailyQ_1910_2020[All_DailyQ_1910_2020$year > 1934, ]
write.csv(ER_Q_35_20, "All_DailyQ_1935_2020.csv")

```

```

#####
# Create plots of Almont and East River

```

```

# _____
par(mfrow=c(1,1), mar=c(4,5,1,1), cex = 1)
All_Q_1910_2020 = All_DailyQ_1910_2020
ER_Q_55_20 <- All_Q_1910_2020[All_Q_1910_2020$year > 1954, ]

# _____
# Create a stacked plot of hydrographs for the period of record
# _____

par(mfrow=c(1,1), mar=c(4,5,2,2), cex = 1.5)

# Create an initial plot to add hydrographs from all years
plot(ER_Q_55_20$yday[ER_Q_55_20$year == 1955],
ER_Q_55_20$Mod_PH_Q_cms[ER_Q_55_20$year == 1955], type = "l",
  ylim = c(0,25), xlab = "Day of Year",
  ylab = expression(paste("Modeled discharge (m3, s-1,)")), lwd = 1,
  main = "East River 1955-2015")

# Create a smaller zoomed in plot to add hydrographs from all years
#plot(ER_Q_55_20$day[ER_Q_55_20$year == 1955], ER_Q_55_20[ER_Q_55_20$year == 1955,
3], type = "l",
#   ylim = c(0,11), xlim = c(160,220), xaxt = "n", xlab = "Day of Year", ylab = "Discharge (cms)",
lwd = 1, main = "East River 1955-2017")

# Create a list of unique years for the period of interest
years = unique(ER_Q_55_20$year)

# A for loop to plot hydrographs for all years on top of one another
for (i in 1:65) {
  years2plot = years[i]
  print(years2plot)
  dat.yr = subset(ER_Q_55_20, year == years2plot)
  print(dat.yr)
  lines(dat.yr$yday, dat.yr$Mod_PH_Q_cms, col = "royalblue1", lwd = 1)
}

# Calculate the mean and 95% confidence level for all hydrographs in the period of interest
AllFlow = ddply(ER_Q_55_20, ~yday, summarise,
  MeanFlow = mean(Mod_PH_Q_cms),
  LCI = quantile(Mod_PH_Q_cms, 0.025, na.rm = TRUE),
  UCI = quantile(Mod_PH_Q_cms, 0.975, na.rm = TRUE))

```

```

# Plot a transparent band representing the 95% confidence level
polygon(c(AllFlow$yday,rev(AllFlow$yday)),c(AllFlow$LCI,rev(AllFlow$UCI)),border=NA,
        col = rgb(red = 0.0, green = 0.0, blue = 0.5, alpha = 0.25))

#-----
# Plot mean hydrographs for 6 time intervals

Q_55_73 = ER_Q_55_20[ER_Q_55_20$year < 1974, ]
Q_74_83 = ER_Q_55_20[ER_Q_55_20$year > 1973 & ER_Q_55_20$year < 1984, ]
Q_84_90 = ER_Q_55_20[ER_Q_55_20$year > 1983 & ER_Q_55_20$year < 1991, ]
Q_91_01 = ER_Q_55_20[ER_Q_55_20$year > 1990 & ER_Q_55_20$year < 2002, ]
Q_02_11 = ER_Q_55_20[ER_Q_55_20$year > 2001 & ER_Q_55_20$year < 2012, ]
Q_12_17 = ER_Q_55_20[ER_Q_55_20$year > 2011, ]
Q_12_15 = ER_Q_55_20[ER_Q_55_20$year > 2011 & ER_Q_55_20$year < 2016, ]

par(mfrow=c(1,1), mar=c(4,4,2,2), cex = 1.5)

# Calculate the mean and 95% confidence level for all hydrographs in the period of interest
Flow73 = ddply(Q_55_73, ~yday, summarise,
              MeanFlow = mean(Mod_PH_Q_cms),
              LCI = quantile(Mod_PH_Q_cms, 0.025, na.rm = TRUE),
              UCI = quantile(Mod_PH_Q_cms, 0.975, na.rm = TRUE))
lines(Flow73$yday, type = "line", #ylim = c(0, 11),
      Flow73$MeanFlow, col = "red", lwd = 2.5,
      xlab = "Day of the year", ylab = "Discharge (cms)") # Plot the mean hydrograph value

# Calculate the mean and 95% confidence level for all hydrographs in the period of interest
Flow83 = ddply(Q_74_83, ~yday, summarise,
              MeanFlow = mean(Mod_PH_Q_cms),
              LCI = quantile(Mod_PH_Q_cms, 0.025, na.rm = TRUE),
              UCI = quantile(Mod_PH_Q_cms, 0.975, na.rm = TRUE))
lines(Flow83$yday,
      Flow83$MeanFlow, col = "orange", lwd = 2.5) # Plot the mean hydrograph value

# Calculate the mean and 95% confidence level for all hydrographs in the period of interest
Flow90 = ddply(Q_84_90, ~yday, summarise,
              MeanFlow = mean(Mod_PH_Q_cms),
              LCI = quantile(Mod_PH_Q_cms, 0.025, na.rm = TRUE),
              UCI = quantile(Mod_PH_Q_cms, 0.975, na.rm = TRUE))
lines(Flow90$yday,
      Flow90$MeanFlow, col = "yellow", lwd = 2.5) # Plot the mean hydrograph value

```

```
# Calculate the mean and 95% confidence level for all hydrographs in the period of interest
Flow01 = ddply(Q_91_01, ~yday, summarise,
  MeanFlow = mean(Mod_PH_Q_cms),
  LCI = quantile(Mod_PH_Q_cms, 0.025, na.rm = TRUE),
  UCI = quantile(Mod_PH_Q_cms, 0.975, na.rm = TRUE))
lines(Flow01$yday,
  Flow01$MeanFlow, col = "green", lwd = 2.5) # Plot the mean hydrograph value
```

```
# Calculate the mean and 95% confidence level for all hydrographs in the period of interest
Flow11 = ddply(Q_02_11, ~yday, summarise,
  MeanFlow = mean(Mod_PH_Q_cms),
  LCI = quantile(Mod_PH_Q_cms, 0.025, na.rm = TRUE),
  UCI = quantile(Mod_PH_Q_cms, 0.975, na.rm = TRUE))
lines(Flow11$yday,
  Flow11$MeanFlow, col = "darkblue", lwd = 3.5) # Plot the mean hydrograph value
```

```
# Calculate the mean and 95% confidence level for all hydrographs in the period of interest
Flow17 = ddply(Q_12_15, ~yday, summarise,
  MeanFlow = mean(Mod_PH_Q_cms),
  LCI = quantile(Mod_PH_Q_cms, 0.025, na.rm = TRUE),
  UCI = quantile(Mod_PH_Q_cms, 0.975, na.rm = TRUE))
lines(Flow17$yday,
  Flow17$MeanFlow, col = "black", lwd = 2.5) # Plot the mean hydrograph value
```

```
par(mfrow=c(1,1), mar=c(4,4,2,2), cex = 1.2)
legend(280, 25, legend = c("1955-1973", "1974-1983", "1984-1990", "1991-2001", "2002-2011",
"2012-2015"),
  col = c("red", "orange", "yellow", "green", "darkblue", "black"),
  lty = 1.2, lwd = 2.5, bg = "gray85")
```

```
#####
```

### ###Stream Flow Frequency Analysis and Recession Limb Quantification

```
#####
```

```
# From time lapse photos and the stage data, bankfull stage appears to occur at about 4 cms
```

```
#####
```

```
#setwd(loadpath)
```

```
#All_DailyQ_1935_2020 = read.csv("All_DailyQ_1935_2020.csv", stringsAsFactors = F)
```

```
#"All_DailyQ_1910_2020.csv", stringsAsFactors = F)
```

```
data = All_DailyQ_1935_2020 #"All_DailyQ_1910_2020.csv", stringsAsFactors = F)
```

```
dat.er = data[,c(2,3,5:9)]
```

```

dat.er$flow.er = dat.er$Mod_PH_Q_cms

# estimate lowflow conditions and a reference basflow by which to measure the recession limb
Lowflow = mean(na.omit(dat.er$flow.er[dat.er$month %in% list("10","11","12","1","2","3")]))
Baseflow = 1.91 #Lowflow #mean(na.omit(dat.er$flow.er[dat.er$month %in% list("9")]))
BFQ = 8 # define a threshold approximation for bankfull discharge
# Estimated bankfull at 8 cms

# Initialize storage variables
years = unique(dat.er$year) # Unique years for indexing (using water years (10/01-9/30))
years = years[years > 1934]

# Aggregate Yearly (or monthly) data by mean, median, max, and min (or anything else)
x = subset(dat.er, year %in% c(1935:2019))
statistics = as.data.frame(as.list(aggregate(flow.er ~ year ,data = x, FUN=function(x) c(mean
=mean(x), median=median(x), max = max(x),min = min(x)))))

maxflow = as.data.frame(matrix(ncol=10,nrow =85)#length(years))
# define the list of column names for the dataframe
names(maxflow) = c("year","peakdate","flow.er","BFflow", "BF_EndDay", "enddate",
"TotalSlope","BFslope","BF_StartDay","PeakSlope")

for (k in 2:85){
  # Skip years where insufficient data was collected using a # of days in year as threshold. bad
  if (length(dat.er$Date[dat.er$year == years[k]]) < 250) {
  }
  else {
    # find peak flows greater than 500cfs and corresponding year and Date
    dat.sub = subset(dat.er, year == years[k]) # Subset larger data set
    dat.sub$Date = as.Date(dat.sub$Date, format="%Y-%m-%d")
    medianflow = mean(dat.sub$flow.er[dat.sub$month %in% list("10","11","12")])
    #median(na.omit(dat.sub$flow)) # find median flow (used as a threshold, need better method)
    maxflow[k,3] = max(na.omit(dat.sub$flow.er)) # find and store peak flows
    maxflow[k,1] = years[k] # store year
    index = tail(which(dat.sub$flow.er == maxflow[k,3]), n=1) # find index of peak flow to
    detrmine the exact Date
    maxflow[k,2] = as.character(dat.sub$Date[index]) # Date of peak flow
    #as.Date(index, origin = dat.sub$Date[1]) #

    # Bankfull flow
    if (max(dat.sub$flow.er >= 8)) {
      indX1 = min(which(dat.sub$flow.er >= 8)) # index the date flow rises above BF
      indX = max(which(dat.sub$flow.er >= 8)) # index the date flow drops below BF
      BF_start = as.character(dat.sub$Date[indX1]) # Assign first date flow exceeds BF
    }
  }
}

```

```

maxflow[k,9] = BF_start # Assign first date flow exceeds BF
BF_end = as.character(dat.sub$Date[indX]) # Assign last date flow drops below BF
maxflow[k,5] = BF_end # Assign last date flow drops below BF
maxflow[k,4] = dat.sub$flow.er[indX]
}
else {
  maxflow[k,5] = NA
  maxflow[k,4] = NA
  maxflow[k,9] = NA
  indX = NA
  BF_start = NA
  BF_end = NA
  print(years[k])
}

## Extracting Recession limb
# This section finds the Dates corresponding to the peakflow (already found above) and a
later
# Date corresponding to "normal" flow conditions. I am currently using the median but it's a
bad
# metric.
# Starting at the index of the peak flow Date, step forward one day (increasing the index by 1)
and
# check if the flow that day is a certain percentage from the median value.
PeakDate = as.character(dat.sub$Date[index]) # used for extracting recession limb
maxdepth = maxflow[k,3] # used for extracting recession limb
repeat{
  index = index+1
  maxdepth = dat.sub$flow.er[index] # flow one day later
  if (is.na(maxdepth)){ # check if no flow was recorded
  } else if (Baseflow > (maxdepth)){ # Check if flow is within X% of median value
    break # was previously ((medianflow) + Qmin) > maxdepth))
    # The "index" term now identifies the obs where Q reaches a baseflow condition ~0.8cms
  } else if (index == length(dat.sub$flow.er)) {
    print(paste(dat.sub$year[1])) # identify the year
    break
    # This forces the loop to break if Q never falls below baseflow
  }
}
}
#*****
# Indexing for bankfull slope calculation
BFDate = maxflow[k,5]

if (is.na(maxflow[k,5]) == FALSE) {

```

```

repeat{
indX = indX+1 #increment one more day after last BF flow
BFQ = dat.sub$flow.er[indX] # flow one day later
if (is.na(BFQ)){ # check if no flow was recorded and do nothing
} else if (Baseflow > (BFQ)){ # Check if flow is within threshold of median value was
previously ((medianflow) + Qmin > (BFQ))
break # Exist loop if Q drops below baseflow and saved that Q value as BFQ
} else if (indX == length(dat.sub$flow.er)) {
print(paste(dat.sub$year[1]))
break # Exit loop if flow does not drop below baseflow
}
}
}
}

```

```

BaseDate = as.character(dat.sub$Date[index])
maxflow[k,6] = as.character(dat.sub$Date[index])
#FirstDate = dat.sub$Date[1] #Set the first date of the year

```

```

# Convert Dates to yday for duration calculations
BaseDay=yday(BaseDate)
PeakDay=yday(PeakDate)
BF_endDay=yday(BF_end)
BF_startDay=yday(BF_start)
Last_index=length(dat.sub$Date)
LastDay = yday(dat.sub$Date[Last_index])
BaseFlow_Date = as.Date(BaseDay, origin = dat.sub$Date[1])

```

```

#####
# Calculate and plot slopes of recession limb at various stages
# _____

```

```

# Calculate recession slope based on best fit regression line between all points
TotSlopeQ = dat.sub$Mod_PH_Q_cms[dat.sub$yday %in% c(PeakDay:BaseDay)]
TotSlopeDate = dat.sub$Date[dat.sub$yday %in% c(PeakDay:BaseDay)]
TotSlopeReg = lm(TotSlopeQ ~ TotSlopeDate)
summary(TotSlopeReg)

```

```

maxflow[k,7] = -1*TotSlopeReg$coefficients[2] #((maxflow[k,3])-Baseflow)/(BaseDay-
PeakDay) # Slope of line from start to end of recession limb
plot(dat.sub$Date, dat.sub$Mod_PH_Q_cms, type = "line", main = paste(years[k]),
ylab = "Discharge (cms)", xlab = NA)
points(TotSlopeDate, TotSlopeQ, pch = 19, col = "violet")
lines(TotSlopeDate, predict(TotSlopeReg), col = "purple", lwd = 2)

```

```

# Calculate slope as line between two points
#maxflow[k,7] = (maxflow[k,3]-Baseflow)/(BaseDay-PeakDay)
#plot(dat.sub$Date, dat.sub$Mod_PH_Q_cms, type = "line", main = paste(years[k]),
#  ylab = "Discharge (cms)", xlab = NA)
#points(TotSlopeDate, TotSlopeQ, pch = 19, col = "violet")
#QPoints = c(maxflow[k,3],Baseflow)
#TotDayPts =c(PeakDate, BaseDate)
#DayPoints = as.Date(TotDayPts, "%Y-%m-%d")
#lines(DayPoints, QPoints, col = "purple", lwd = 2)

# Calculate the recession slope from the peak to bankfull flow as the best fit line
if (is.na(maxflow[k,4])) {
  maxflow[k,10] = NA #Calculate slope of highest peak lower than bankfull to baseflow
}
else {

# Calculate recession slope based on best fit regression line between all points
PeakSlopeQ = dat.sub$Mod_PH_Q_cms[dat.sub$yday %in% c(PeakDay:BF_endDay)]
PeakSlopeDate = dat.sub$Date[dat.sub$yday %in% c(PeakDay:BF_endDay)]
PeakSlopeReg = lm(PeakSlopeQ ~ PeakSlopeDate)
summary(PeakSlopeReg)
points(PeakSlopeDate, PeakSlopeQ, pch = 20, col = "pink")
lines(PeakSlopeDate, predict(PeakSlopeReg), col = "red", lwd = 2)
maxflow[k,10] = -1*PeakSlopeReg$coefficients[2] #((maxflow[k,3])-
(maxflow[k,4]))/(BF_endDay-PeakDay) #Slope from peak to bankfull

# Calculate slope as line between two points
#maxflow[k,10] = (maxflow[k,3]-maxflow[k,4])/(BF_endDay-PeakDay)
#points(PeakSlopeDate, PeakSlopeQ, pch = 20, col = "pink")
#QPoints = c(maxflow[k,3],maxflow[k,4])
#PeakDayPts =c(PeakDate, BF_end)
#DayPoints = as.Date(PeakDayPts, "%Y-%m-%d")
#lines(DayPoints, QPoints, col = "red", lwd = 2)
}

# Calculate the bankfull slope from bankfull to base flow
if (is.na(maxflow[k,4])) {
  maxflow[k,8] = NA #Calculate slope of highest peak lower than bankfull to baseflow
}
else {
  # Calculate recession slope based on best fit regression line between all points
  BFSlopeQ = dat.sub$Mod_PH_Q_cms[dat.sub$yday %in% c(BF_endDay:BaseDay)]
  BFSlopeDate = dat.sub$Date[dat.sub$yday %in% c(BF_endDay:BaseDay)]
}

```

```

BFSlopeReg = lm(BFSlopeQ ~ BFSlopeDate)
summary(BFSlopeReg)
points(BFSlopeDate, BFSlopeQ, pch = 20, col = "lightblue")
lines(BFSlopeDate, predict(BFSlopeReg), col = "blue", lwd = 2)
maxflow[k,8] = -1*BFSlopeReg$coefficients[2]

# Calculate slope as line between two points
#maxflow[k,8] = (maxflow[k,4]-Baseflow)/(BaseDay-BF_endDay)
#points(BFSlopeDate, BFSlopeQ, pch = 20, col = "lightblue")
#QPoints = c(maxflow[k,4],Baseflow)
#BFDayPts =c(BF_end,BaseDate)
#DayPoints = as.Date(BFDayPts, "%Y-%m-%d")
#lines(DayPoints, QPoints, col = "blue", lwd = 2)

}

# Save year-days for duration calculations
maxflow[k,11] = BF_startDay
maxflow[k,12] = PeakDay
maxflow[k,13] = BF_endDay
maxflow[k,14] = BaseDay
maxflow[k,15] = BF_endDay - BF_startDay # Duration Of recession Limb
maxflow[k,16] = BaseDay - PeakDay # Duration Of recession Limb
maxflow[k,17] = BaseFlow_Date
maxflow[k,18] = LastDay # Last recorded day of the year

# Cumulative days before and after bankfull
if (is.na(BF_endDay)==FALSE) { # If there was a bankfull flow (i.e., BF_endDay is not NA)
  maxflow[k,19] = LastDay - BF_endDay # Calculate the days since BF ended
}
else { # if there was no bankfull flow that year...
  maxflow[k,19] = LastDay + maxflow[k-1,19] # add the total number of days in the year to the
days since BF in the previous year
}

if (is.na(BF_endDay)==FALSE) { # If there was a bankfull flow (i.e., BF_endDay is not NA)
  maxflow[k,20] = BF_startDay + maxflow[k-1,19] # Days since bankfull
}
else {
  maxflow[k,20] = LastDay + maxflow[k-1,19]
}
BaseStart = min(which(dat.sub$flow.er >= Baseflow))
maxflow[k,21] = dat.sub$yday[BaseStart]

```

```

}
}

names(maxflow) = c("year", "peakdate", "flow.er", "BFflow", "BF_EndDate", "enddate",
  "TotalSlope", "BFslope", "BF_StartDate", "PeakSlope", "BF_startDay",
  "PeakDay", "BF_endDay", "Base_endDay", "BankfullDuration", "RecDuration",
  "BaseFlow_Date", "LastDay", "CummDaysAfterBF", "CummDaysBeforeBF",
  "Base_startDay")

#maxflow = na.omit(maxflow) # Remove missing flow
#if (is.na(maxflow[,2]) == FALSE) {}
#maxflow$peakdate = as.Date(maxflow$peakdate)
#maxflow$enddate = as.Date(maxflow$enddate)
maxflow$duration = yday(maxflow$enddate)-yday(maxflow$peakdate) # Duration Of recession
Limb

# Generate ranks (note that R ranks opposite of what is desired)
maxflow$rank = (length(maxflow$year)+1)-rank(maxflow$flow.er)
maxflow$RI = (length(maxflow$year)+1)/maxflow$rank
# Calculate exceedence probability
maxflow$exceedence = 1/maxflow$RI
#maxflow$NonBFdays = maxflow$LastDay - (maxflow$BF_endDay - maxflow$BF_startDay)
#THis does not account for days before first and last BF day that do not have BF flow
maxflow$BaseDuration = maxflow$Base_endDay - maxflow$Base_startDay #THis does not
account for days before first and last BF day that do not have BF flow

maxflow1 = maxflow[2:85,]
maxflow = maxflow[,c(1,9,2,5,6,3,4,7,10,8,20,21,22,23,26,11:19,24,25)]

setwd(savepath)
write.csv(maxflow1, file = "Maxflow1_6.29.20_Base_1.91_BestFit.csv")
write.csv(maxflow, file = "Maxflow_6.29.20_Base_1.91_BestFit.csv")

#*****
# Create plots
maxflow1$enddate = as.Date(maxflow1$enddate, format="%Y-%m-%d")
maxflow1$peakdate = as.Date(maxflow1$peakdate, format="%Y-%m-%d")

plot(flow.er ~ maxflow1$RI, maxflow1, log = 'x',
  xlab = "Recurrence Interval (years)",
  ylab = "Annual Maximum discharge (cfs)",
  main = "Flood Frequency Curve of Estimated Peak Flows")

rm(list=setdiff(ls(), c("maxflow", "dat", "dat.almont", "dat.bc", "dat.er",

```

```
"hydrobounds","statistics","yearstats","years","colfunc",  
"loadpath","savepath","mod2","best.span", "Baseflow"))))
```

```
#####
```

```
#
```

```
# Recession Limb Characteristics
```

```
#
```

```
#####
```

```
hydrobounds = as.data.frame(matrix(ncol = 2, nrow = 85)) # create data frame for flow regime  
characteristics
```

```
names(hydrobounds) = c("start","end") # create colums for end and start dates for bankfull  
flow
```

```
#hydrobounds$start = maxflow$BF_StartDay
```

```
#hydrobounds$end = maxflow$BFdata
```

```
hydrobounds$EndDay = maxflow$BaseDay # assign the ending date
```

```
#maxflow$BF_StartDate = as.Date(maxflow$BF_StartDay)
```

```
for (k in 1:85){
```

```
  #print(k)
```

```
  years2plot = years[k] # create a list of each of the 83 years of record
```

```
  dat.sub = subset(dat.er, year%in%years2plot) # create a subset of data for the current year
```

```
  FirstDate = dat.sub$Date[1] #Set the first date of the year
```

```
  #
```

```
  # Calculate cummulative annual volume of water discharged by East River
```

```
  #dat.sub$yearVol[1] = dat.sub$flow.er[1]*86400 # set initial flow volume for 1st day
```

```
  dat.sub$AnnualVol[1] = dat.sub$flow.er[1]*86400 # set initial flow volume for 1st day
```

```
  for (n in 2:length(dat.sub$Date)){ # create for loop to add consecutive Q resulting in  
  cumulative annual Q
```

```
    dat.sub$AnnualVol[n] = dat.sub$AnnualVol[n-1] + dat.sub$flow.er[n]*86400 # sum each  
  consecutive flow volume for cummulative volume
```

```
  }
```

```
  #print(n)
```

```
  maxflow$AnnualVol[k] = dat.sub$AnnualVol[n] # assign the total ANnual volume of discharge  
  for each year
```

```
  dat.sub$BFVol = NA #create column for bankfull flow volume and fill with NA
```

```
  #
```

```
  # Calculate cummulative volume of overbank flow discharged by the East River
```

```

for (m in 1:length(dat.sub$Date)) {

  if (is.na(maxflow$BF_StartDate[k]) == FALSE) {
    # Set initial volume for first day above Bankful flow
    dat.sub$BFVol[which(maxflow$BF_StartDate[k]==dat.sub$Date)] =
dat.sub$flow.er[which(maxflow$BF_StartDate[k]==dat.sub$Date)]*86400 # set initial flow
volume for 1st day
    #Create indices for the start and end of bankfull flow
    BF_StartIndex = which(maxflow$BF_StartDate[k]==dat.sub$Date) # Index the row for the first
day of bankful flow begins
    BF_EndIndex = which(maxflow$BF_EndDate[k]==dat.sub$Date) #index the row for the last
day of bankful flow ends

    #Creat a loop to add cumulative volume of bankfull discharge
    for (p in BF_StartIndex+1:(BF_EndIndex-BF_StartIndex)) { # create for loop to add consecutive
Q resulting in cumulative annual Q
      #print(p)
      # Old calculations that estimates max BF volume for all days between 1st and last day of
bankfull flow. THis is an iver estimate
      dat.sub$BFVol[p] = dat.sub$BFVol[p-1] + dat.sub$flow.er[p]*86400 # sum each consecutive
flow volume for cummulative volume
      #print(dat.sub$Date[p])
    }
    maxflow$BFVol[k] = dat.sub$BFVol[p] # Assign yearly volume of flow above bankful to the
annual summary
  }
  else {
    dat.sub$BFVol[m] = NA #Assign days without bankful flow as NA values
    maxflow$BFVol[k] = NA #Assign years without bankful flow as NA values
    p=NA

  }
}

hydrobounds$cvol.er[k] = dat.sub$AnnualVol[length(dat.sub$AnnualVol)]
hydrobounds$BFVol[k] = dat.sub$BFVol[max(which(is.na(dat.sub$BFVol) == FALSE))]

### Model peaks and valleys

baseflowinitial = mean(dat.sub$flow.er[dat.sub$month %in% list("1", "2")]) # Set initial
baseflow conditions as the mean of flow in Jan and Feb
baseflowend = mean(dat.sub$flow.er[dat.sub$month %in% list("12")]) # Set ending baseflow
conditions as the mean flow in Dec

```

```

#create column index for the peaks defined by a rise in flow followed by a decline in flow
occurring in three consecutive days
peaks = which(diff(sign(diff(dat.sub$flow.er)))==2)+1
#create column index for the valleys defined by a decrease in flow followed by an increase in
flow occurring in three consecutive days
valleys = which(diff(sign(diff(dat.sub$flow.er)))==2)+1

peakbase = dat.sub$flow.er[peaks]-baseflowinitial
#print(peakbase)
valleybase = dat.sub$flow.er[valleys] - baseflowinitial
hydrographstart = 1 # Define HYDRGRAPHSTART

for (n in 1:length(peakbase)){
  if (length(valleys) < 1){
    hydrographstart = peaks[n]
    peaks[n]
    break
  }

  if(peakbase[n] > 40){ # Check if threshold was met
    if (peaks[n] < valleys[1]) { # Check if first peak is greater than threshold
      hydrographstart = peaks[n]
      break
    }
    else {
      firstvalley = max(valleys[valleys<peaks[n]])
    }

    hydrographstart = firstvalley
    break
  }
}

bankfullflow = dat.sub$flow.er[dat.sub$flow.er > 8]
maxflow$bankfullvol[k] = sum((bankfullflow)*86400) # sum the volume of water exceeding
bankfull flow
maxflow$bankfulldays[k] = length(bankfullflow)
hydrobounds[k,1] = hydrographstart
BaseDays = dat.sub$flow.er[dat.sub$flow.er > Baseflow]
maxflow$BaseflowDays[k] = length(BaseDays)
maxflow$NonBFdays[k] = maxflow$LastDay[k] - maxflow$bankfulldays[k]

if (k%%10 == 0){

```

```

}
hydrobounds$startdate[k] = as.character(dat.sub$Date[hydrobounds$start[k]])
}

# Write csv file of the temporary dat.sub datasheets for each year
#setwd(savepath)
write.csv(maxflow, "AnnualStats_6.29.20_Base_1.91_BestFit.csv", row.names = TRUE)

rm(list=setdiff(ls(), c("maxflow","dat","dat.almont","dat.bc","dat.er",
                        "hydrobounds","statistics","yearstats","years","colfunc",
                        "loadpath","savepath","mod2", "best.span")))

#### Extract Local Peaks above a specific flow rate above "bankfull"
#library("signal", lib.loc=~R/win-library/3.2")
library("signal")

# Estimated bankfull at 8 cms

for (k in 1:85){
  years2plot = years[k]
  dat.sub = subset(dat.er,year == years2plot)
  x1 = dat.sub$flow.er
  x1
  y1 = dat.sub$day

  #myfilter = butter(1, .2, type = 'low', plane='z')
  myfilter2 = filter(filt = sgolay(p = 12, n = 23), x = x1) # PEak Filter started at 11
  #myfilter3 = fftfilt(rep(1, 10)/10, x1, n = 365)
  myfilter4 = filter(filt = sgolay(p = 7, n = 15), x = x1) # p = 5, n = 17 # 10 & 15 Oct 2017 # VALLEY
  filter good as it gets

  #yfiltered = as.matrix(filter(myfilter, x1)) # apply filter
  yfiltered = myfilter2
  zfiltered = myfilter4
  ##print("*****")
  ##print(years2plot)
  plot(dat.sub$flow.er,type = "n", main = paste(years2plot))
  lines(yfiltered,col = "red")
  lines(dat.sub$flow.er)
  points(dat.sub$flow.er)

  #points(yfiltered[peaks]~dat.sub$day[peaks], pch = 19)

```

```

# PEaks
peaks = which(diff(sign(diff(yfiltered)))== -2)+1 #identify the peaks by setting a threshold
where the next point decreases by 2
##print(peaks)
points(yfiltered[peaks]~dat.sub$yday[peaks], pch = 20, col = "orange")
peaks2keep = (peaks[yfiltered[peaks] > 8])
##print("peaks 2 keep")
##print(length(peaks2keep))
#SortPeaks <- peaks2keep[order(dat.sub$flow.er)]
###print(SortPeaks)
##print(peaks2keep)
points(yfiltered[peaks2keep]~dat.sub$yday[peaks2keep], pch = 19, col = "red")

# Valleys
valleys = which(diff(sign(diff(zfiltered)))== 2)+1 #identify the trophs by setting a threshold
where the next point increases by 2
print("valleys")
print(valleys)
points(zfiltered[valleys]~dat.sub$yday[valleys], pch = 20, col = "green")
valleys2keep = (valleys[zfiltered[valleys] < 100])
print("valleys2keep")
print(valleys2keep)
points(zfiltered[valleys2keep]~dat.sub$yday[valleys2keep], pch = 19, col = "blue")

#PeakFlows = yfiltered(dat.sub$flow.er[peaks2keep])

truepeak = c()
truepeak[1] = tail(which(dat.sub$flow.er == maxflow$flow.er[k]), n=1) # Find the date of the
max flow and assign to peak flow
###print(truepeak)

RealPeaks = c()
leftthresh = c()
rightthresh = c()
PeakCount = 1
#NotPeak = 0
p = 0
Rp = 0
IsPeak = c()

for (n in 1:length(peaks2keep)) {

  if (length(peaks2keep) == 0){ # If no peaks exceed bankfull...

```

```

    #truepeak = yday(maxflow$peakdate[k]) #Determine julian day of max peakflow if below
bankfull
    ###print(peaks2keep)
    PeakCount = 0
    ##print(PeakCount)
    break
}

```

```

IsPeak[n] = "N"
leftthresh[n] = max(valleys2keep[valleys2keep < peaks2keep[n]]) # identify the valley
immediately before each peak above bankfull
rightthresh[n] = min(valleys2keep[valleys2keep > peaks2keep[n]]) # identify the valley
immediately after each peak aboe bankfull
p=p+1

```

```

##print(valleys2keep)
##print(leftthresh[n])
##print(peaks2keep[n])
##print(rightthresh[n])
##print(years[k])
##print(leftthresh[n])
##print(dat.sub$flow.er[leftthresh[n]])
##print(peaks2keep[n])
##print(dat.sub$flow.er[peaks2keep[n]])
##print(rightthresh[n])
##print(dat.sub$flow.er[rightthresh[n]])
##if (abs(yfiltered[peaks2keep[n]]-yfiltered[leftthresh[n]]) < 5 | # was <50 eliminates
# abs(yfiltered[peaks2keep[n]]-yfiltered[rightthresh[n]]) < 4){ # was <50
#q = 0
if (
    ((dat.sub$flow.er[peaks2keep[n]] - dat.sub$flow.er[leftthresh[n]]) > 2)
    & # peaks that are >2 cms from valey to left
    (dat.sub$flow.er[peaks2keep[n]] - dat.sub$flow.er[rightthresh[n]]) > 2 & # peaks that are
>2 cms from valey to right
    ((dat.sub$flow.er[rightthresh[n]]) < 10 | (dat.sub$flow.er[leftthresh[n]]) < 10) &
    #(n < length(peaks2keep) & peaks2keep[n+1] < rightthresh[n]) |
if (n > 1) {
    TRUE
    if (peaks2keep[n-1] < leftthresh[n]) {
        TRUE
    }
    else {
        FALSE
    }
}

```

```

        #IsPeak[n] = "N"
    }
} else {TRUE} #Just changed this from FALSE to TRUE
)
{
    truepeak[n] = leftthresh[n]-1+tail(which(dat.sub$flow.er[leftthresh[n]:rightthresh[n]] ==
max(dat.sub$flow.er[leftthresh[n]:rightthresh[n]])),n=1)
    Rp = Rp + 1
    RealPeaks[Rp] = peaks2keep[n]
    IsPeak[n] = "Y"
    #print("1st check _____")
    #print(peaks2keep[n])
    #print(IsPeak[n])
    ##print(p)
    ##print("1st Peaks to keep")
    ##print(peaks2keep[n])
    ##print(dat.sub$flow.er[peaks2keep[n]])
    ##print(rightthresh[n])
    ##print(dat.sub$flow.er[rightthresh[n]])
    ##print("Real peaks")
    ##print(length(RealPeaks))
    ##print(RealPeaks)
    ##print(RealPeaks[p])
    ##print(peaks2keep[n-1])
    ##print(RealPeaks[p-1])
}

else {
    ##print("Length of peaks 2 keep")
    ##print(length(peaks2keep))
    ##print("RealPeaks")
    ##print(length(RealPeaks))
    IsPeak[n] = "N"

if (length(peaks2keep) == 2 & n == 1) { #length(RealPeaks == 0) {
    #Rp = Rp + 1
    RealPeaks[1] = peaks2keep[n]
    IsPeak[n] = "Y"
    Rp = Rp + 1
    RealPeaks[Rp] = peaks2keep[n]
    ##print(length(RealPeaks))
    ##print("conditional met")
    ##print(length(RealPeaks))
    #print("3rd check _____")
}
}

```

```

# print(peaks2keep[n])
# print(IsPeak[n])
} else {

# Check all but the last and first point for issues
if ((n > 1) & (n < length(peaks2keep))) { # NEED TO CORRECT THIS LINE
  ## print("checking small cluster peaks")
  # print("4th check _____")
  # print(peaks2keep[n])
  # print(IsPeak[n])
  IsPeak[n] = "N"
  # TRUE

if(
  (((dat.sub$flow.er[peaks2keep[n]] - dat.sub$flow.er[rightthresh[n]]) > 2) &
  (((dat.sub$flow.er[peaks2keep[n]] - dat.sub$flow.er[leftthresh[n]]) < 2))# |
  #(dat.sub$flow.er[leftthresh[n]] > 10))
  &
  ((IsPeak[n-1] == "N") &
  (dat.sub$flow.er[leftthresh[n]] < 10 | dat.sub$flow.er[leftthresh[n-1]] < 10 ))) |

  (((dat.sub$flow.er[peaks2keep[n]] - dat.sub$flow.er[rightthresh[n]]) < 2) &
  (((dat.sub$flow.er[peaks2keep[n]] - dat.sub$flow.er[leftthresh[n]]) > 2)) &
  (dat.sub$flow.er[leftthresh[n]] < 10) &
  (leftthresh[n] > peaks2keep[n-1] | IsPeak[n-1] == "N") &
  rightthresh[n] < peaks2keep[n+1])
  #& (IsPeak[n-1] == "N")
  # This creates an error because there is no value when there is no peak detected
  )
  {
  # TRUE
  truepeak[n] = leftthresh[n]-1+tail(which(dat.sub$flow.er[leftthresh[n]:rightthresh[n]] ==
  max(dat.sub$flow.er[leftthresh[n]:rightthresh[n]])), n=1)
  Rp = Rp + 1
  RealPeaks[Rp] = peaks2keep[n]
  IsPeak[n] = "Y"
  # print("5th check _____")
  # print(peaks2keep[n])
  # print(IsPeak[n])
  ## print(Rp)
  ## print("2nd Peaks to keep")
  ## print(peaks2keep)
  ## print(peaks2keep[n])
  ## print(peaks2keep[n-1])

```

```

##print(dat.sub$flow.er[peaks2keep[n]])
##print(rightthresh[n])
##print(dat.sub$flow.er[leftthresh[n]])
##print(dat.sub$flow.er[peaks2keep[n]])
##print("Real peaks")
##print(length(RealPeaks))
##print(RealPeaks) # Results in NA with no detected peak
##print(RealPeaks[Rp])
##print(RealPeaks[Rp-1])

}

} else {
IsPeak[n] = "N"
#print("6th check_____")
#print(peaks2keep[n])
#print(IsPeak[n])

}

#Check last point and first point for discrepancies
if (n == length(peaks2keep)) {
  #print("8th check_____")
  #print(peaks2keep[n])
  IsPeak[n] = "N"
  #print(IsPeak[n])
  TRUE

  if( ((dat.sub$flow.er[peaks2keep[n]] - dat.sub$flow.er[leftthresh[n]]) > 2 &
      (dat.sub$flow.er[peaks2keep[n]] - dat.sub$flow.er[rightthresh[n]]) > 1 & # peaks that
are >2 cms from valey to right
      (dat.sub$flow.er[leftthresh[n]]) < 10 &
      leftthresh[n] > peaks2keep[n-1]) |

      (((dat.sub$flow.er[peaks2keep[n]] - dat.sub$flow.er[rightthresh[n]]) > 2) &
      (((dat.sub$flow.er[peaks2keep[n]] - dat.sub$flow.er[leftthresh[n]]) < 2)) &
      #(IsPeak[n-1] == "N" |
      (leftthresh[n] != rightthresh[n-1])) #|

      #(((dat.sub$flow.er[peaks2keep[n]] - dat.sub$flow.er[rightthresh[n]]) < 2) &
      # (((dat.sub$flow.er[peaks2keep[n]] - dat.sub$flow.er[leftthresh[n]]) > 2)) &
      # (dat.sub$flow.er[leftthresh[n]] < 10))# &
      # leftthresh[n] > peaks2keep[n-1] &
      #rightthresh[n] < peaks2keep[n+1])

```

```

)
{
  TRUE
  truepeak[n] = leftthresh[n]-1+tail(which(dat.sub$flow.er[leftthresh[n]:rightthresh[n]] ==
max(dat.sub$flow.er[leftthresh[n]:rightthresh[n]])), n=1)
  Rp = Rp + 1
  RealPeaks[Rp] = peaks2keep[n]
  IsPeak[n] = "Y"
  #print("9th check _____")
  #print(peaks2keep[n])
  #print(IsPeak[n])
}

} else {
  FALSE
  if (n == 1) {
    #print("10th check _____")
    #print(peaks2keep[n])
    #print(IsPeak[n])
    ##print(dat.sub$flow.er[peaks2keep[n]])
    ##print(dat.sub$flow.er[rightthresh[n]])
    TRUE

    if ((dat.sub$flow.er[peaks2keep[n]] - dat.sub$flow.er[rightthresh[n]]) > 2 &
      (dat.sub$flow.er[peaks2keep[n]] - dat.sub$flow.er[leftthresh[n]]) > 2 &
      dat.sub$flow.er[leftthresh[n]] < 10 &
      dat.sub$flow.er[rightthresh[n]] < 10 &
      rightthresh[n] < peaks2keep[n+1]) {
      TRUE
      IsPeak[n] = "Y"
      Rp = Rp + 1
      RealPeaks[Rp] = peaks2keep[n]
      #print("11th check _____")
      #print(peaks2keep[n])
      #print(IsPeak[n])
    }
  }
}

}
}
if (length(RealPeaks) == 0 & length(peaks2keep) != 0) {
  #TRUE

```

```

    RealPeaks[1] = 1
  }
  PeakCount = length(RealPeaks) #PeakCount + p
  ##print("PeakCount")
  ##print(PeakCount)
}

truepeak = na.omit(truepeak)
##print(truepeak)
##print(peaks2keep)
#points(dat.sub$flow.er[truepeak]~dat.sub$day[truepeak], pch = 19)
#points(yfiltered[valleys]~dat.sub$day[valleys], pch = 19, col = "blue")

#hydrobounds$peak[k] = length(truepeak)
hydrobounds$peak[k] = PeakCount
bankfullflow = dat.sub$flow.er[dat.sub$flow.er > 8] # define bankfull flow threshold
hydrobounds$bankfullvol[k] = sum((bankfullflow)*86400) # sum the volume of water
exceeding bankfull flow
hydrobounds$bankfulldays[k] = length(bankfullflow)

}

yearstats = cbind(maxflow[,-c(4,5)],hydrobounds[,-c(1,2)],statistics[,-1])
# You will have to rename the headers in excel unless I get some time to go back and clean
things up a bit

#setwd(savepath)
write.csv(yearstats,"YearlyStatistics_6.29.20_Base_1.91_BestFit.csv")

rm(list=setdiff(ls(), c("maxflow","dat","dat.almont","dat.bc","dat.er",
  "hydrobounds","statistics","yearstats","years","colfunc",
  "loadpath","savepath","mod2", "best.span")))

# This code will average variables for periods between imagery along the East River

# Author: Nicholas A. Sutfin
# Date: April 2020

library("plyr")
#library("smwrBase", lib.loc=~R/win-library/3.2")
library("lattice") #, lib.loc="C:/Program Files/R/R-3.3.0/library")

```

```

library("lubridate")
library("hydroGOF")

# User space same as save path from steps 1-4
savepath = '/Users/NicholasSutfin/Documents/EastRiver/ER_Rcode/Baseflow_1.91_BestFit/' #
Calculating slope as line between 1st and last points (2p)
setwd(savepath)
# Load ALmont data for 2015-2017 as csv file, convert to SI units, code the date as a date, and
define the year
#Alm_Q <- read.csv("ER_AlmQ_2015-2017.csv", header=TRUE)
AnnualStats <- read.csv("YearlyStatistics_6.29.20_Base_1.91_BestFit.csv", header=TRUE)
AnnualStats$period = NA

for (i in 2:length(AnnualStats$year)) {
  #AnnualStats$TimeSinceBF[i] = AnnualStats$BF_startDay[i] + AnnualStats$DaysSinceBF[i-1]
  if (AnnualStats$year[i] < 1955){
    AnnualStats$period[i] = "before1955"
  }
  if (AnnualStats$year[i] > 1954 & AnnualStats$year[i] < 1974){
    AnnualStats$period[i] = "1955to1973"
  }
  if (AnnualStats$year[i] > 1973 & AnnualStats$year[i] < 1984){
    AnnualStats$period[i] = "1974to1983"
  }
  if (AnnualStats$year[i] > 1983 & AnnualStats$year[i] < 1991){
    AnnualStats$period[i] = "1984to1990"
  }
  if (AnnualStats$year[i] > 1990 & AnnualStats$year[i] < 2002){
    AnnualStats$period[i] = "1991to2001"
  }
  if (AnnualStats$year[i] > 2001 & AnnualStats$year[i] < 2012){
    AnnualStats$period[i] = "2002to2011"
  }
  if (AnnualStats$year[i] > 2011 & AnnualStats$year[i] < 2016){
    AnnualStats$period[i] = "2012to2015"
  }
  if (AnnualStats$year[i] > 2015){
    AnnualStats$period[i] = "after2015"
  }
}

#na.rm(AnnualStats)

DecadalStats = ddp(AnnualStats, ~period, summarise,

```

```

    MeanPeakDay = mean(PeakDay),
    MeanPeakQ = mean(flow.er), MaxPeakQ = max(flow.er),
    MeanBFDuration = mean(BankfullDuration, na.rm=TRUE), MaxBFDuration =
max(BankfullDuration, na.rm=TRUE),
    MeanBFDays = mean(bankfulldays, na.rm=TRUE), MaxBFDays = max(bankfulldays,
na.rm=TRUE),
    MeanBaseDuration = mean(BaseDuration, na.rm=TRUE), MaxBaseDuration =
max(BaseDuration, na.rm=TRUE),
    MeanBaseDays = mean(BaseflowDays, na.rm=TRUE), MaxBaseDays =
max(BaseflowDays, na.rm=TRUE),
    MeanDaysAfterBF = mean(CummDaysAfterBF, na.rm=TRUE), MaxDaysAfterBF =
max(CummDaysAfterBF),
    MeanDaysB4_BF = mean(CummDaysBeforeBF, na.rm=TRUE), MaxDaysB4_BF =
max(CummDaysBeforeBF, na.rm=TRUE),
    MeanNonBFdays = mean(NonBFdays, na.rm=TRUE), MaxNonBFdays =
max(NonBFdays, na.rm=TRUE),
    MeanBaseDay = mean(Base_endDay, na.rm=TRUE), MeanBF_EndDay =
mean(BF_endDay, na.rm=TRUE),
    MeanPeaks = mean(peak, na.rm=TRUE), MaxPeaks = max(peak, na.rm=TRUE),
    MeanTotSlope = mean(TotalSlope, na.rm=TRUE), MaxTotSlope = max(TotalSlope,
na.rm=TRUE),
    MeanBFSlope = mean(BFSlope, na.rm=TRUE), MaxBFSlope = max(BFSlope,
na.rm=TRUE),
    MeanPeakSlope = mean(PeakSlope, na.rm=TRUE), MaxPeakSlope = max(PeakSlope,
na.rm=TRUE),
    MeanAnnualVol = mean(AnnualVol), MaxAnnualVol = max(AnnualVol),
    TotAnnualVol = sum(AnnualVol),
    # ALtered 6.26.2020 to include volume for days above BF rather than all days
between first and last BF days
    MeanBFVol = mean(bankfullvol,na.rm=TRUE), MaxBFVol =
max(bankfullvol,na.rm=TRUE),
    TotBFDuration = sum(BankfullDuration, na.rm=TRUE), TotBaseDuration =
sum(BaseDuration, na.rm=TRUE),
    TotNonBFdays = sum(NonBFdays, na.rm=TRUE), TotBF_EndDay = sum(BF_endDay,
na.rm=TRUE),
    TotDaysB4_BF = sum(CummDaysBeforeBF, na.rm=TRUE), TotDaysAfterBF =
sum(CummDaysAfterBF),
    TotBFVol = sum(BFVol, na.rm=TRUE))

#setwd(savepath)
write.csv(DecadalStats, "TimePeriodStats_6.29.20_1.91_BestFit.csv", row.names = TRUE)

# This code will examine 15 min hydrograph datasets from the ALmont gage and East River
study site

```

```
# to quantify fluctuations above and below bankfull along the recession limb
```

```
# Author: Nicholas A. Sutfin
```

```
# Date: Oct. 18th 2017
```

```
# This code will examine to hydrograph dataset, select matching days
```

```
# and times and conduct a regression that can be used to fill in missing data
```

```
# Author: Nicholas A. Sutfin
```

```
# Date: Oct. 18th 2017
```

```
library(plyr)
```

```
library(chron)
```

```
library(tidyr)
```

```
#library(smwrBase, lib.loc=~R/win-library/3.2)
```

```
library(lattice) #, lib.loc=C:/Program Files/R/R-3.3.0/library)
```

```
library(lubridate)
```

```
library(hydroGOF)
```

```
library(OHLCMerge)
```

```
library(corrplot)
```

```
library(lmtest)
```

```
library(car)
```

```
library(MASS)
```

```
library(Hmisc)
```

```
# Set user space on LANL PC
```

```
loadpath = '/Users/NicholasSutfin/Documents/EastRiver/ER_Rcode'
```

```
savepath = '/Users/NicholasSutfin/Documents/EastRiver/ER_Rcode'
```

```
setwd(loadpath)
```

```
#setwd("/Users/306722/Documents/EastRiver/ER_Rcode")
```

```
# Load Almont data for 2015-2017 as csv file, convert to SI units, code the date as a date, and  
define the year
```

```
Alm_15Q <- read.csv("Almont_30minQ_1987_2020.csv", header=TRUE) #load USGS discharge  
data
```

```
Alm_15Q$Discharge_cfs =
```

```
as.numeric(levels(Alm_15Q$Discharge_cfs))[Alm_15Q$Discharge_cfs] # convert Q factors to  
numeric values
```

```
which(is.na(Alm_15Q$Discharge_cfs) == TRUE) #Check for NA values
```

```
Alm_15Q$AlmQ_cms = Alm_15Q$Discharge_cfs*0.0283168 # Calculate Q conversion from cfs to  
cms
```

```
which(is.na(Alm_15Q$Discharge_cfs) == TRUE) # check for NA values after numeric conversion
```

```
Alm_15Q$date = as.Date(Alm_15Q$date, format="%m/%d/%y") # convert Q factors to numeric  
values
```

```

Alm_15Q$DaTime = paste(Alm_15Q$date, Alm_15Q$time)
Alm_15Q$DateTime = as.POSIXct(Alm_15Q$DaTime, format = "%Y-%m-%d %H:%M")
Alm_15Q$year = year(Alm_15Q$Date)
Alm_15Q$month = month(Alm_15Q$Date)
Alm_15Q$Calday = day(Alm_15Q$Date)
Alm_15Q$Yday = yday(Alm_15Q$Date)
#Alm_15Q$Yday = yday(Alm_15Q$Date)
Alm_15Q = as.data.frame(Alm_15Q)
#
# Load Pump house data for 2015-2017 as csv file, convert to SI units, code the date as a date,
and define the year
PH_10Q <- read.csv("PHQ_2014_2018.csv", header=TRUE)
#PH_10Q <- read.csv("PH_10Q.csv", header=TRUE) #load East River pump house discharge data
PH_10Q$DateTime = as.POSIXct(PH_10Q$date, format = "%m/%d/%y %H:%M")
PH_10Q$year = year(PH_10Q$DateTime)
PH_10Q$month = month(PH_10Q$DateTime)
PH_10Q$Calday = day(PH_10Q$DateTime)
PH_10Q$Time = format(as.POSIXct(strptime(PH_10Q$DateTime, "%Y-%m-%d %H:%M", tz="")),
,format = "%H:%M")
PH_10Q$Yday = yday(PH_10Q$DateTime)
PH_10Q = as.data.frame(PH_10Q)
#plot(PH_10Q$DateTime, PH_10Q$PHQ_cms, type = "l", col = "blue")

#
# Find matching date-time combinations and create new dataset
#PH_Q_match =
Alm_15Qnew1 = Alm_15Q[,c(4,6,7,8,9,2,10)][!duplicated(Alm_15Q$DateTime),]
Alm_15Qnew = Alm_15Qnew1[which(is.na(Alm_15Qnew1$DateTime) == FALSE),]
PH_10Qnew = PH_10Q[,c(2:8)]

Q_int <- intersect.POSIXct(PH_10Qnew$DateTime, Alm_15Qnew$DateTime)
Alm_Q_match <- Alm_15Qnew[Alm_15Qnew$DateTime %in% Q_int, ] #Alm_15Q[Q_int, ] #
PH_Q_match <- PH_10Qnew[PH_10Qnew$DateTime %in% Q_int, ] #PH_10Q[Q_int, ] #
Q_diff <- setdiff(PH_Q_match$DateTime, Alm_Q_match$DateTime)
#which(PH_Q_match$DateTime == NA)
#which(Alm_Q_match$DateTime == NA)
All_Qmatch <- cbind(Alm_Q_match, PH_Q_match)

# Create a smaller zoomed in plot to view Q around Bankfull Q (8 cms)
plot(All_Qmatch$DateTime, All_Qmatch$PHQ_cms, type = "l",
ylim = c(5,10), xlab = "Day of Year", ylab = "Discharge (cms)", lwd = 1, main = "East River 2015
recession")

# Plot discharge data

```

```

plot(All_Qmatch$DateTime, All_Qmatch$AlmQ_cms, col = "blue", type = "l")
lines(All_Qmatch$DateTime, All_Qmatch$PHQ_cms, col = "royalblue", type = "l")
# _____
# Linear regression between the Almont and PH gauges 2014-2016

Qreg <- lm(All_Qmatch$PHQ_cms ~ All_Qmatch$AlmQ_cms, data = All_Qmatch)
summary(Qreg)
Qreg # adjusted R squared = 0.95
# For all days: PHQ = -0.081804 + 0.211284(Alm)
# Excluding frozen days, regression output: PHQ = 0.010948 + 0.211611(Alm)

par(mfrow=c(1,1), mar=c(4,4,2,2), cex = 1, lwd = 1)
plot(All_Qmatch$AlmQ_cms, All_Qmatch$PHQ_cms, col = "blue",
     xlab = "Discharge at Almont (cms)", ylab = "Discharge at Study Site (cms)")
lines(All_Qmatch$AlmQ_cms, Qreg$coefficients[1] +
      Qreg$coefficients[2]*All_Qmatch$AlmQ_cms,
      col = "black")
par(cex = 0.6)
#points(All_Qmatch$AlmQ_cms, All_Qmatch$PHQ_cms, pch = 19, col = "red")
text(10, 15, expression("r"^{2} ~"= 0.94"), cex = 1.5)

# Use regression to extend daily Q for PH based on Almont flow
# _____
# regression output: PHQ = -0.081804 + 0.211284(Alm)

# Reduce Almont Data size
Alm_15Q_sel = Alm_15Qnew[((Alm_15Qnew$time == "0:00") | (Alm_15Qnew$time == "1:00")
| (Alm_15Qnew$time == "2:00") |
      (Alm_15Qnew$time == "3:00") | (Alm_15Qnew$time == "4:00") |
(Alm_15Qnew$time == "5:00") |
      (Alm_15Qnew$time == "6:00") | (Alm_15Qnew$time == "7:00") |
(Alm_15Qnew$time == "8:00") |
      (Alm_15Qnew$time == "9:00") | (Alm_15Qnew$time == "10:00") |
(Alm_15Qnew$time == "11:00") |
      (Alm_15Qnew$time == "12:00") | (Alm_15Qnew$time == "13:00") |
(Alm_15Qnew$time == "14:00") |
      (Alm_15Qnew$time == "15:00") | (Alm_15Qnew$time == "16:00") |
(Alm_15Qnew$time == "17:00") |
      (Alm_15Qnew$time == "18:00") | (Alm_15Qnew$time == "19:00") |
(Alm_15Qnew$time == "20:00") |
      (Alm_15Qnew$time == "21:00") | (Alm_15Qnew$time == "22:00") |
(Alm_15Qnew$time == "23:00") |
      (Alm_15Qnew$time == "24:00")), ]

```

```

All_Q_1987_2020 = Alm_15Q_sel[which(is.na(Alm_15Q_sel$AlmQ_cms) == FALSE), ] #[
,c(6,1,7:9,2,10,4)]
All_Q_1987_2020$Mod_PHQ_cms = Qreg$coefficients[1] +
Qreg$coefficients[2]*All_Q_1987_2020$AlmQ_cms

# Plot a zoomed in window of the recession limb for 2017
Flow2017 = All_Q_1987_2020[All_Q_1987_2020$year == 2017,]
Recession2017 = Flow2017[Flow2017$month == 6,]
Recession2017 = Recession2017[Recession2017$Calday > 6,]
DailyQ = ddply(Recession2017, ~Yday, summarise,
  MeanQ = median(Mod_PHQ_cms),
  DateTime = min(DateTime))

Rmax = max(Recession2017$DateTime)
Rmin = min(Recession2017$DateTime)
window1 <- data.frame(xmin=Rmin, xmax=Rmax, ymin=8, ymax=11)
window2 <- data.frame(xmin=Rmin, xmax=Rmax, ymin=5, ymax=12)

ggplot(data=Recession2017, aes(x=DateTime, y=Mod_PHQ_cms)) +
  geom_path() +
  geom_line(data = DailyQ, aes(x = DateTime , y = MeanQ, colour = 003399)) +
  geom_line(data=Recession2017, aes(x=DateTime, y=Mod_PHQ_cms)) +
  labs(y = expression(paste("Discharge (m3", "s-1",")"), x = "")) +
  theme(axis.title.x = element_blank()) +
  theme(text = element_text(size=13)) +
  scale_y_continuous(minor_breaks = seq(6,16,1), breaks = seq(6,16,2)) +
  geom_rect(data=window2, aes(xmin=Rmin, xmax=Rmax, ymin=5, ymax=10), fill="blue",
alpha=0.20, inherit.aes = FALSE) +
  geom_rect(data=window1, aes(xmin=Rmin, xmax=Rmax, ymin=7.95, ymax=8.05), fill="red",
alpha=0.5, inherit.aes = FALSE)

#geom_rect(x=x, aes(xmin=Rmin, xmax=Rmax, ymin=8, ymax=11, alpha=.5))
#geom_density(aes(, alpha=.5))

#####

#####
# Recession Limb Characteristics
#####

#####

```

```

years = c("1988", "1989", "1990", "1991", "1992", "1993", "1994", "1995", "1996",
          "1997", "1998", "1999", "2000", "2001", "2002", "2003", "2004", "2005",
          "2006", "2007", "2008", "2009", "2010", "2011", "2012", "2013", "2014",
          "2015", "2016", "2017", "2018", "2019")

DielYears = data.frame("Years" = years)
DielYears$PeakDate = as.POSIXlt(All_Q_1987_2020$DateTime[1], format = "%Y-%m-%d
%H:%M:%S")
par(cex = 1, mar = c(4,4,2,1))
BFmin = 5
BFmax = 10
DielFluctuation = 2

for (p in 1:length(years)) {
  DataYear = years[p]
  DielData = subset(All_Q_1987_2020, year%in%DataYear)
  DielRec = 0
  AllDiel = 0
  DielYears$PeakFlow[p] = max(DielData$Mod_PHQ_cms[which(is.na(DielData$Mod_PHQ_cms)
== FALSE)]) #max(DielData$Mod_PHQ_cms)
  DielYears$PeakDate[p] = as.POSIXlt(DielData$DateTime[max(which(DielData$Mod_PHQ_cms
== DielYears$PeakFlow[p]))], format = "%Y-%m-%d %H:%M:%S")
  DielYears$PeakDay[p] = yday(DielYears$PeakDate[p])
  DielYears$PostPeakDays[p] = max(DielData$Yday) - DielYears$PeakDay[p]
  PeakIndex = which(DielData$DateTime == DielYears$PeakDate[p])
  DielPeaks = c()
  DielTotal = 0
  maxDiel = 0
  minDiel = 0
  #print("_____")
  #print(years[p])
  #print(DielPeaks)
  #print(minDiel)
  #print(maxDiel)
  #print(AllDiel)
  #print(DielRec)

#Find unique days for the year on record
UniqDays = unique(DielData$Yday)
PostPeakUniq = UniqDays[UniqDays > DielYears$PeakDay[p]]

```

```

if (DielYears$PeakFlow[p] > 6) {

  for (r in 2:length(UniqDays)) {
    # Assign daily max and min discharge values
    DailyFlow = subset(DielData, DielData$Yday == UniqDays[r])
    Dmax = max(DailyFlow$Mod_PHQ_cms)
    #DmaxIndex = which(DailyFlow$Mod_PHQ_cms == Dmax)
    Dmin = min(DailyFlow$Mod_PHQ_cms)

    if (((Dmax < BFmax) | (Dmin > BFmin)) & ((Dmax - Dmin) > DielFluctuation)) {
      AllDiel = AllDiel + 1
    }
    DielYears$AllDiel[p] = AllDiel # Record number of times Q crosses BF during the entire year
  }
  #print("-----")
  #print(years[p])
  #print("YES")
  for (q in 1:length(PostPeakUniq)) {
    # Assign daily max and min discharge values
    DailyFlow = subset(DielData, DielData$Yday == PostPeakUniq[q])
    Dmax = max(DailyFlow$Mod_PHQ_cms)
    #DmaxIndex = which(DailyFlow$Mod_PHQ_cms == Dmax)
    Dmin = min(DailyFlow$Mod_PHQ_cms)

    if (((Dmax < BFmax) | (Dmin > BFmin)) & ((Dmax - Dmin) > DielFluctuation)) {

      DielRec = DielRec + 1
      DielPeaks[DielRec] = DailyFlow$Yday # Index the day of year for each Q that crosses BF
after peak flow
      #print(length(DielPeaks))
      #print(DielPeaks)
      maxDiel = max(DielPeaks)
      minDiel = min(DielPeaks)
      DielRange = Dmax - Dmin
      DielTotal = DielTotal + DielRange
      DielYears$minDiel[p] = minDiel
      DielYears$maxDiel[p] = maxDiel

      # Plot portion of recession limb within bankfull window
      days = c(minDiel, maxDiel)
      Qlow = c(BFmin, BFmin)
      Qhigh = c(BFmax, BFmax)
      #plot(DielData$day, DielData$Mod_PHQ_cms, type = "l", main = paste(years[p]),

```

```

#ylim = c(6,10), xlim = c(DielYears$minDiel[p]-1,DielYears$maxDiel[p]+1),
#xlab = "Day of Year", ylab = "Discharge (cms)", lwd = 1)
#lines(c(0,250), c(8,8), col="blue")

# plot a transparent band around the bankfull window
#polygon(c(days, rev(days)), c(Qlow, Qhigh), border = NA,
#col = rgb(red = 0.0, green = 0.0, blue = 0.5, alpha = 0.4))
}
AveDielRange = DielTotal/DielRec
DielYears$TotalDielRange[p] = DielTotal
DielYears$AveDielRange[p] = AveDielRange
DielYears$DielRec[p] = DielRec # Record number of times Q crosses BF during recession limb

}
#plot(DielData$day, DielData$Mod_PHQ_cms, type = "l", main = paste(years[p]),
#xlab = "Day of Year", ylab = "Discharge (cms)", lwd = 1)
}

else {
#print("-----")
#print(years[p])
#print("NO")
DielYears$TotalDielRange[p] = NA
DielYears$AveDielRange[p] = NA
DielYears$DielRec[p] = NA
DielYears$minDiel[p] = 0
DielYears$maxDiel[p] = 0
}
}

```

## DielYears

```

# THis data was combined with the average statistics form the hydrologic and
# imagery analysis to produce the datasheet used below

```

```

#####
#####
# Conduct Multiple Regression to examine role of diel fluctuations on erosion
#####
#####

```

```

# Load data on Mac with slope analysis from primary 60 year analysis derived from daily mean
data
# Set user space

```

```

savepath =
'/Users/NicholasSutfin/Documents/EastRiver/ER_Rcode/Baseflow_0.49_2p_corrected/' #
Calculating slope as line between 1st and last points (2p)
setwd(savepath)
write.csv(DielYears,"DielRecessionDate_6.30.20_2cms_>6_5_10.csv")

# Load other hydrologic variables from baoder analysis and 6 year hydro record
YearlyHydroStats <- read.csv("DielRecessionRegData_6.29.20.csv", header=TRUE)

# cbind annual hydrologic data with diel data
DielRegData = cbind(DielYears, YearlyHydroStats)

DielRegData = DielRegData[(which(is.na(DielRegData$DielRec) == FALSE)), ]

for (i in 1:length(DielRegData$Years)) {
  if (DielRegData$DielRec[i] == 0) {
    DielRegData$AveDielRange[i] = 0
  }
}

#=====
#Assign variables
#RespVar = DielRegData$AveDielRange
Preds = subset(DielRegData, select = c(6:9,16:18)) #c(3:6,9:52))
Preds[, c(1:7)] <- sapply(Preds[, c(1:7)], as.numeric)

# examine subset correlations
par(mfrow=c(1,1), mar=c(3,3,3,2), cex = 1.3)
DataCorr = cor(Preds, method = "pearson")
corrplot(DataCorr)

CorrT = rcorr(as.matrix(Preds), type = "pearson")
CorrRtable = data.frame(CorrT$r)
CorrPtable = data.frame(CorrT$p)
CorrT

write.csv(CorrRtable, file = "DielData_RCorrs_6.30.20_2cms_>6_5_10.csv") # with new data
from new stats calculated June 2020
write.csv(CorrPtable, file = "DielData_PCorrs_6.30.20_2cms_>6_5_10.csv")

#####
# Number of Diel Fluctuations
# _____

```

```
cor.test(Preds$TotalSlope, Preds$DielRec)
DielRecReg = lm(Preds$TotalSlope ~ Preds$DielRec, data=Preds)
summary(DielRecReg)
```

```
ggplot(Preds, aes(x=TotalSlope, y=DielRec)) +
  geom_point(color='#D55E00', size = 3) +
  geom_smooth(method=lm, color='#2C3E50', linetype="dashed") +
  theme(text = element_text(size=13)) +
  labs(title = "2cms fluctuations >6cms from 5-10cms window",
        y=expression(paste("Number of diel fluctuations > 2 m3", "s-1")),
        x = expression(paste("Slope of recession limb (m3", "s-1", "day-1,"))))
```

```
#####
# Total sum magnitude of diel fluctuation
# _____
```

```
cor.test(Preds$TotalSlope, Preds$TotalDielRange)
```

```
ggplot(Preds, aes(x=TotalSlope, y=TotalDielRange)) +
  geom_point(color='#D55E00', size = 3) +
  geom_smooth(method=lm, color='#2C3E50', linetype="dashed") +
  theme(text = element_text(size=13)) +
  labs(title = "2cms fluctuations >6cms from 5-10cms window",
        y=expression(paste("Summed magnitude of diel fluctuation")),
        x = expression(paste("Slope of recession limb (m3", "s-1", "day-1,"))))
```

```
#####
# Average magnitude of diel fluctuation
# _____
```

```
cor.test(Preds$TotalSlope, Preds$AveDielRange)
```

```
ggplot(Preds, aes(x=TotalSlope, y=AveDielRange)) +
  geom_point(color='#D55E00', size = 3) +
  geom_smooth(method=lm, color='#2C3E50', linetype="dashed") +
  theme(text = element_text(size=13)) +
  labs(title = "2cms fluctuations >6cms from 5-10cms window",
        y=expression(paste("Average magnitude of diel fluctuation (m3", "s-1", ")")),
        x = expression(paste("Slope of recession limb (m3", "s-1", "day-1,"))))
```

Supporting Information for

## **River bank erosion and lateral accretion linked to hydrograph recession and flood duration in a snowmelt-dominated system**

**Nicholas A Sutfin<sup>1\*</sup>, Joel Rowland<sup>1</sup>, Mulu Fratkin<sup>1</sup>, Sophie Stauffer<sup>1</sup>, Rosemary Carol<sup>2</sup>, Wendy Brown<sup>3</sup>, Ken Williams<sup>4</sup>**

<sup>1</sup>Earth and Environmental Sciences Division, Los Alamos National Laboratory, Los Alamos, NM

<sup>2</sup>Division of Hydrologic Sciences, Desert Research Institute, Reno, NV

<sup>3</sup>Rocky Mountain Biological Laboratory, Gothic, CO

<sup>4</sup>Lawrence Berkeley National Laboratory, Berkeley, CA

\* Current affiliation: Dept. of Earth, Environmental, and Planetary Sciences, Case Western Reserve University, Cleveland, OH

Corresponding authors: Nicholas A. Sutfin ([Nicholas.sutfin@case.edu](mailto:Nicholas.sutfin@case.edu)), Joel Rowland ([jrowland@lanl.gov](mailto:jrowland@lanl.gov))

### **Contents of this file**

Introduction to supporting information

Figure S1

Figure S2

Figure S3

Table S1

Table S4

Table S5

### **Additional Supporting Information (Files uploaded separately)**

Captions for Table S2

Captions for Table S3

Captions for Table S6

### **Introduction**

Figures and tables below are cited within the text of Sutfin et al. to provide supporting information and summary data. In addition, we briefly provide explanation of the statistical transformations conducted for analyses and referenced in the text.

Multiple linear regression model residuals met assumptions of homoscedasticity and normality (at the 95% confidence level) after a natural log transform of annual floodplain vertical accretion rate and boxcox power transformations with lambda ( $\lambda$ ) exponent coefficients of 0.1010101 and 0.2626263 for the area of floodplain eroded and laterally accreted, respectively. Eroded and accreted areas appearing in equations 2 and 3 in the main text contain exponents of the reciprocal of these lambda values, necessary if one

were to attempt calculation of erosion or accretion based on parameters listed in those equations.

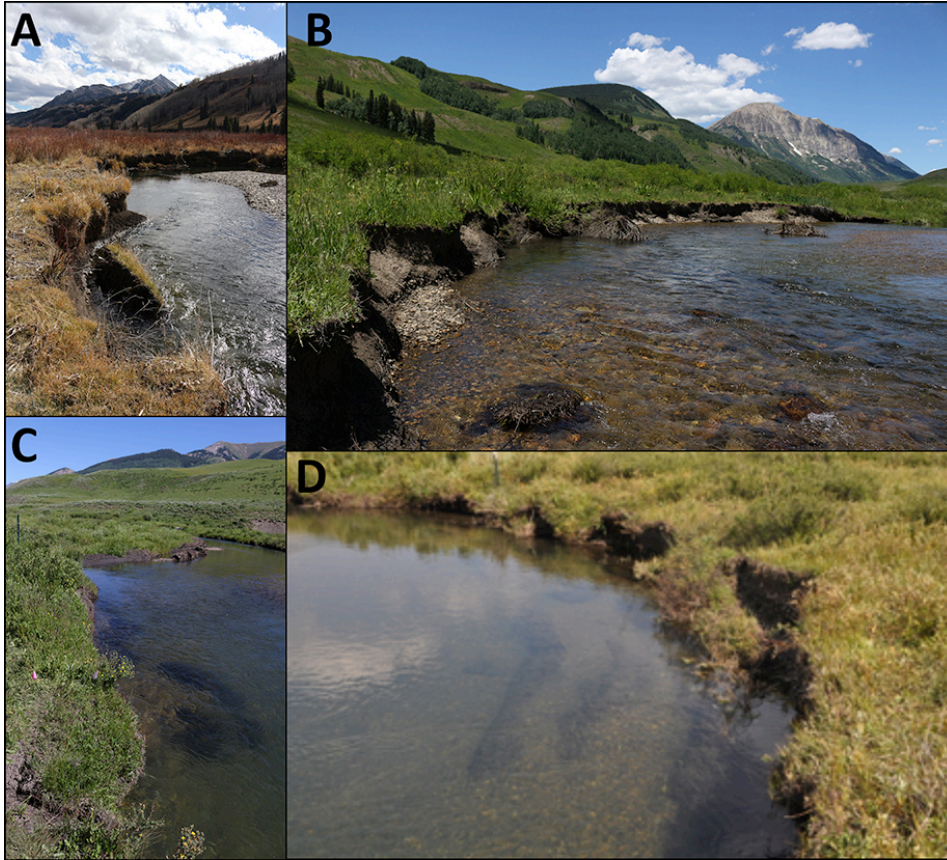


**Figure S1:** Bank erosion commonly observed along the East River. The upper fine-grained portion of floodplain sediment collapses in large blocks on the outside of channel bends. Following undercutting and erosion of underlying sandy gravel, channel banks crack (A, C) and eventually fall into the channel (A, B, D) where they remain on the channel bed at low flows (A, B) and can be buried by gravel during higher flows (C,D).

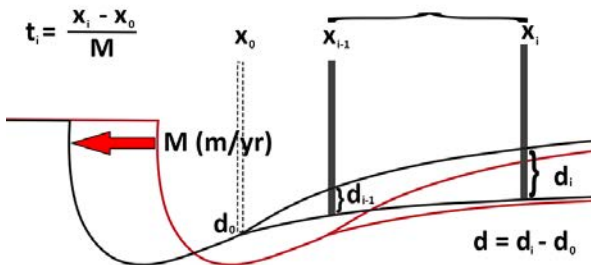
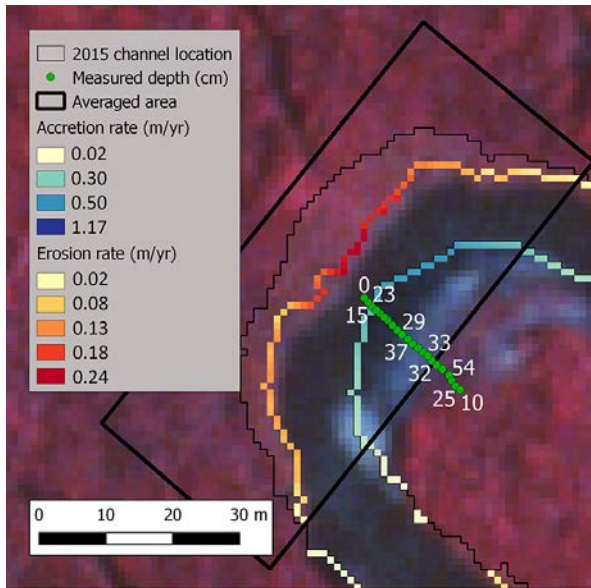


**Figure S2.** At each bend where a transect of measured depths was located, linear erosion rates along the bank (depicted as the outer bank in 1973 by the yellow-red spectrum) and accretion rates (depicted as the inner bank in 2015 by the yellow-blue spectrum) were averaged within a rectangle. The rectangle was drawn to capture the accreted bank pixels with a boundary defined by the approximate location where the outer bank from 1973 intersect the outer bank from 2015 (thin black line). The difference in the horizontal distances ( $x_i$  and  $x_{i-1}$ ) between consecutive depth measurements ( $d_i$  and  $d_{i-1}$ ) was divided by the mean migration rate to determine the duration of sediment deposition at each point ( $t_i$ ). Vertical accretion rate at each point was then calculated by the difference in measured depth between consecutive points divided by the time between points. This point-by-point method was conducted in addition to that described in the main text, but yielded inconsistent results as a function of small changes in floodplain topography and possible alternative periods of point bar erosion and deposition, so this analysis was not used for the results presented.

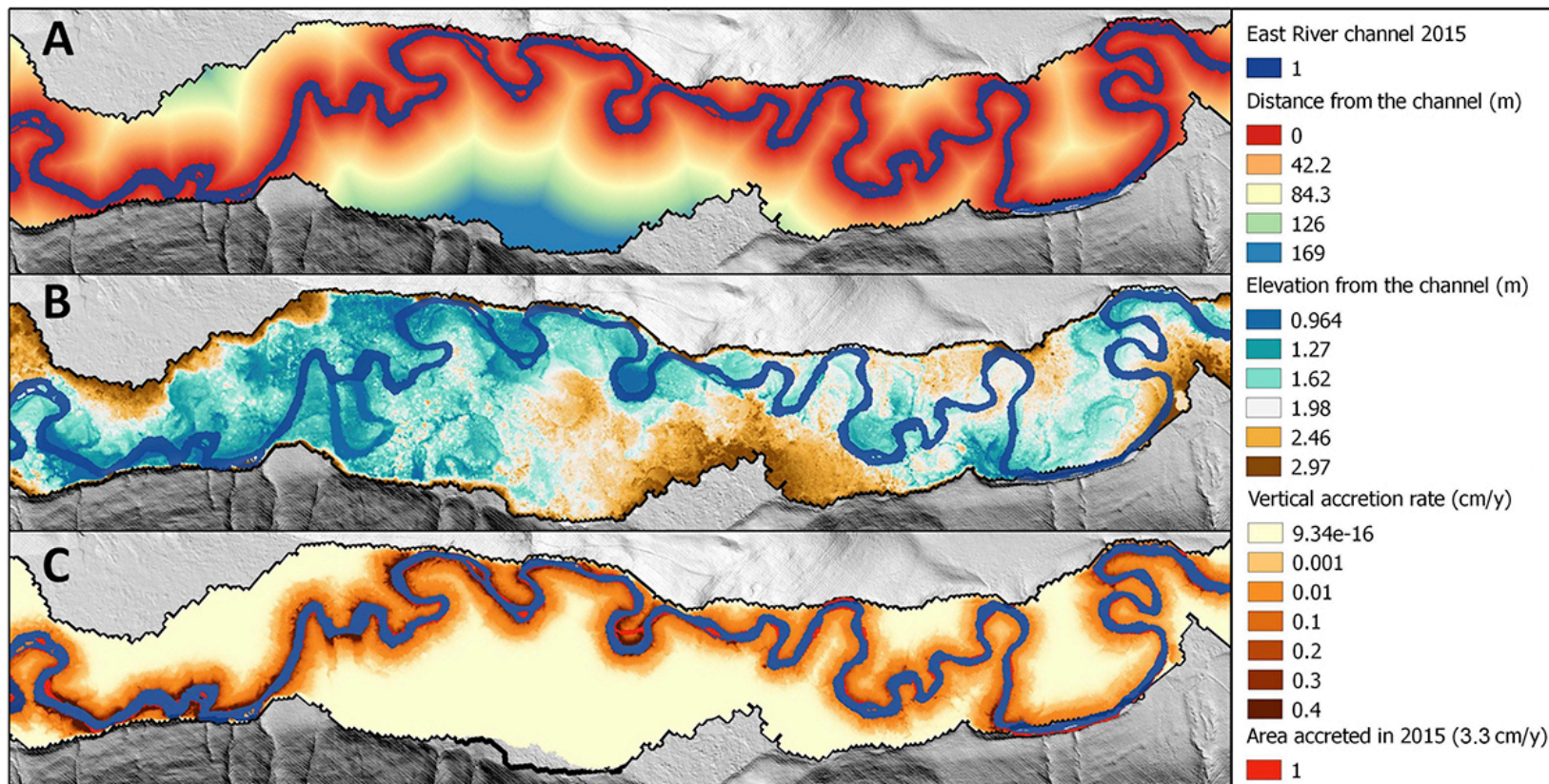


**Figure S3** Example from the 2015 pixel grid calculations. Distance from the channel (A) for each time period and relative elevation (B) for all time periods were used in a multiple linear regression to estimate mean overbank vertical accretion rate ( $r_{va}$ ) across the floodplain (C) using the following equation.  $\ln(r_{va}) = 1.204490 - 0.072038x - 1.205276z$  where  $x$  is distance from the channel along a transects orthogonal to the channel and  $z$  is elevation from the channel. As indicated in the legend, areas in red on the vertical accretion map are those identified from SCREAM analysis from differences in channel masks in consecutive years. Long-term deposition from measured depths within 10 m from the active channel indicated a mean vertical accretion rate of  $3.3 \text{ cm y}^{-1}$ , which was applied to the area of lateral accretion. Overbank deposition outside of the red accreted areas was estimated using relationships determined in multiple regression equation 3.

## TABLES

Years	Erosion	Accretion
1973-1983	17%	14%
1983-1990	25%	14%
1990-2001	16%	16%
2001-2011	19%	13%
2011-2015	41%	25%

**Table S1 .** Percentage error in floodplain area estimates from SCREAM, as calculated and outlined by Rowland et al. (2016). As described in the text, estimates of error for the time period between 1955 and 1973 were not obtainable through SCREAM, thus errors presented in Table 1 and Figure 3 are estimated as two times the maximum error from other time periods.

**Table S2.** Field and remotely sensed data for stepwise multiple linear regression of measured floodplain fine sediment depths at 315 points across 51 transects.

**Table S3.** Annual hydrologic indices for synthetic hydrographs at the East River study site constructed using a linear regression with the USGS East River at Almont stream gage and parameters extracted using code provided.

Variable	Floodplain vertical accretion	
	Considered	Included
Surface elevation (m)	X	√**
Elevation of gravel surface (m)	X	
Distance from the channel (m)	X	√***
Relative elevation from the channel (m)	X	
Duration (years)	X	
Channel width (m)	X	
Valley width (m)	X	X
Confinement (m <sup>2</sup> /m <sup>2</sup> )	X	√**
Reach valley slope (m/m)	X	
Reach sinuosity (m)	X	X
Reach channel slope (m/m)	X	
Local valley slope (m/m)	X	
Local sinuosity (m/m)	X	
Local Channel slope (m/m)	X	X
Bend orientation angle	X	X
Radius of curvature	X	√-
Inside of bend	X	X
Outside of bend	X	

**Table S4.** Variables considered (X) before elimination following reduction of collinearity and examined (X) using stepwise multiple linear regression for vertical accretion. Among variables examined, those marked with (√) indicate variables retained in the optimal multiple linear regression model. Significance of variables in the regression model is denoted at confidence levels of 99.9% \*\*\*, 99% \*\*, 95% \*, 90% . , or not significant <90% -

Variable	Floodplain area along nine reaches over 6 time periods			Entire study segment over 6 time periods		
	Examined			Examined		
	Considered	Erosion	Accretion	Considered	Erosion	Accretion
Channel slope	X	X	X			
Valley Slope	X					
Confinement	X	X	X			
Mean Channel width	X	X	√*			
Sinuosity	X	√**	√***			
Mean Day of Peak Flow	X		X	X		
Mean Peak Flow (m <sup>3</sup> s <sup>-1</sup> )	X			X		
Max Peak Flow (m <sup>3</sup> s <sup>-1</sup> )	X			X		
Mean Bankfull Duration (days)	X	X		X		
Max Bankfull Duration (days)	X			X		
Mean Days Above Bankfull Flow	X			X		
Max Days Above Bankfull Flow	X		X	X		√.
Mean Duration Above Baseflow (days)	X		X	X		
Max Duration Above Baseflow (days)	X	√*	X	X		
Mean Days Above Baseflow	X	X		X		
Max Days Above Baseflow	X		√*	X		
Mean Days Since Bankfull Flow	X			X		
Max Days Since Bankfull Flow	X			X		
Mean Day Baseflow Ends	X			X		
Mean Day Bankfull Flow Ends	X	X		X		
Mean No. Peaks Above Bankfull	X			X		
Maximum No. Peaks Above Bankfull	X			X		
Mean Total Recession Slope (m <sup>3</sup> s <sup>-1</sup> day <sup>-1</sup> )	X			X		
Max Total Recession Slope (m <sup>3</sup> s <sup>-1</sup> day <sup>-1</sup> )	X	√***		X	√**	
Mean Bankfull Recession Slope (m <sup>3</sup> s <sup>-1</sup> day <sup>-1</sup> )	X			X		
Max Bankfull Recession Slope (m <sup>3</sup> s <sup>-1</sup> day <sup>-1</sup> )	X		√.	X		
Mean Total Annual Volume (km <sup>3</sup> )	X			X		
Max Total Annual Volume (km <sup>3</sup> )	X			X		
Mean Bankfull Volume (km <sup>3</sup> )	X			X		
Max Bankfull Volume (km <sup>3</sup> )	X	X		X		
Power transformation coefficient (lambda)		0.1010101	0.2626263		NA	NA
Coefficient of determination (r <sup>2</sup> )		0.59	0.55		0.91	0.59
Regression model p-value		<0.0001	<0.0001		0.003	0.074

**Table S5.** Variables considered (X) before elimination following reduction of collinearity and examined (X) using stepwise multiple linear regression for lateral erosion and accretion. Among variables examined, those marked with (√) indicate variables retained in the optimal multiple linear regression model. Significance of variables in the regression model is denoted at confidence levels of 99.9% \*\*\*, 99% \*\*, 95% \*, 90% . , or not significant <90% -

**Table S6.** Correlation matrix for variables considered in multiple linear regression analysis to examine linkages between hydrologic flow conditions, erosion, and accretion.